January 2008

Design of a Two-Receiver Interferometer on Motorized Tracks

Eric Marklein
University of Massachusetts Amherst

DESIGN OF A TWO-RECEIVER INTERFEROMETER ON MOTORIZED TRACKS

A Thesis Presented

by

ERIC R. MARKLEIN

Submitted to the Graduate School of the
University of Massachusetts Amherst in partial fulfillment
of the requirements for the degree of

MASTER OF SCIENCE IN ELECTRICAL AND COMPUTER ENGINEERING

May 2008

Electrical and Computer Engineering

DESIGN OF A TWO-RECEIVER INTERFEROMETER ON MOTORIZED TRACKS

A Thesis Presented

by

ERIC R. MARKLEIN

Approved as to style and content by:

Daniel H. Schaubert, Chair

Calvin T. Swift, Member

Marinos N. Vouvakis, Member

C. V. Hollot, Department Chair
Electrical and Computer Engineering

To Harold Myhre.

ACKNOWLEDGMENTS

Thank you.

ABSTRACT

DESIGN OF A TWO-RECEIVER INTERFEROMETER ON MOTORIZED TRACKS

MAY 2008

ERIC R. MARKLEIN

B.S.E.E., UNIVERSITY OF MASSACHUSETTS AMHERST

M.S.E.C.E., UNIVERSITY OF MASSACHUSETTS AMHERST

Directed by: Professor Daniel H. Schaubert

A 94.8 GHz interferometric imaging system utilizing aperture synthesis and tomography is developed for the Center for Advanced Sensor and Communication Antennas. Whereas typical interferometer designs employ multiple antennas to synthesize an aperture for image reconstruction, this unique interferometer will reproduce a scene's brightness temperature with only two antennas. To achieve this, the aperture synthesis is done with one antenna remaining stationary while the second antenna is moved at discrete increments along two controlled tracks. The two signals received by the antennas are cross-correlated to produce measured visibility function samples. The visibility samples reconstruct the scene brightness temperature through an inverse Fourier transform relationship.

TABLE OF CONTENTS

LIST OF TABLES

Table **Page**

LIST OF FIGURES

Figure **Page**

CHAPTER 1

INTRODUCTION

Microwave remote sensing of the earth's surface with an interferometer is a well-known method of passively measuring various parameters including ocean salinity, soil moisture or rainfall. An antenna pointed towards a given target covers a resolution cell with dimensions determined by the antenna's aperture size and distance away from the targeted scene. However, the need for finer spatial resolution requires an increase in the antenna's aperture size [1]. Rather than constructing an entire aperture, aperture synthesis is a commonly used alternative for achieving similar results. When properly designed, synthetic apertures have the benefit of reducing the total system weight and volume while providing the spatial resolution of the full-sized antenna aperture.

With two antennas spaced a distance d apart, received signals between the two are cross-correlated, producing a single Fourier component of the brightness temperature, known as a visibility function in radio astronomy. The visibility function is unique for each value of d and is non-zero only when the antennas share a field of view [2]. By measuring the visibility function over numerous discrete distances across the entire aperture, the brightness temperature of the scene is obtained by application of the inverse Fourier transform. One implementation for measuring brightness temperature employs a thinned array format [3] [4] [5]. The thinned array design places antennas at appropriate integer half-wavelength spacings that insure the cross-correlation signals will have every half-wavelength spacing up to the maximum spacing distance using the fewest samples possible. This minimum redundancy linear array contains the fewest duplicate samples as redundant samples do not improve spatial resolution [6].

However, when working at a high frequency of 94.8 GHz, the cost of designing multiple receivers for a thinned array implementation is extremely costly for a proof-of-concept. The alternative used in this thesis utilizes only two 94.8 GHz antenna receivers to provide all the cross-correlating terms to complete the scene reconstruction. The design builds upon the two antenna correlating procedure that was discussed earlier. One antenna remains stationary with the second antenna moving along a track at appropriate discrete, half-wavelength spacings that fill the desired aperture size. The drawback to this design is that several hours are needed to measure an entire scene.

The current system consists of two linear drives creating the separations between two radiometers. Measurements taken by the radiometers are introduced to an analog correlator, producing samples of the complex visibility function. These samples are collected by an A/D converter and stored on a local computer. The data collection and movement of the linear drives is done through custom built software integrating the pieces of hardware. The collected data are placed through additional post-processing code to reproduce the final brightness temperature of a measured, stationary scene.

This thesis provides a proof-of-concept for recreating a brightness temperature scene using two antennas on moveable tracks. The successful implementation of this system will permit further advancements in the design to be made. The final version of this system will incorporate numerous antenna receivers into a thinned array format, generating multiple fan beams simultaneously. This thinned array would be fixed on a spoke that would sweep 180° in steps such that the Nyquist rate is satisfied. The generation of multiple fan beams into the system would reduce the inherent time consumption needed in measurement taking in the current version.

CHAPTER 2

THEORY

A simplistic imaging system with a single antenna is shown in Figure 2.1. The antenna's aperture from a height h covers a spatial resolution cell of the earth's surface of approximately $L \times W$. Typically, the antenna is scanning off-nadir at some angle θ. The dimensions of the resolution cell are approximated as:

$$L = h\frac{\lambda}{D}\sec^2\theta \quad W = h\frac{\lambda}{D}\sec\theta \tag{2.1}$$

These equations reduce to:

$$L = W = h\frac{\lambda}{D} \tag{2.2}$$

at nadir where λ is the operating frequency wavelength and D is the maximum antenna aperture dimension. It's apparent from Equations 2.1 and 2.2 the need to increase the aperture size to provide finer spatial resolution. Instead, using multiple smaller antennas and aperture synthesis can provide the same resolution results [1].

Figure 2.2 shows an idealized correlating scheme with two antennas. The two antennas share a field of view. One antenna remains fixed and represents the origin of the defined coordinate system. The measured scene is assumed flat and both antennas are placed a height h above the scene. The second antenna is placed at a location $(D_x, D_y, 0)$ away from the stationary antenna. The received RF signals from each antenna are cross-correlated. The cross-correlated signal is the Fourier transform

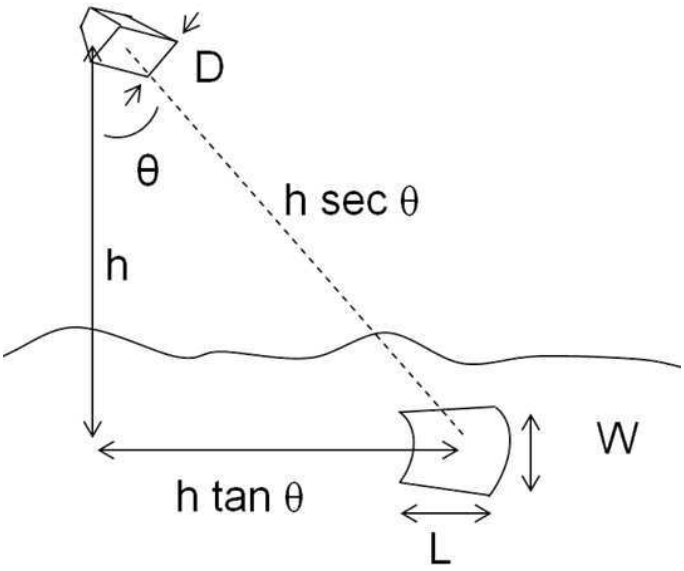

Figure 2.1. Simple imaging system with resolution cell dimensions

of the brightness temperature, known as the visibility function. The visibility function is given by:

$$V(u,v) = \frac{c}{4\pi} \int_0^{2\pi} \int_0^{\pi} T_\Omega(\theta,\phi)\, G(\theta,\phi) e^{j2\pi(u\sin\theta\cos\phi + v\sin\theta\sin\phi)} \sin\theta \, d\theta \, d\phi \tag{2.3}$$

With

V in degrees Kelvin

$u = \frac{D_x}{\lambda} \quad v = \frac{D_y}{\lambda}$

D_x, D_y are antenna spacings

λ is the free-space wavelength of the antenna's operating frequency and c is some constant value that is solved for by measuring a uniform scene of temperature T_0. G is the gain of the receiving antenna and T_Ω is the incident brightness temperature per steradian. For an antenna with a pencil beamwidth θ_B, such that:

$$G(\theta,\phi) = \begin{cases} \frac{16}{\theta_B^2} & : \quad \theta \leq \frac{\theta_B}{2} \\ 0 & : \quad \theta \geq \frac{\theta_B}{2} \end{cases}$$

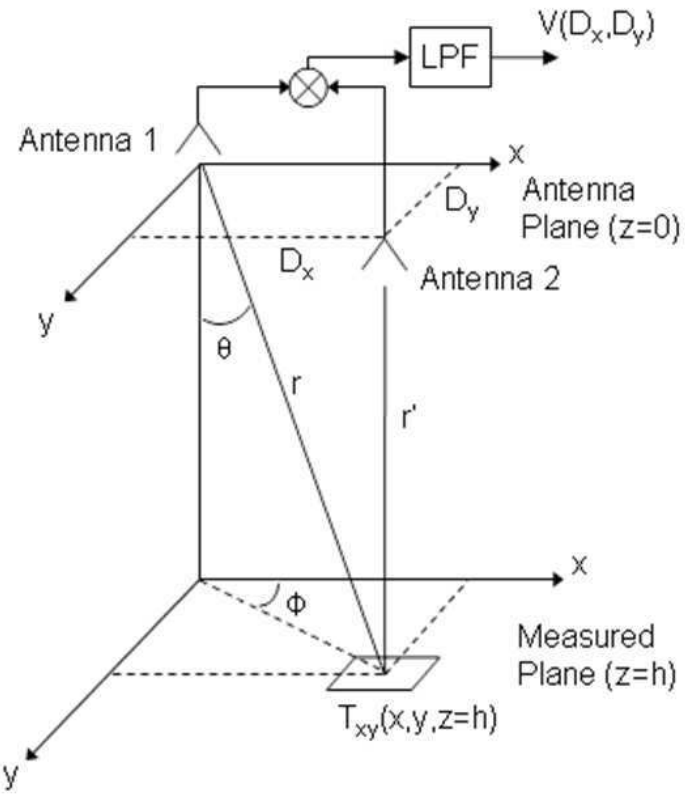

Figure 2.2. Two-dimensional interferometer capable of producing visibility function samples, $V(D_x, D_y)$ of the measured scene brightness temperature, $T_{xy}(x, y)$

the visibility function in rectangular coordinates is approximated as:

$$V(u,v) = \frac{c}{\pi} \int_{-1}^{1} \int_{-\sqrt{1-\bar{y}^2}}^{\sqrt{1+\bar{y}^2}} T_\Omega(\bar{x},\bar{y}) e^{j\pi\theta_B(u\bar{x}+v\bar{y})}\, d\bar{x}\, d\bar{y} \tag{2.4}$$

With

$\bar{x} = \frac{x}{\left(\frac{h\theta_B}{2}\right)}$ $\quad \bar{y} = \frac{y}{\left(\frac{h\theta_B}{2}\right)}$

If Equation 2.4 is sampled at integer multiples of a distance d in both directions, the real and imaginary components of the visibility function (V_I and V_Q, respectively) become:

$$V_I(md, nd) = \frac{c}{\pi} \int_{-1}^{1} \int_{-\sqrt{1-\bar{y}^2}}^{\sqrt{1+\bar{y}^2}} T_\Omega(\bar{x}, \bar{y}) \cos\left(\pi\theta_B \frac{d}{\lambda}(m\bar{x} + n\bar{y})\right) d\bar{x}\, d\bar{y}$$

$$V_Q(md, nd) = \frac{c}{\pi} \int_{-1}^{1} \int_{-\sqrt{1-\bar{y}^2}}^{\sqrt{1+\bar{y}^2}} T_\Omega(\bar{x}, \bar{y}) \sin\left(\pi\theta_B \frac{d}{\lambda}(m\bar{x} + n\bar{y})\right) d\bar{x}\, d\bar{y} \tag{2.5}$$

In this form, Equation 2.5 is a truncated Fourier series that can be inverted to produce the scene brightness temperature through the equation

$$T(x, y) \cong \frac{c}{\pi} \sum_{m=1}^{M} \sum_{n=1}^{N} V_{mn} e^{-j\pi\theta_B \frac{d}{\lambda}(mx+ny)} \tag{2.6}$$

$$V_{mn} = V_I(md, nd) + jV_Q(md, nd) \tag{2.7}$$

By moving the second antenna across the entirety of the desired aperture in discrete intervals, enough visibility function samples are accumulated to use the inverse Fourier transform in Equation 2.6 to reproduce the scene's brightness.

One such block diagram implementation for producing a complex, cross-correlating output is shown in Figure 2.3. The two received signals, S_1, centered at f_1 and S_2, centered at f_2, each containing the same bandwidth B are combined and square-law detected. One of the output terms is the correlation of the two signals received by the antennas, $(S_1 S_2)$, centered at the difference frequency $(f_1 - f_2)$. A bandpass filter preserves and eliminates unwanted terms of $(S_1 + S_2)^2$ before demodulation by an LO signal operating at this difference frequency. Lastly, the output is integrated to produce the sampled visibility function.

Radiometer measurements at microwave frequencies have an unavoidable noise floor ΔV due to the finite integration time τ in the correlator. For an array with N elements, the noise floor is given by the function [7]

$$\Delta V = \frac{T_B + T_R}{\sqrt{B\tau}} \tag{2.8}$$

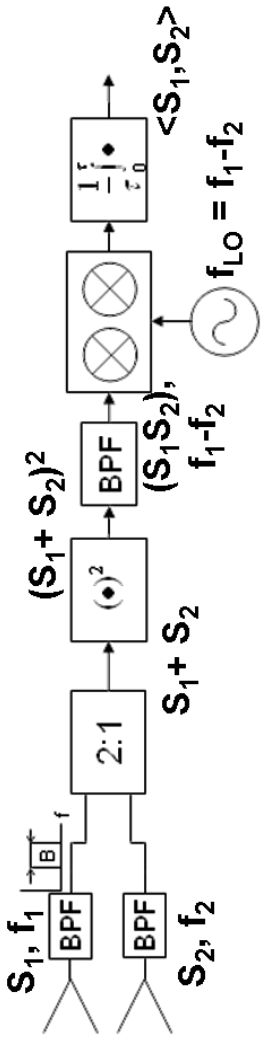

Figure 2.3. Interferometer correlating block diagram for two receivers

ΔV is the noise floor the measurement in degrees Kelvin

B is the system bandwidth in Hz

T_B is the ambient brightness temperature in degrees Kelvin

T_R is the receiver noise temperature in degrees Kelvin

This noise floor is related to the overall image resolution ΔT of the scene brightness temperature by

$$\Delta T = \Delta V \frac{D}{d} \sqrt{\frac{\pi}{8}} \tag{2.9}$$

Combining Equations 2.8 and 2.9

$$\Delta T = \frac{D}{d} \sqrt{\frac{\pi}{8}} \frac{T_B + T_R}{\sqrt{B\tau}} \tag{2.10}$$

D is the array size

d is the element spacing

ΔT is the brightness resolution in degrees Kelvin

For imaging applications of this kind, an acceptable brightness temperature resolution is $\Delta T = 1$ K.

CHAPTER 3

SYSTEM OVERVIEW AND RADIOMETER FRONT-END

This chapter provides a detailed look at the radiometer electronics, linear drives and remaining support structures. Section 3.1 gives detailed information on the high-frequency radiometers and noise source used in the design, along with issues encountered with these components. In Section 3.2, the linear drives that are used to create the numerous separations between the two radiometers are described. Section 3.3 discusses the custom built support structures that were made for containing the two radiometers and the linear drives.

3.1 Radiometers and Noise Source

In this section, an overview of the 94.8 GHz radiometers and noise source is given. These three pieces of electronics were constructed by Millitech under the supervision of Professor Calvin Swift. Information on issues found with these microwave components is given as well.

3.1.1 Radiometer Electronics

The block diagram for the receiver subsystems are shown in Figure 3.1. The two system receivers are identical to each other except for physically being mirror-images of one another. These receivers are high-frequency, weatherized radiometers. The radiometers operate at a RF center frequency of 94.8 GHz and have noise figures of 5.4 dB. Both radiometers produce their 91.8 GHz LO signal from a single, 100 MHz reference signal. The 100 MHz reference signal is contained in only one of the

radiometers. The 100 MHz reference signal is sent through a 2:1 power divider, with one output being sent to the second radiometer through a coaxial cable. The 100 MHz reference signal drives a 15.3 GHz single, phase-locked loop oscillator found in each radiometer. The phase noise of the PLL oscillator is typically -115 dBc/Hz at a 20 kHz offset. The output from the oscillator is first doubled in frequency, to 30.6 GHz, and then frequency multiplied by 3 to achieve the 91.8 GHz LO signal that will produce the down-converted 3 GHz IF signal. A stage of amplification follows so that the power level input into the LO channel of the demodulator is roughly 6 dBm before the RF signal demodulation. The 91.8 GHz LO signal offers roughly the same phase noise performance of the original 15.3 GHz signal from the PLL oscillator.

The remainder of the radiometer's layout is now described as follows. A standard, circular corrugated horn that is RHCP is used. The horn antennas have a nominal 25 degree half-power beamwidth, an axial ratio that is approximately ideal and features excellent E- vs. H-plane pattern match, with pattern and gain plots shown in Figures 3.2, 3.3 and 3.4. Each signal received by the radiometers is sent through a W-band waveguide into the receiver. A linear-circular polarizer follows to only allow circularly polarized energy from the antenna into the following components. After the polarizer, a circular to rectangular waveguide transition is included in order to compact the overall mechanical layout. The signal is then amplified by 20 dB with a low noise figure of approximately 6 dB. A ferrite single junction isolator stage comes next for good impedance matching between components and alleviates any potential oscillations. An Iris coupled bandpass cavity filter stage comes next to provide lower sideband rejection before entering the I/Q demodulator. The filter's precision machining gives high repeatability with no tuning elements and a high Q. The demodulator has single stage low-noise amplifiers integrated into the quadrature mixer design. Phase balance is achieved to within $\pm$ 10 degrees across the operating bandwidth. A final IF bandpass filter with steep passband characteristics below 3

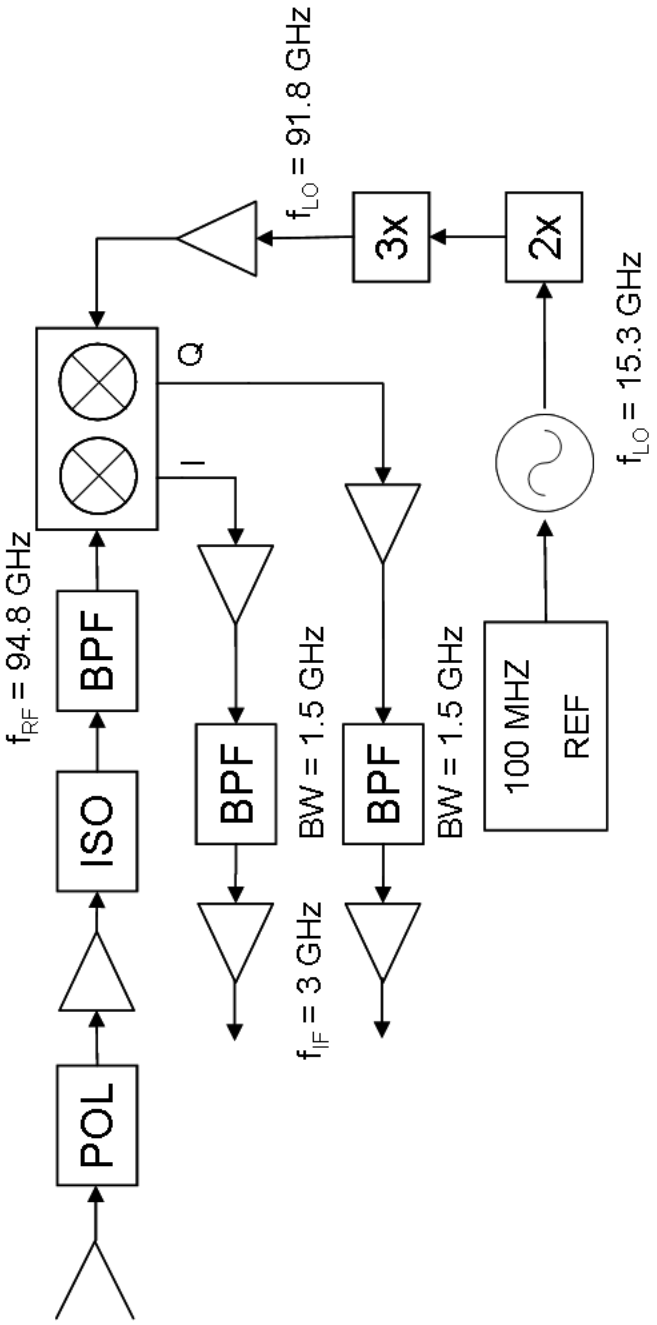

Figure 3.1. Block diagram of 94.8 GHz radiometers

GHz provides an output bandwidth of 1.5 GHz at IF. An amplification stage occurs before the two receiver outputs are fed into the correlator subsystem, as discussed in the next chapter. The total power output level is in the range of -10 to 0 dBm. The output power plots of the two radiometers before being introduced to the complex correlator are shown in in Figures 3.5 and 3.6, respectively. These power output levels are when each radiometer observes an ambient scene and highlight the output bandwidth. For the present implementation of the imaging system, only the in-phase component is needed for signal correlating, the quadrature component is connected to a matched load.

3.1.2 Noise Source

The noise source by Millitech was constructed to be used as a test source and common reference point for the measurements taken. An idealized noise point source in a measured scene would be seen as a "hot-spot" in a reproduced image. For a point noise source of the form:

$$T_B(\bar{x}, \bar{y}) = T_0 \delta(\bar{x} - \bar{x}_0)\delta(\bar{y} - \bar{y}_0) \tag{3.1}$$

The discrete visibility function samples are:

$$V_{mn} = \frac{T_0}{\pi} e^{jm\pi\theta_B \bar{x}_0 \frac{d}{\lambda}} e^{jn\pi\theta_B \bar{y}_0 \frac{d}{\lambda}} \tag{3.2}$$

Applying the previously discussed Fourier relation and applying phased array theory, the resulting reconstructed brightness temperature is of the form

$$\hat{T}_B(\bar{x}, \bar{y}) = \frac{T_0}{\pi} \frac{sin\left[\pi\theta_B(M + \frac{1}{2})(\bar{x} - \bar{x}_0)\frac{d}{\lambda}\right]}{sin\left[\pi\frac{\theta_B}{2}(\bar{x} - \bar{x}_0)\frac{d}{\lambda}\right]} \frac{sin\left[\pi\theta_B(N + \frac{1}{2})(\bar{y} - \bar{y}_0)\frac{d}{\lambda}\right]}{sin\left[\pi\frac{\theta_B}{2}(\bar{y} - \bar{y}_0)\frac{d}{\lambda}\right]} \tag{3.3}$$

Which resembles the form of the array factor in traditional array theory.

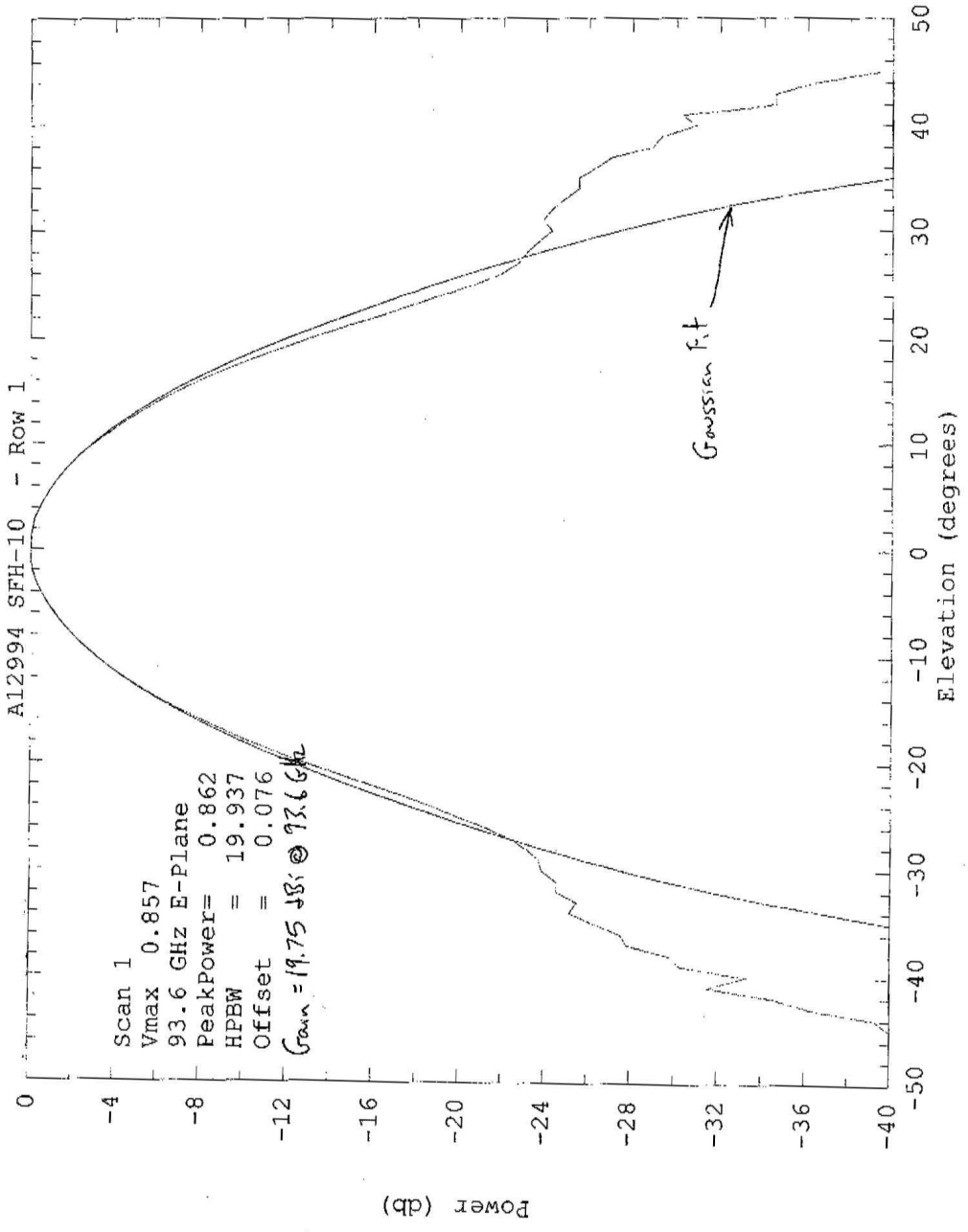

Figure 3.2. Normalized elevation pattern of radiometer's circular corrugated horn antenna, provided by Millitech, Inc.

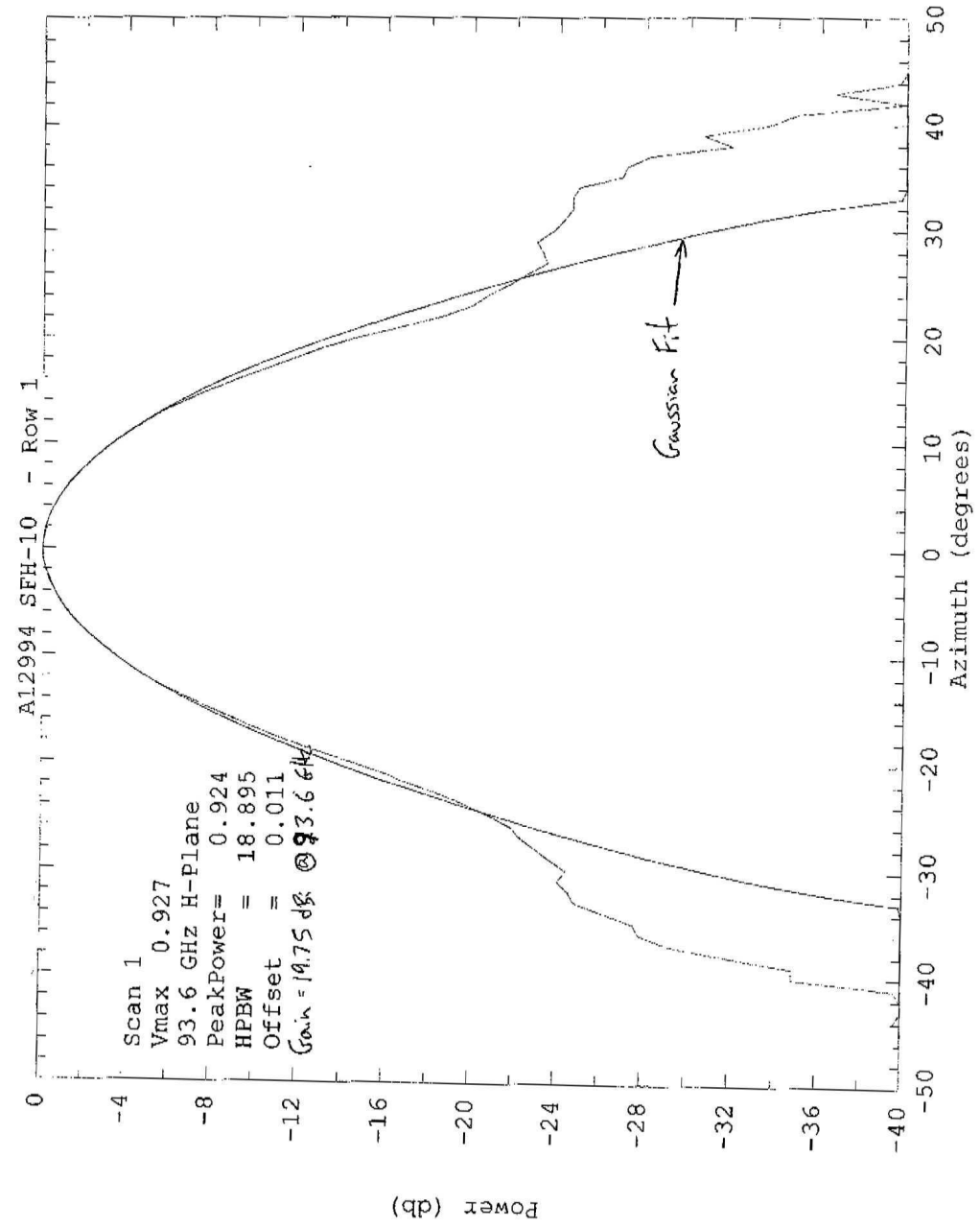

Figure 3.3. Normalized azimuth pattern of radiometer's circular corrugated horn antenna, provided by Millitech, Inc.

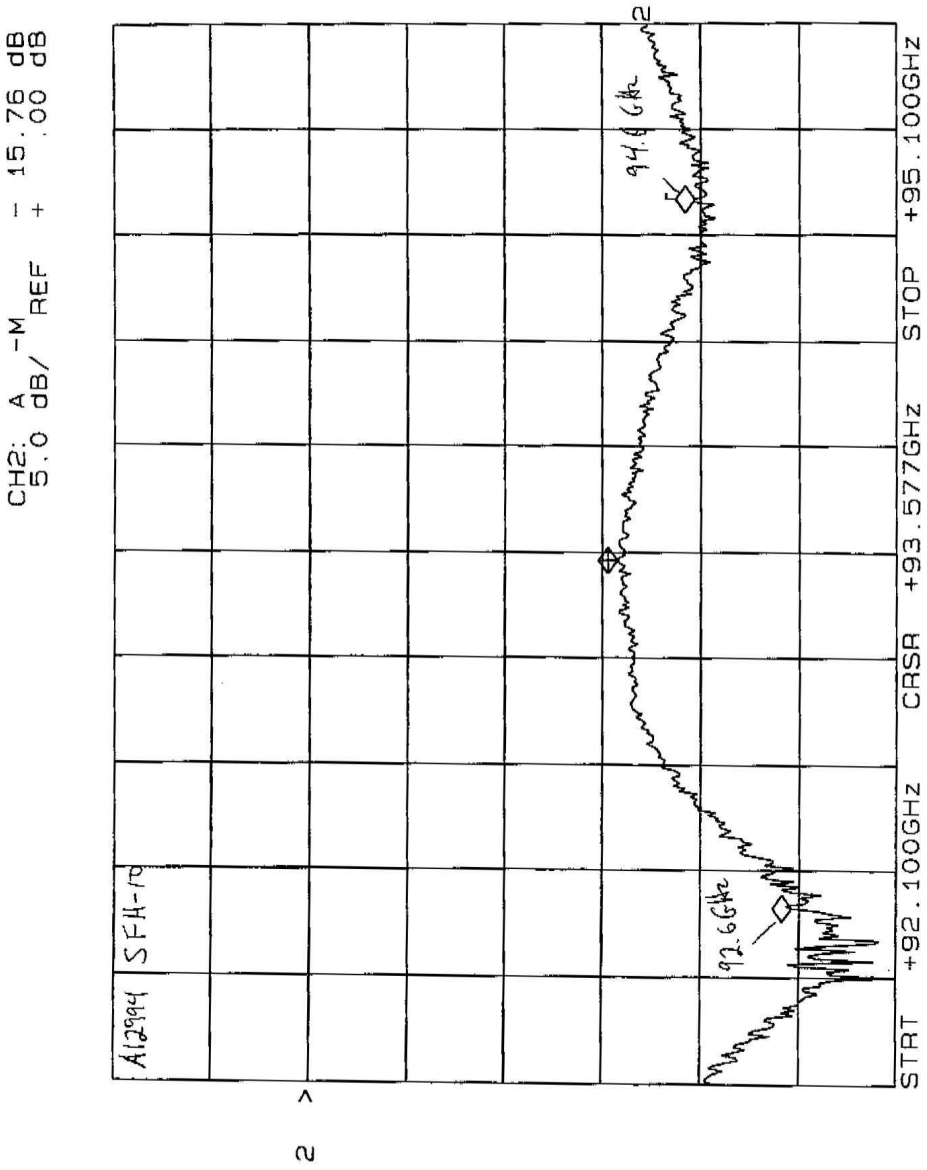

Figure 3.4. Broadside gain of radiometer's circular corrugated horn antenna, provided by Millitech, Inc.

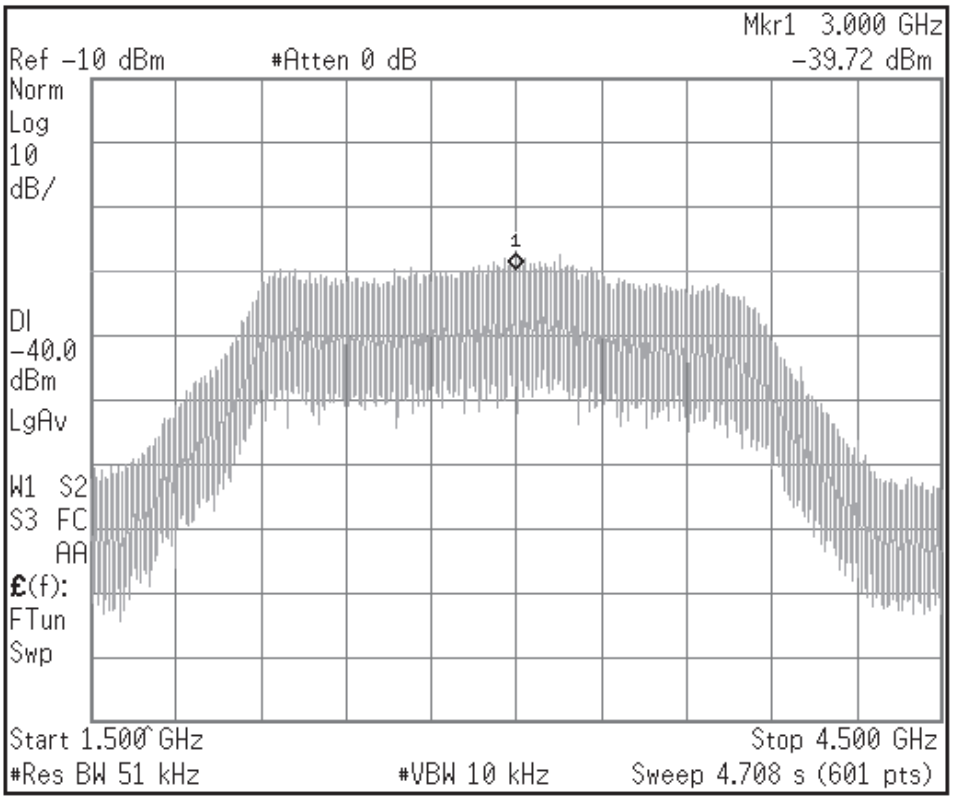

Figure 3.5. Output power plot for receiver 1

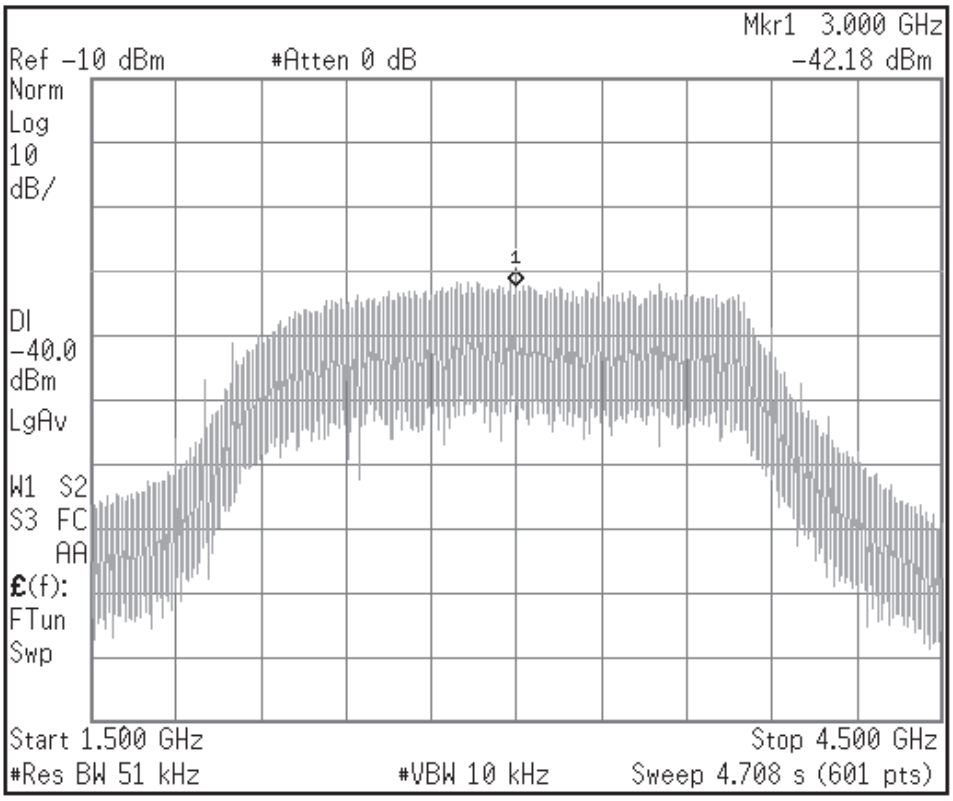

Figure 3.6. Output power plot for receiver 2

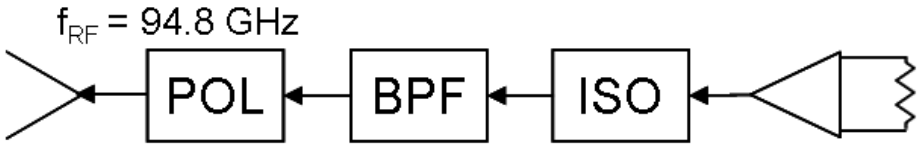

Figure 3.7. Block diagram of 94.8 GHz noise source

The noise source block diagram is shown in Figure 3.7. The nominal 25 dB ENR is obtained by placing a matched load to the input of a low noise amplifier, which is identical to the model used in the radiometer front end. A ferrite single junction isolator stage follows for impedance matching. Bandwidth is limited with an Iris coupled bandpass cavity filter. A linear-circular polarizer is next, allowing only the circularly polarized energy into the transmitted output. The noise signal is transmitted out of a RHCP, circular corrugated horn antenna. The microwave components used in the noise source are of the same make used in the previously described radiometers.

3.1.3 Radiometer Problems

Initial measurements were taken using a lossy, 1 meter RG402 coaxial cable connecting the 100 MHz reference between the two radiometers. When this cable experienced major movements, unwanted fluctuations in the visibility function sample outputs occurred. Since this system is intended to be tested in outdoor environments where winds could cause these kinds of cable movements, the RG402 was replaced with a sturdier coaxial cable. Manual tests of the cable's rigidity were found to remove the fluctuations in the correlator output.

It was also discovered that multipath signals between the two radiometers interfered with the desired correlated signal. By simply moving a hand between the two radiometers the output visibility function samples featured large signal variation. In addition, it was believed that one of the radiometers experienced signal leakage in the waveguide transition between the corrugated horn and the internal RF components. This exposed area was covered in copper tape and secured further. The multipathing was removed by placing a 7 inch $\times$ $9\frac{1}{2}$ inch piece of $2\frac{1}{4}$ inch thick absorber around each horn antenna's aperture, with a hole cut out to fit the receiving horn antennas, shown in Appendix C.

3.2 Linear Drive System

The discrete steps taken with one of the radiometers is accomplished on two 406XR Positioner linear drive tracks manufactured by Parker Automation. This section will detail the arrangement of the linear drives and their additional hardware components, along with their setup and performance capabilities for this imaging application.

3.2.1 Linear Drive Setup

The linear drives provide complete synthesized aperture capabilities for imaging with a 2 meter $\times$ 1 meter synthetic aperture. Each linear drive features a carriage that completes the distance movement executed by the user. The carriages move on a 10 mm thread ballscrew that is connected to a rugged servo motor. The servo motor contains a rotary encoder with signal feedback for enhanced movement precision. The 2 meter carriage supports the 1 meter linear drive at mid-section, with the arrangement shown in Figure 3.8. Each linear drive is connected to its own Gemini GV-U3E Digital Servo Drive. These digital servo drives store each drives' performance configuration and transmit the step-direction commands to the servo motors. The configuration of the drives is discussed in the following section.

The linear drives each contain a set of 3 sensors that are used as end-of-limits and homing triggers. A metal plate found on the side of each carriage will trigger a sensor if it moves over it. The sensor contains either a sinking switch, where the output provides an electrical path to ground, or a sourcing switch, where the output provides an electrical path to a positive voltage. The sensors contain 4 wires, one of which is used for the limit or home switch depending on the switch type. Depending on the sensor's use, the unused wire is left unwired. The sensors can be relocated to different positions on the linear drives; however, the manufacturer's recommendation is to not tamper with their mechanically set positions.

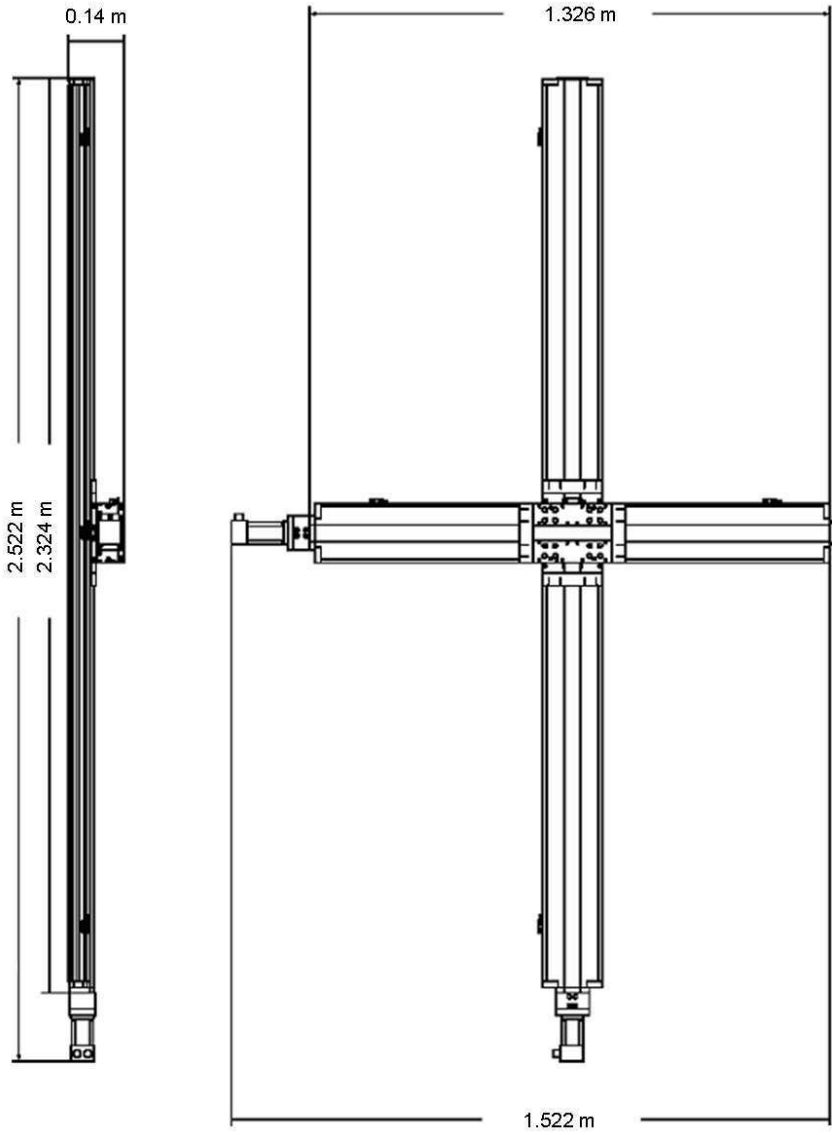

Figure 3.8. Linear Drive Configuration

Control of the digital servo drives is done in turn through the 6K2 2-axis Controller. The 6K2's communication to the host computer is done with a RS232 cable. The 6K2 acts as the hub for all communication done with the two servo drives. In addition, the 6K2 recognizes the status of the limit and homing sensors found on the linear drives.

For this thesis, measurements are taken in standard rectangular coordinate movements. However, if future designs choose to incorporate measurements in polar coordinates or in a spiral, as is the need for many remote sensing applications [8], the linear drives are capable of meeting such requirements.

3.2.2 Performance of Linear Drives

The servo drives operate internally in rotary units, with 8000 counts being completed in a full 360° rotary motor revolution of 10 mm. Scaling is incorporated in the software to operate in linear steps. Additionally, each linear drive carriage supports a significant load and needs to be considered during a tuning process done with the software provided by the manufacturer. The tuning process is done iteratively by the user to determine proportional and velocity gain values to achieve a 1st order response. A 1st order response gives minimal overshoot and close position tracking. A diagram of a desired 1st order response is shown in Figure 3.9. Each drives' load-to-rotor inertia ratio LJRAT needs to be accounted for as well and is done by the following equation:

$$\text{LJRAT} = \frac{\text{load intertia}}{\text{motor rotor inertia}} \tag{3.4}$$

If the linear drives are correctly tuned and the load-to-rotor inertia ratio is correct, a positional accuracy of 159 micrometers, $\lambda/20$ at 94.8 GHz, or better is attainable. The current system calibration has exhibited positional accuracy no worse than $\lambda/50$ (60 micrometers) through measurement tests.

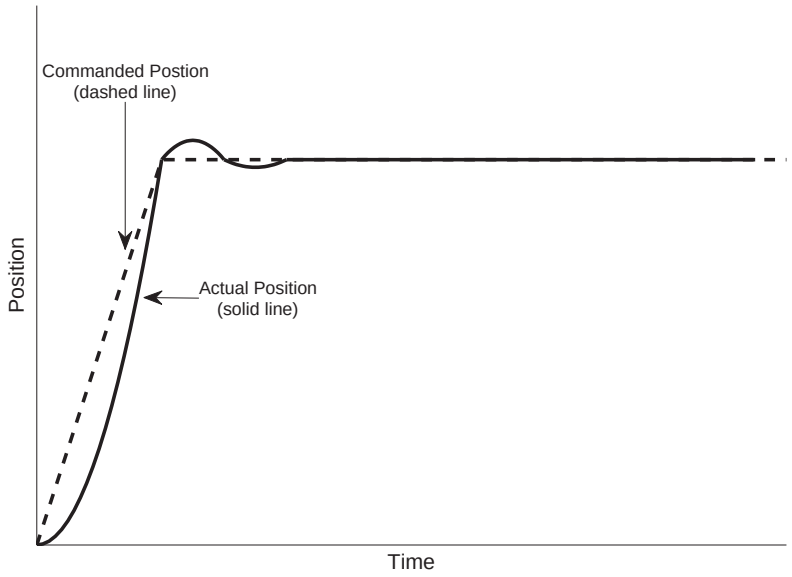

Figure 3.9. Desired 1st order movement response of 406XR drives

It's ideal that all the sensors be either all sinking switches or all sourcing switches to take advantage of the just the Limits/Home connector found on the 6K2. Curiously, the sensor sets found on the linear drives each came with a different sensor model. The sensors on axis 1 were PNP (sinking switches) while axis 2 sensors were NPN (sourcing switches). Instead of wiring axis 1's sensors to the Limits/Home connector, they were specially connected to the 6K2's Trigger/Outputs connector. Pin outs for both axes 1 and 2 are shown in Appendix B. Additional controller configuration needed to be done and is given in Appendix D.

The motion of the linear drives can be controlled through a complete coding environment designed by the manufacturer. However, since the linear drive motion is integrated with data acquisition code, the manufacturer's programming environment was circumvented through an automation server also provided by the manufacturer, called the Communications Server. The 32-bit OLE server completes all communication done between the 6K controller and Gemini drives with PC applications, in

this case the data acquisition software developed in-house. The integration of the Communications Server with acquiring measured data is discussed in Chapter 5.

3.3 Support Structures

Each radiometer is attached to a custom built, $\frac{1}{2}$ inch thick aluminum support structure, each of which is shown in Figure 3.10. The stationary radiometer's structure has to hover over drives so as to allow clearance of the traveling 1 meter track. The moving radiometer's structure is attached to the carriage of the 1 meter track. Both support structures can be manually adjusted so that the two radiometer antennas are as close as possible to each other before measurements are taken. The two structures also have 6 inches or more of clearance below the radiometers to accommodate the power and signal output cables. Dimensions of the two strucutres can be found in Appendix B.

The linear drive tracks are securely connected to a 96 inch $\times$ 36 inch $\times$ 1 $\frac{3}{4}$ inch maple wood block. The maple block in turn is secured to a support structure shown in Figure 3.11. The rectangular frame was specifically built so that the antennas are tilted approximately $\pm 15^{\circ}$ from horizontal. This was done so that the half-beamwidth angle of the corrugated horn antennas is parallel to the earth.

After initial movement profiles were completed with all of the hardware secured, numerous vibrations in the entire structure were found during movements. These vibrations were causing the stationary radiometer to shake, resulting in a questionable origin position. Since the stationary support structure needed to hang over the 1-m track, shaking from the motion profiles was inevitable. In addition to the mechanical vibrations, the stationary structure would need more support to resist any intrusive outdoor elements. Strengthening angles and various braces were put in to dampen the effects to some degree, until finally aluminum pieces were fastened on to the structure at the critical joints.

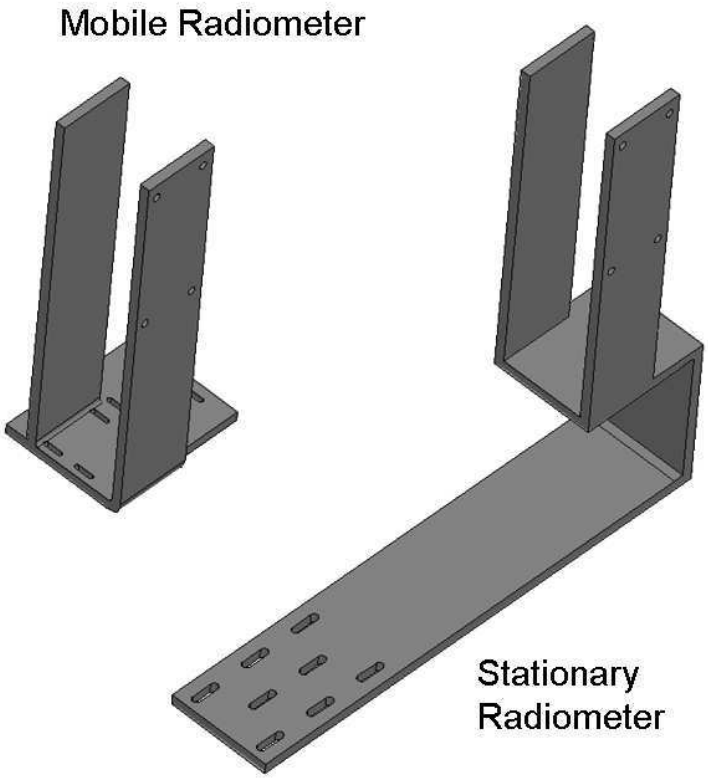

Figure 3.10. Support structures for receiver in motion and stationary receiver

Figure 3.11. Support structure for linear drives and radiometers

CHAPTER 4

CORRELATOR SYSTEM

The details of the analog complex correlator designed for the interferometer are given in this chapter. The function of the correlator is to produce the discrete visibility function samples for the numerous antenna separations. An explanation of the correlator's operation verification is given as well as complete details of problems that emerged during the complex correlator's design and development.

4.1 Correlator Layout

This section discusses the methodology, electrical design and physical layout used to create the complex visibility function samples. The correlator design is unique and will be compared with prior methods done for signal correlation.

4.1.1 Complex Correlator

The complex correlator block diagram that produces the visibility function samples in the interferometer is shown in Figure 4.1. All connections between transmission lines and the components are 50 Ω SMA coaxial. Transmission lines connecting the components were built using semi-rigid coaxial cable. To avoid any confusion in the following section, the stationary radiometer will be referred to as RX-1 and the mobile radiometer as RX-2. The signal from RX-1 is introduced to a XMC3000-1000 bandpass filter. The filter has a center frequency of 3 GHz and a passband of ±.5 GHz. The signal is then fed through two stages of amplification. The first amplifier is a ZX60-5916M high isolation amplifier, with 17 dB of gain at 3 GHz. The second

amplifier provides an additional 24 dB of gain through a high-power amplifier, model AML26P2403. The signal from RX-2 is introduced to a XMC3000-1000 bandpass filter and a ZX60-5916M amplifier, having the same performance as the ones used for RX-1 signal. Following the stage of amplification, the RX-2 signal is mixed with a 1.2 GHz LO signal. The J2080HB mixer has typical conversion loss of 6.5 dB to the signal. The upconverted 4.2 GHz output is the desired component and is preserved with a XMC4200-1000 bandpass filter, centered at 4.2 GHz with a $\pm.5$ GHz passband. A stage of amplification follows, using a ZX60-6013E broadband amplifier with 13 dB of gain.

At this point, both RX-1 and RX-2 signals are introduced to a wideband mixer J2080LB. The direct signal multiplication in the wideband mixer correlates the RX-1 and RX-2 signals. Conversion loss in the mixer is 6.5 dB. The 3 GHz RX-1 signal acts as the driving LO signal and the 4.2 GHz RX-2 signal represents the RF signal. The desired downconverted, correlated IF signal is centered at 1.2 GHz, while the remaining harmonic terms need to be rejected. A stage of amplification and filtering at the IF frequency follow the correlating stage. A ZX60-6013E amplifier provides 16 dB of gain across the IF output. The unwanted harmonic terms are suppressed by a XMC1200-1000 bandpass filter. This bandpass filter has a $\pm.5$ GHz passband at the 1.2 GHz center frequency. The correlation of the two signals requires a final stage of demodulation to extract the complex terms of the visibility sample. A QD0717X quadrature demodulator extracts the in-phase and quadrature components of the correlated signal. The demodulator divides the 1.2 GHz correlated signal and multiplies the signals by 1.2 GHz LO signals that are 0° and 90° out of phase, respectively. The demodulated in-phase and quadrature outputs are each baseband signals up to 500 MHz.

The 1.2 GHz local oscillator signal is derived from a ZX95-1600W voltage controlled oscillator. The power output of the oscillator at 1.2 GHz is 9 dBm or better.

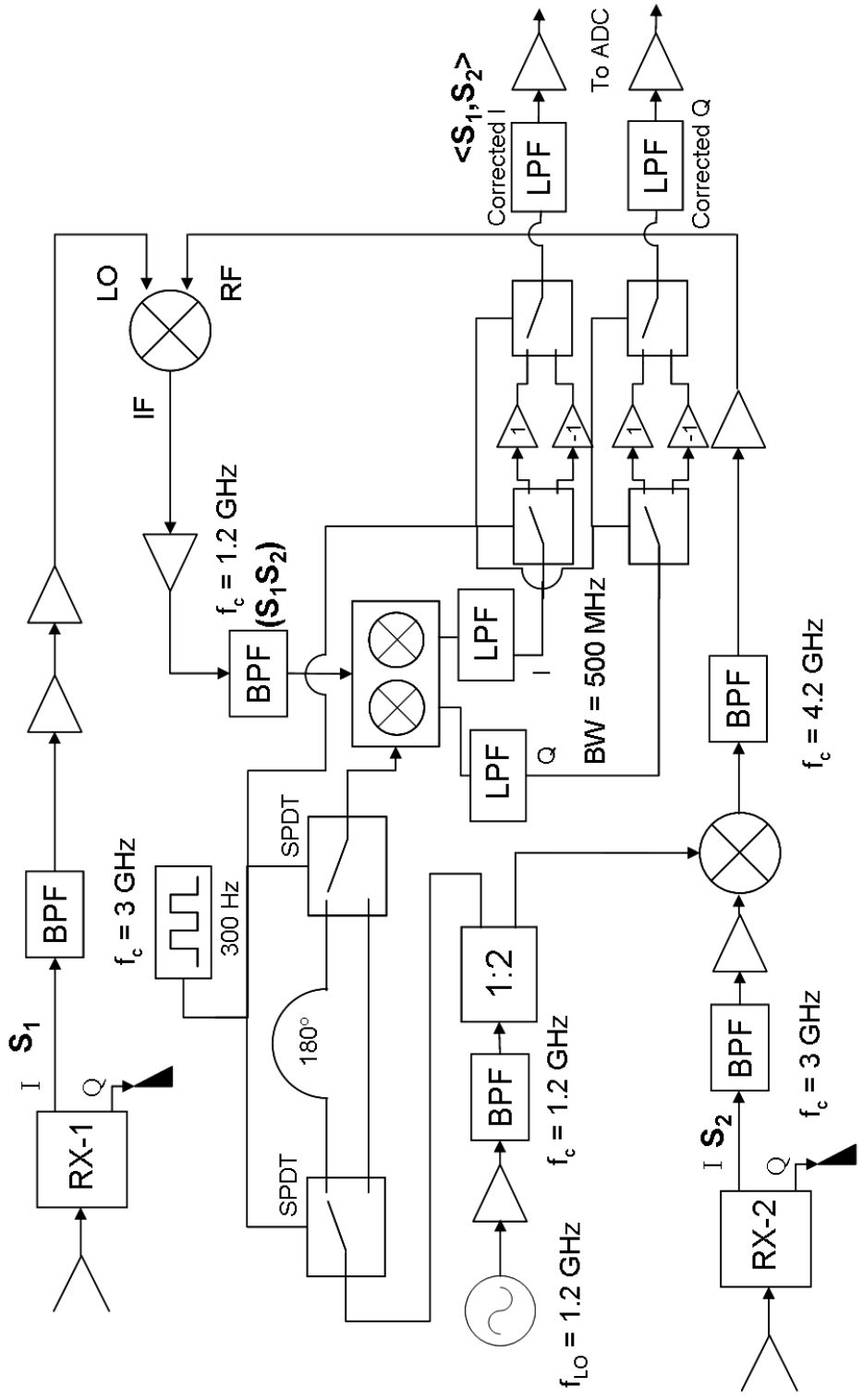

Figure 4.1. Complex correlator block diagram

A ZX60-4016E amplifier increases the power output to almost 18 dBm, in order to drive the J2080HB mixer's power specification. After the signal amplification the LO is introduced to a 1.2 GHz bandpass filter to remove higher frequency LO harmonics that were amplified in the process. The LO signal is introduced to a power divider; model ZN2PD2-50. The power divider has 3.7 dB of insertion loss across both channels. One signal is sent to the J2080HB mixer to upconvert the RX-2 signal to 4.2 GHz. The second signal is fed to a SPDT pin diode switch that switches between 2 output ports by a 300 Hz clock. The ZMSW-1211 by Mini Circuits has 1.3 dB of insertion loss during the ON state and 30 dB of isolation during the OFF state for both channels. Depending on the switches state, the LO signal is directed to one of two paths that are 180° out of phase with each other. The signal is output to another SPDT switch alternating at the same 300 Hz clock rate. The output of this switching circuit is a 1.2 GHz LO whose phase shifts by 180° at a rate of 300 Hz. The purpose of the LO phase-shifting is to remove any DC bias introduced in the quadrature demodulator and will be explained in greater detail in the following paragraphs. This modulated 1.2 GHz LO is introduced to the quadrature demodulator's LO port. The microwave component layout inside the correlator is shown in Figure 4.2.

After the signal demodulation, the in-phase and quadrature components enter a circuit board containing the circuitry to demodulate the 300 Hz prior to the analog to digital conversion. The printed circuit board is constructed on an 3.1 inch × 5.8 inch, GML 1000 copper clad, high frequency laminate. Traces are only featured on a single side, using 1 ounce copper. The top side layout of the printed circuit board, featuring all electronic parts, is shown in Figure 4.3. The bottom side of the printed circuit board contains all copper traces and is shown in Figure 4.4. Unmarked components are wire connections to traces. Resistor and capacitor values are in Table 4.1. The circuit board inputs are the in-phase and quadrature components, +5V, - 5 V and +2

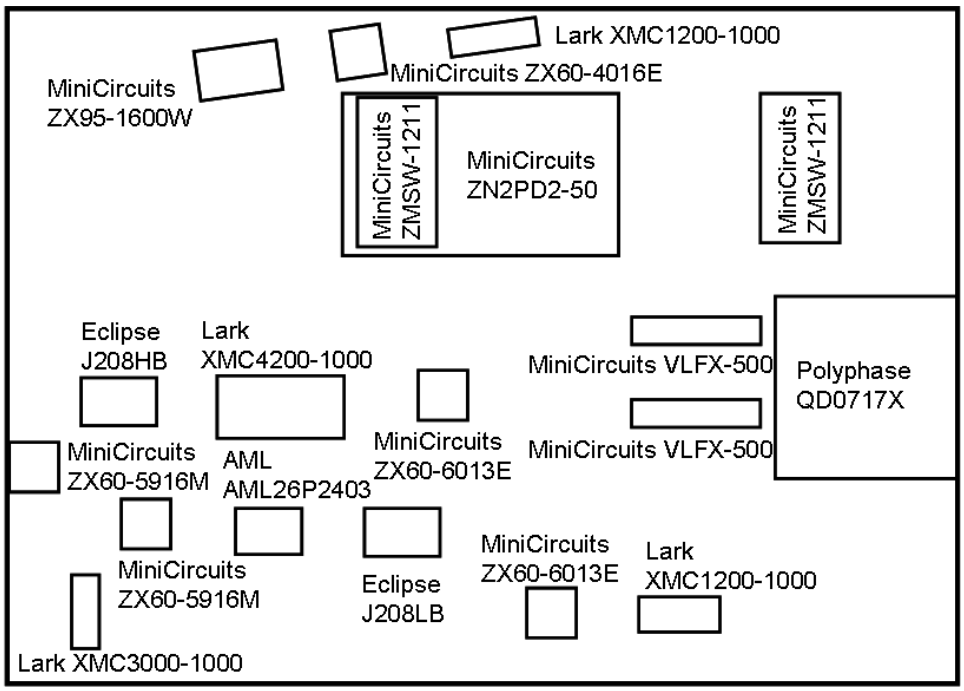

Figure 4.2. Microwave component layout of complex correlator

V DC, two clock lines and analog ground. A block diagram for the following signal processes is shown in Figure 4.5 and schematic for it is shown in Figure 4.6.

Each in-phase and quadrature signal is input into a SPDT switch. Switching occurs at 300 Hz and depending on the TTL logic state, will switch between 1 and -1. Both unity and inverted gains are produced with a single LMH6609 operational amplifier. The output from this switch demodulates the 300 Hz modulated in-phase and quadrature components, but modulates by 300 Hz any DC bias offsets introduced by the quadrature demodulator.

A passive low pass filter follows the switching stage and accomplishes the signal integration of the complex correlated signals and removes any 300 Hz modulated DC bias from the previous stage. The low pass filter has an integration time τ determined by the system noise floor. The the integration time is set by the RC time constant

$$\tau = RC \tag{4.1}$$

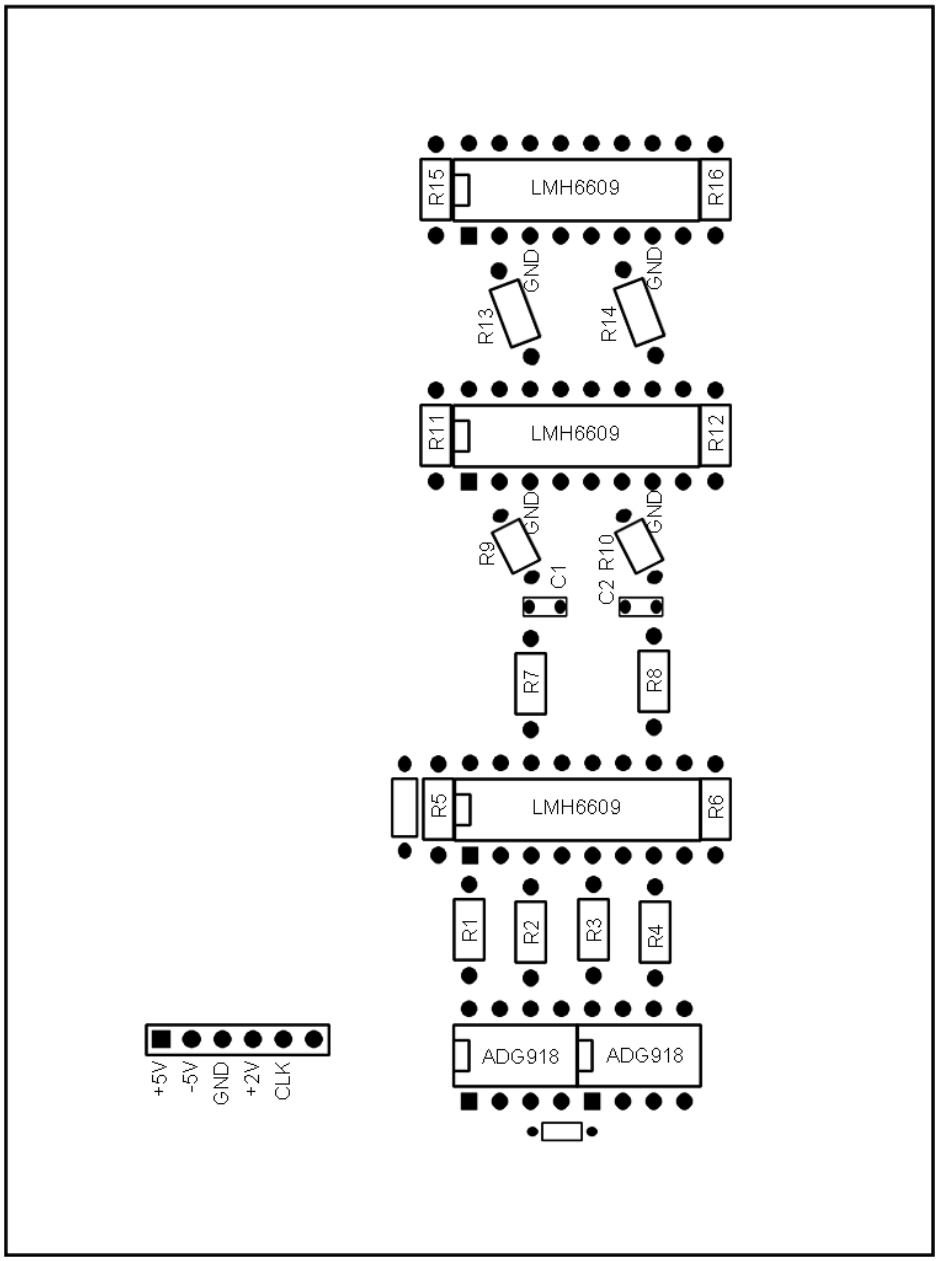

Figure 4.3. Demodulator circuit board top side layout

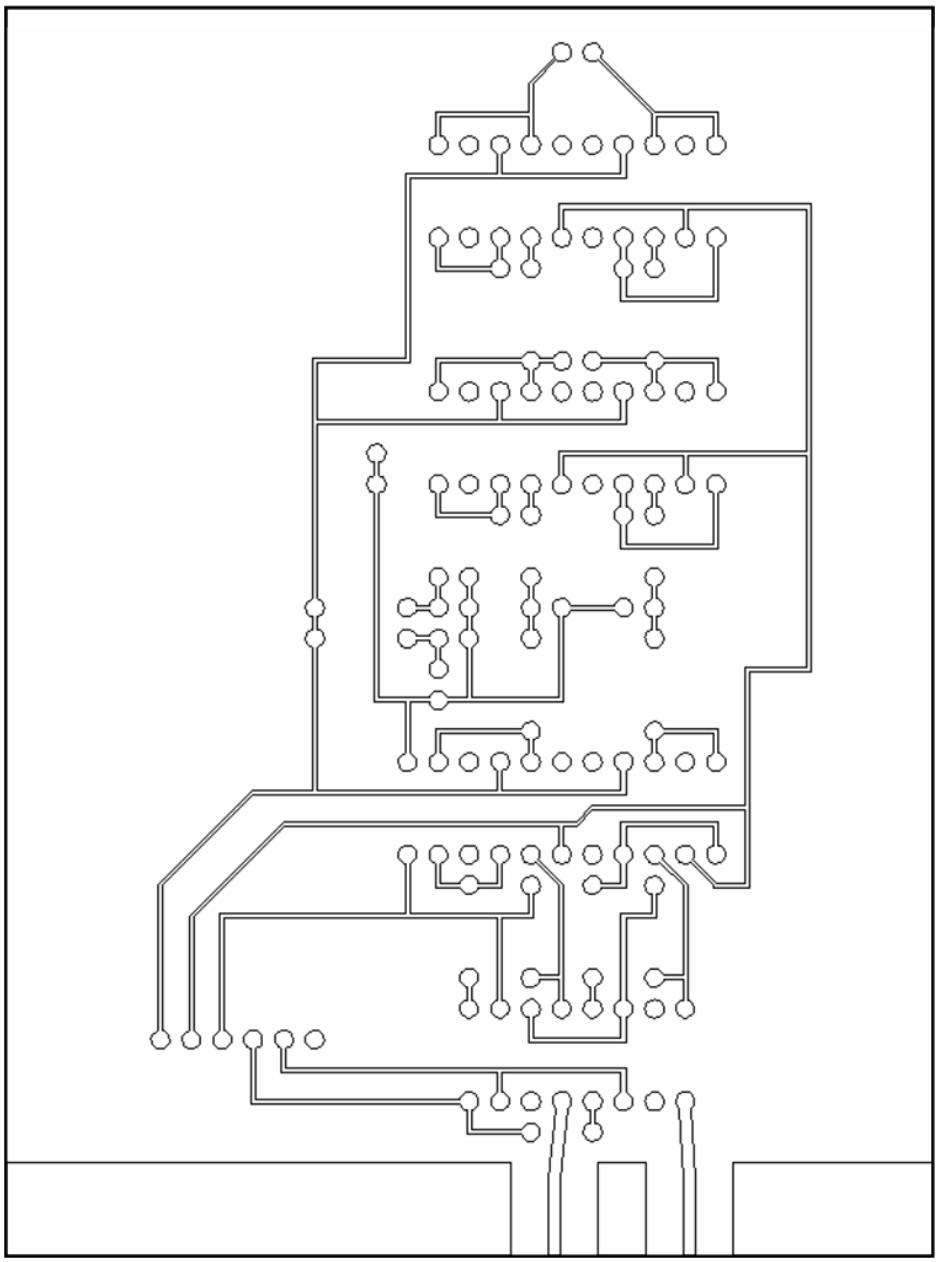

Figure 4.4. Demodulator circuit board bottom side layout

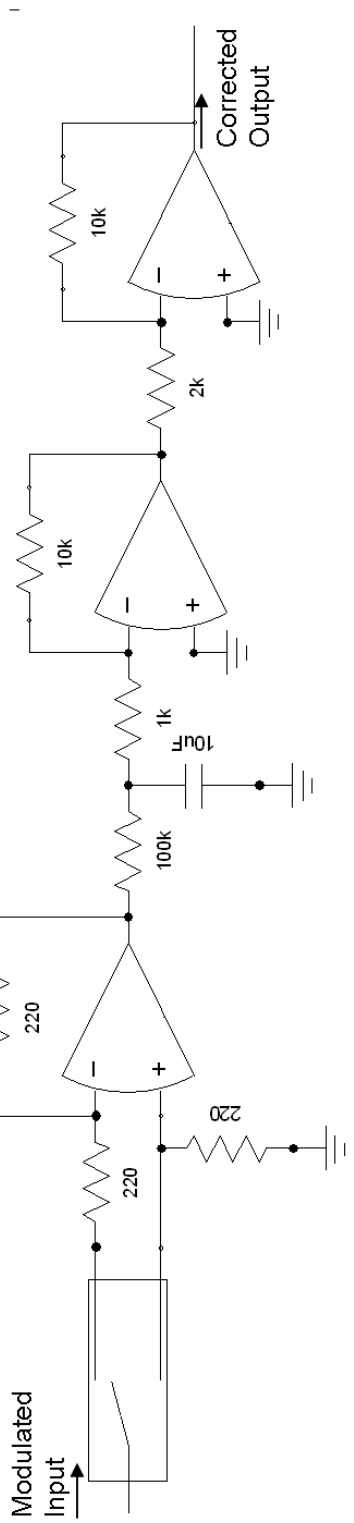

Figure 4.5. Demodulator circuit board block diagram for a single complex correlated component

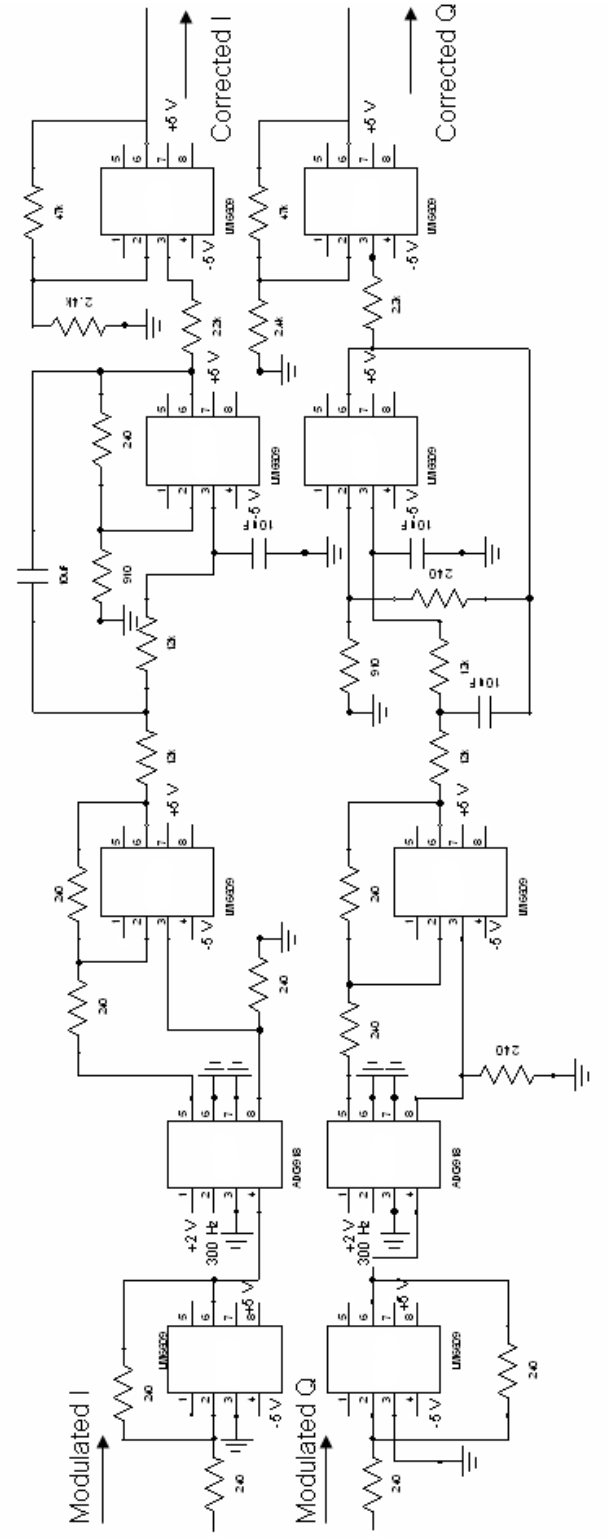

Figure 4.6. Demodulated circuit board schematic

Table 4.1. Demodulator circuit board resistor and capacitor values

Resistors Ω	Capacitors μF
R1 = 220	C1 = 10
R2 = 220	C2 = 10
R3 = 220	
R4 = 220	
R5 = 220	
R6 = 220	
R7 = 100 k	
R8 = 100 k	
R9 = 1 k	
R10 = 1 k	
R11 = 10 k	
R12 = 10 k	
R13 = 2 k	
R14 = 2 k	
R15 = 10 k	
R16 = 10 k	

With

R = 100 kΩ

C = 10 μF

A stage of amplification follows to amplify the in-phase and quadrature signals to within a -1 V to +1 V range. The gain of this stage is

$$G = -\frac{R_2}{R_1} = -10 = 10dB \tag{4.2}$$

With

R_1 = 1 kΩ

R_2 = 10 kΩ

If a DC bias exists at the outputs, they can be removed through a offset voltage input into the positive amplifier node. Traces for biasing circuit are shown in Figure

4.4. After this amplifier stage the signal can be read by the A/D converter or amplified further with a second stage of amplification. The second amplifier stage amplifies the in-phase and quadrature signals to within a -5 V to +5 V range. The gain of the stage is

$$G = -\frac{R_2}{R_1} = -5 = 7dB \tag{4.3}$$

With

$R_1 = 2$ kΩ

$R_2 = 10$ kΩ

The output levels at this stage can be introduced to the to the analog to digital converter, which is discussed in the next chapter. It should be noted that each LMH6609 depicted Figure 4.3 is two 8-pin LMH6609 chips, SOIC packaged, connected to a 16-pin SOIC to DIP adapter. The 8-pin ADG918 is MSOP packaged and connected to a 8-pin MSOP to DIP adapter. Further details of the parts used in the correlator including diagrams and specifications are given in Appendix B. The component layout of the correlator is found in Appendix B as well.

4.1.2 Signal Correlation

The unique aspect of this complex correlator is how the use of a mixer to correlate the two received signals. Previous complex correlator designs created have used a power combiner and Schotkky diode to produce the signal correlation. A simplified implementation is shown in Figure 4.7. The correlated signal is derived from the square-law properties of the Schotkky diode. The correlation of the two signals is centered at the difference frequency of the two input signals. The following quadrature demodulator produces the complex components at baseband, with the final stage of integration before being sampled by an A/D converter.

The initial approach for the complex correlator was to implement this method using prepackaged power combiner and Schotkky diode. However, all prepackaged Schotkky diodes considered for the design featured a capacitance at the output that removed the desired correlated signal at 1.2 GHz. Rather than custom order a suitable Schotkky diode, wideband mixers were readily available and were instead used for producing the correlation of the two signals.

4.2 Correlator Testing

Testing of the correlator was done to verify the system's performance under a set of test cases. All test measurements were done at the passive RC low pass outputs, as amplifier gains were not set at that time. Correction of the signal gain differences was done in software. The first test done was a phase test to verify the correlator's ability to measure the input phase changes. A 3 GHz narrowband signal was placed through a 2:1 power divider with each correlator input channel receiving the signal. A variable phase shifter was placed at the input of the Receiver 2 channel. The path length for Receiver 2's signal was extended for 10 unique points and measured, the results for this test are shown in Figure 4.8. The phase shifter introduces magnitude loss in the Receiver 2 channel, resulting in a spiraling of the in-phase and quadrature output voltage levels. The any gain differences not corrected for in the software also contributed in creating an elliptical rather than circular shape in the I and Q plot.

The second test done on the complex correlator was to measure the linearity of the system between the correlator's input and output channels. The same setup used in the phase test was used, however the phase shifter used in the Receiver 2 channel was removed. Varying power levels from -30 to -20 dBm were introduced through the two channels. The results for the real and imaginary components of the visibility samples are shown in Figure 4.9. The output data remains linear until around -24 dBm (0.004 mW), where the output power begins to level off. This should be expected as the

amplified 3 GHz LO signal is inputting a power large enough that the mixer loses its linearity output characteristics.

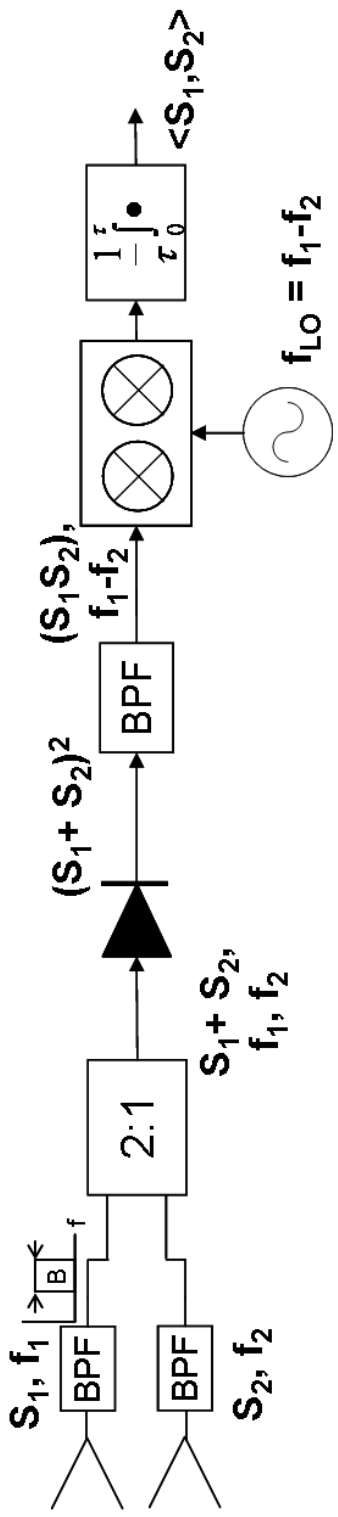

Figure 4.7. Basic complex correlator using a power combiner and diode detector

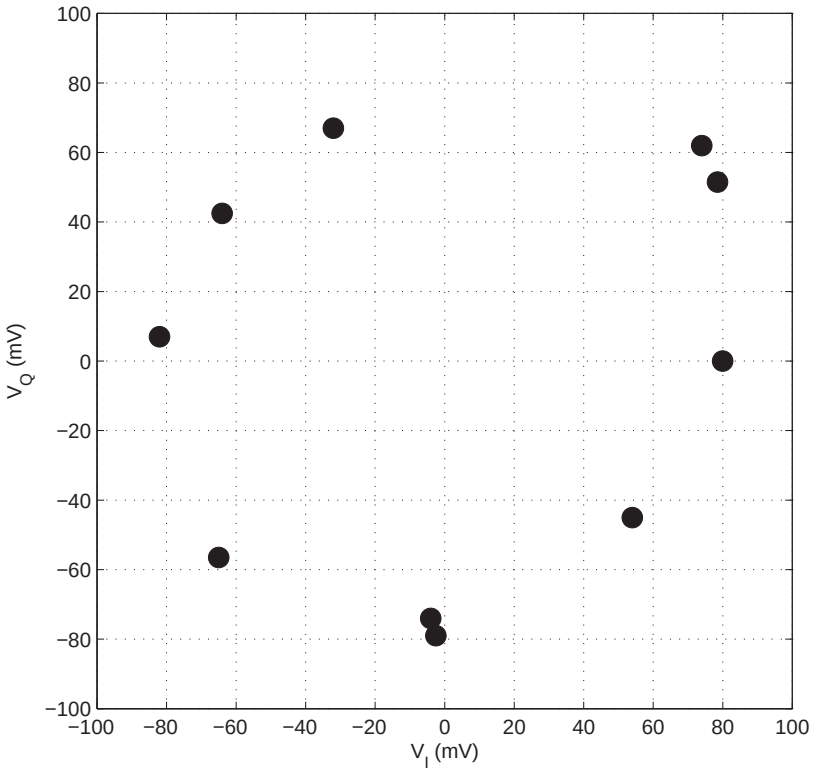

Figure 4.8. In-phase and quadrature circle of correlator for varying phase lengths

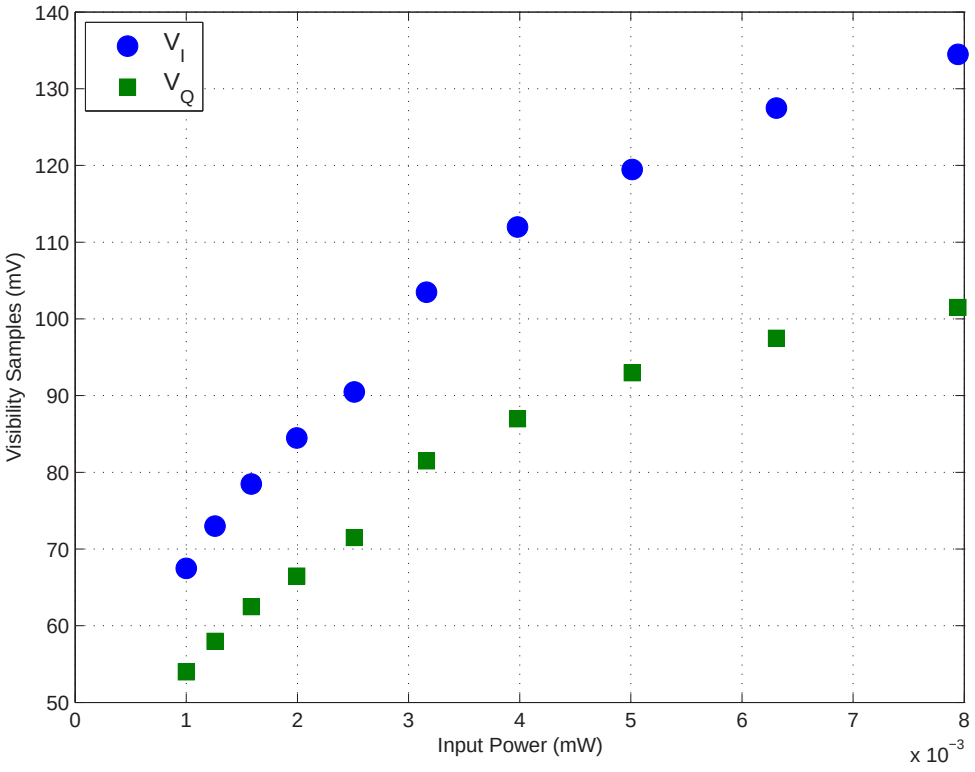

Figure 4.9. Input vs. output linearity perfomance of correlator

CHAPTER 5

DATA ACQUISITION AND IMAGE RECONSTRUCTION

This chapter details the acquisition of the visibility sample data through A/D conversion. Acquiring visibility sample data required software integration of the linear drive and data acquisition hardware. A custom runtime application was programmed to enact the step-measurement procedure on the host computer. Post-processing code was created for reconstructing the brightness image of stationary scenes as discussed in Chapter 2. Image focusing was also incorporated to account for measurements taken within the antenna array's near-field region.

5.1 Data Acquisition

Acquisition of the DC visibility function samples is done using a Dataq DI-148U-SP A/D converter. The DI-148U-SP features 10-bit sampling resolution and an adjustable sampling rate that is controlled through the host computer. Throughput ranges can be as large as 14,400 Hz and can be as small as sub-hertz. The integration time of low pass filter stage τ determines the minimum sample rate of the A/D converter. For the low pass filter's 1 second integration time, a minimum 2 samples/sec or better is required. The A/D receives the correlated inputs through separate screw-terminals. The A/D converter has four sampling input channels and 6 digital I/O screw terminals. Two input channels are string pot channels that are left unused. The two remaining channels 3 and 4 receive the in-phase and quadrature components, respectively. Channel-to-channel crosstalk rejection is -60 dB and the

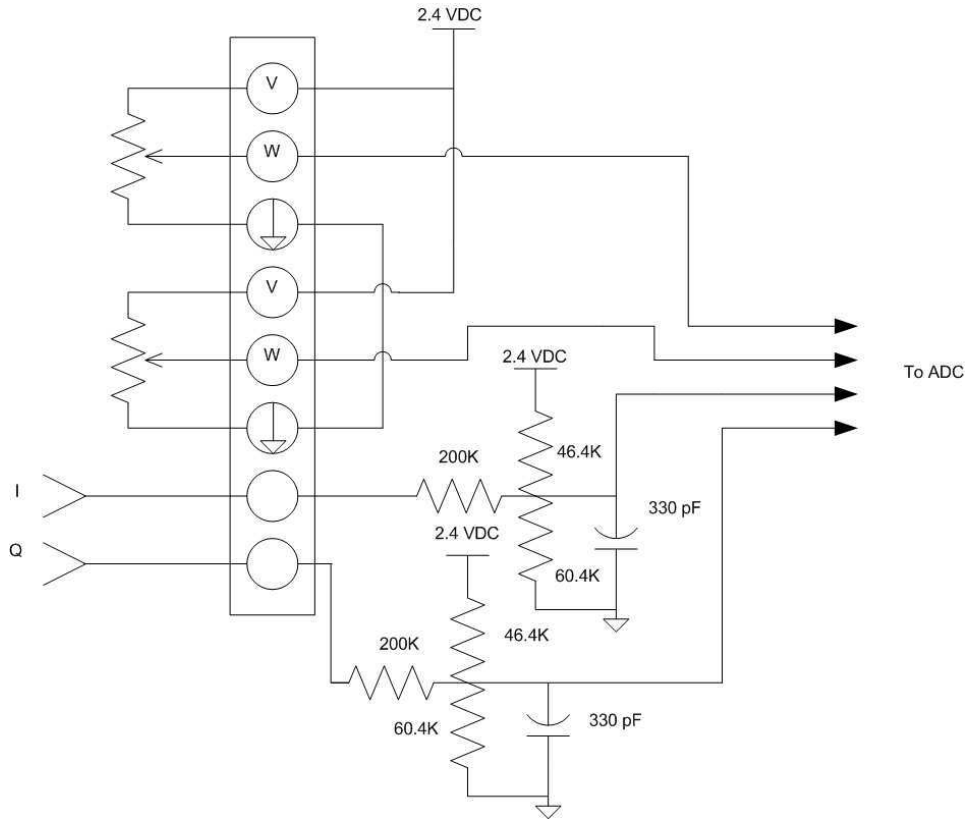

Figure 5.1. Input diagram of DI-148U-SP A/D converter

maximum voltage input into each channel is ± 10 V. The signal input diagram of the DI-148U-SP before entering the A/D converter is shown in Figure 5.1.

The A/D converter samples each signal and stores the data in a sample buffer. The maximum amount of sampled data that can be stored in the buffer is 2 kilobytes. Command lines programmed by the user set the sample rate and buffer read conditions. When the data stored in the sample buffer has accumulated the user-defined amount, the buffer data is sent to the local computer where it is written to a data file.

The A/D converter is packaged in a 2.6 inch × 2.6 inch × 1.1 inch casing that is itself placed in the correlator enclosure described in Chapter 6. The I and Q outputs from the complex correlator are wired to the screw terminal inputs. The A/D

converter contributes a DC bias to the measured visibility samples, approximately 0.4 V. This bias is removed as best as possible in the calibration section described in the following section. Power is supplied to the DI-148U-SP from the local computer through its USB interface. The sampled visibility function is transmitted to the local computer through this USB interface also.

5.2 Measurement Software

The Parker 6K2, mentioned in Chapter 3, and the Dataq A/D converter both offer their own individual software programs for conducting their respective tasks. The integration of both products' capabilities was done by creating a Visual Basic application to command both pieces of hardware together. The 6K2's Communication Server executes tasks to the linear drives commanded in this Visual Basic application. The third-party shareware software recommended by Dataq, UltimaSerial ActiveX, is used for controlling the A/D converter commands executed in the application. The code created to control both pieces of hardware can be found in Appendix E.

The software application requires the user to calibrate the linear drives before starting any a measurement process. The linear drives travel to both of their positive and negative end-of-travel limits, whereby the program determines the midpoint and origin positions for all measurement processes. The origin position is located at the 2 meter drive's midpoint and the 1 meter drive's positive end-of-travel limit. The linear drives relocate to this origin position. During calibration, 50 Ω matched loads should be placed on each correlator input channel so that the DC bias produced by the A/D converter can be sampled and averaged out of the measurements during post-processing. Upon completion of the linear drive calibration, measurement of the visibility function can begin.

The movement procedure for a 2-D measurement scan is illustrated for a 5×5, 25 element measurement process is shown in Figure 5.2. When starting a measurement

process, the two antennas should be placed directly next to each other. The first movement shifts the mobile radiometer to the negative Y end of the scanning area and stops for a measurement. The antenna dwells long enough to satisfy the integration time τ for collecting the appropriate amount of samples. The radiometer moves a half-wavelength step down, stops and collects data. This step is repeated until the radiometer hits the maximum D_x antenna separation. When the radiometer has reached the maximum D_x separation designated by the user, the antenna shifts a half-wavelength over and returns to the top of the linear drive. Having the carriage return to the positiveend-of-travel limit is done to minimize error accumulation in the X-axis. When the antenna has completed this movement it stops to take a measurement. The antenna then steps down a half-wavelength and stops to collect data. The antenna repeats those two basic motion profiles until it has reached the positive end of the scanning area and the maximum D_x antenna separation. A final data sample is collected, at which point the antenna returns to its initial position.

Before the antenna moves on to a new measurement position, the following data is added to the final data output file: (1) the commanded movement position, (2) any movement error incurred in both directions, (3) the averaged complex visibility sample at that position, (4) and the standard deviation in the complex visibility sample. The output data sequence for a single measurement location is given below:

$$\mathrm{y,x,y}_{error},\mathrm{x}_{error},\mathrm{V}_i\mathrm{(x,y)},\mathrm{V}_q\mathrm{(x,y)},\mathrm{V}_{iDev}\mathrm{(x,y)},\mathrm{V}_{qDev}\mathrm{(x,y)}$$

The final output file also contains the linear drive calibration data.

Handshaking between the different software platforms was attempted, but is not operational yet in the current implementation. The purpose of the the handshaking is to resolve a timing issue with the 6K2 Communication Server. When a command is sent to the 6K2, the program does not wait for the 6K2's response, instead it executes the remaining lines of code. A generic delay subroutine was written to prevent the program from executing lines of code before a 6K2 command had been completed.

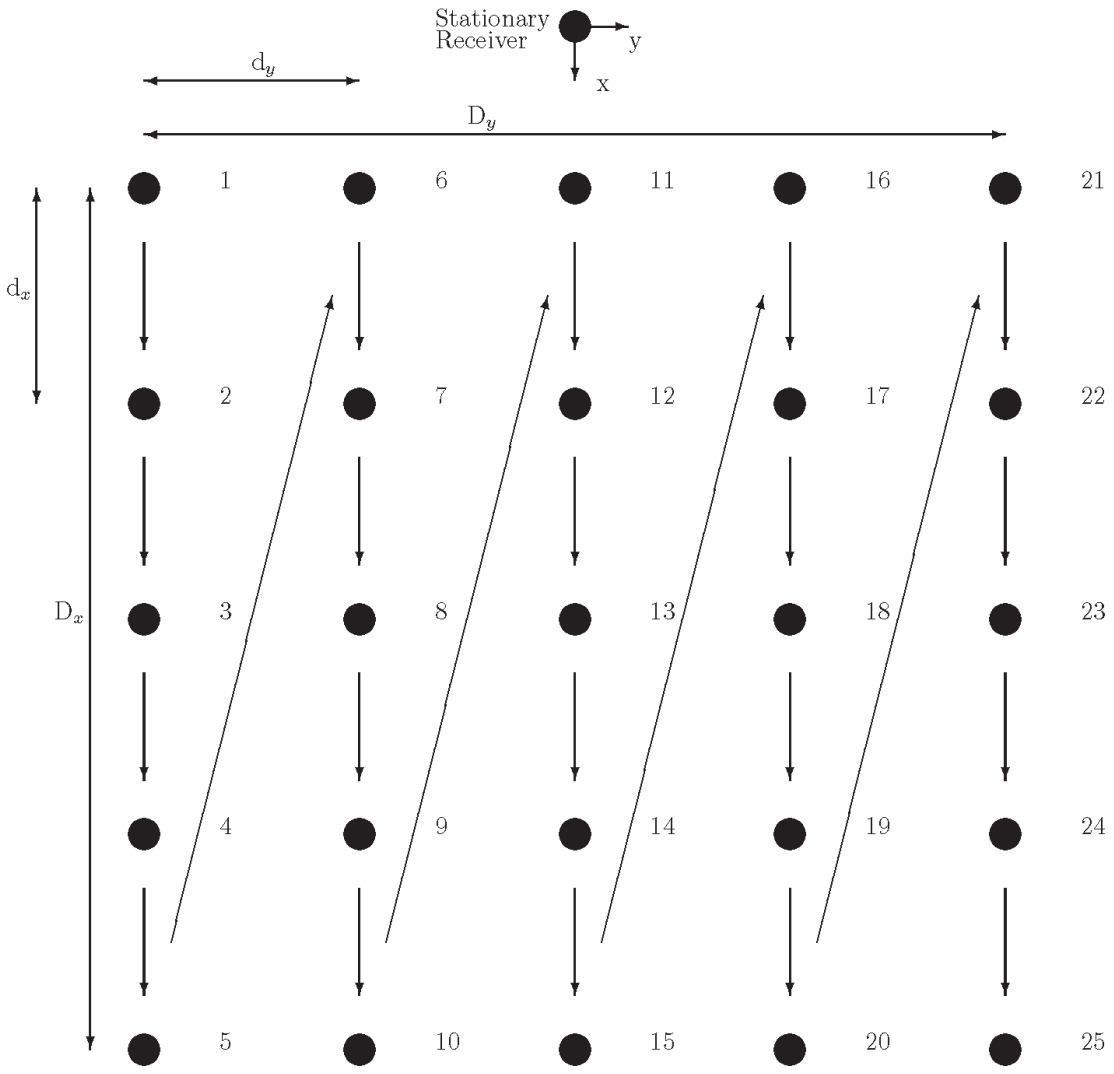

Figure 5.2. Sample radiometer movement path for a 5×5, 25 element measurement scan

For movement commands, the delay time before moving on to the next program line is determined by the equation

$$t_{delay} = 2\frac{D}{V} + 8\frac{V}{A} \tag{5.1}$$

With

D is the programmed distance

V is the programmed velocity rate

A is the programmed acceleration rate

This equation is based on modified equations given in the 6K2 manual for calculating time required for a movement profile. Those equations account for acceleration, average acceleration and jerk rates. The modification of the manual's equations was due to the fact that the equations given did not provide enough delay for tested movement profiles to complete and therefore had to be extended. For slower moevement rates, this time delay is longer than necessary, however for faster movement rates this time delay is required.

5.3 Reconstruction Formulation

The data file containing the measured data for each discrete position is uploaded into a Matlab code for image reconstruction. The Matlab code implements the reconstruction formulation theory given in Chapter 2, applying the Fourier transform for image reproduction.

The code takes into account focusing of the data when measurements are done in the near-field. When working with a large synthesized array, the large aperture and small wavelength result in a large near-field. A 1 meter synthesized array aperture will be in the near field up to 625 meters away. Near-field measurements have an additional quadratic phase component that must be corrected in the reconstruction

formulation. The discrete visibility function sample is multiplied by the weighting function:

$$W(h,u,v) = e^{j\pi\frac{\lambda}{h}(u^2+v^2)} \tag{5.2}$$

With

$u = \frac{D_x}{\lambda}$

$v = \frac{D_y}{\lambda}$

Substituting this modified visibility function into Equation 2.6 given in Chapter 2 results in the modified brightness temperature equation:

$$T(x,y) \cong \frac{c}{\pi}\sum_{m=1}^{M}\sum_{n=1}^{N} V_{mn} e^{-j\pi\theta_B\frac{d}{\lambda}(mx+ny)} e^{j\pi\frac{d^2}{\lambda h}(m^2+n^2)} \tag{5.3}$$

The user must select the correct focusing distance h to produce the resolved image.

Though the distance and visibility measurement errors are not used in recreating the image, they are provided in the data file as supplemental information should the user have need for them. In the case that a reconstructed image is poor, the user might find that there was a great deal of signal or position variation during the measurement process. There are optional lines of code included to remove any additional DC offsets in the data that might still persist.

CHAPTER 6

GENERAL ELECTRONICS AND PACKAGING

The power supply for the two radiometers and noise source was constructed by Millitech. The block diagram for this power supply is shown in Figure 6.1. The DC voltages for the supply are all derived from 120 VAC at 60 Hz. A fan is attached to the back of the system and operates from the 120 VAC signal. The power supply features a main power switch and three secondary switches that are found within the system. DC voltages of +12, -12, +15 and individual grounds are produced from three separate AC/DC power supplies. The 120 VAC input is connected to a dual-fuse, IEC inlet filter which features a DPDT switch for turning on the power supplies. The +12, -12 and +15 VDC power supplies each contain the appropriate fuse before being introduced to the main terminal strip. The 6 signal lines are connected to 3 Cannon 7-pin circular connector lines. Each line provides power to either radiometers or the noise source. The pin outputs for the voltage supplies are identified in Appendix A.

The 6K2 controller requires a 24 VDC, +/-10%, 1 Amp supply for proper operation. A 24 VDC SOLA power supply is used to provide power for the 6K2 and sensor circuits. The power supply is powered by a 120 VAC signal and has auto-select capabilities if the supply source is either 120/230 VAC. The supply provides a maximum 2.4 A of current to the devices and has drive shutdown capabilities if overdriven. The power supply also features a tunable knob that can be adjusted to provide a voltage output between the ranges of 24 to 28 VDC. The positive terminal of the power supply is connected to the 24 VDC terminal on the 6K2 and the negative

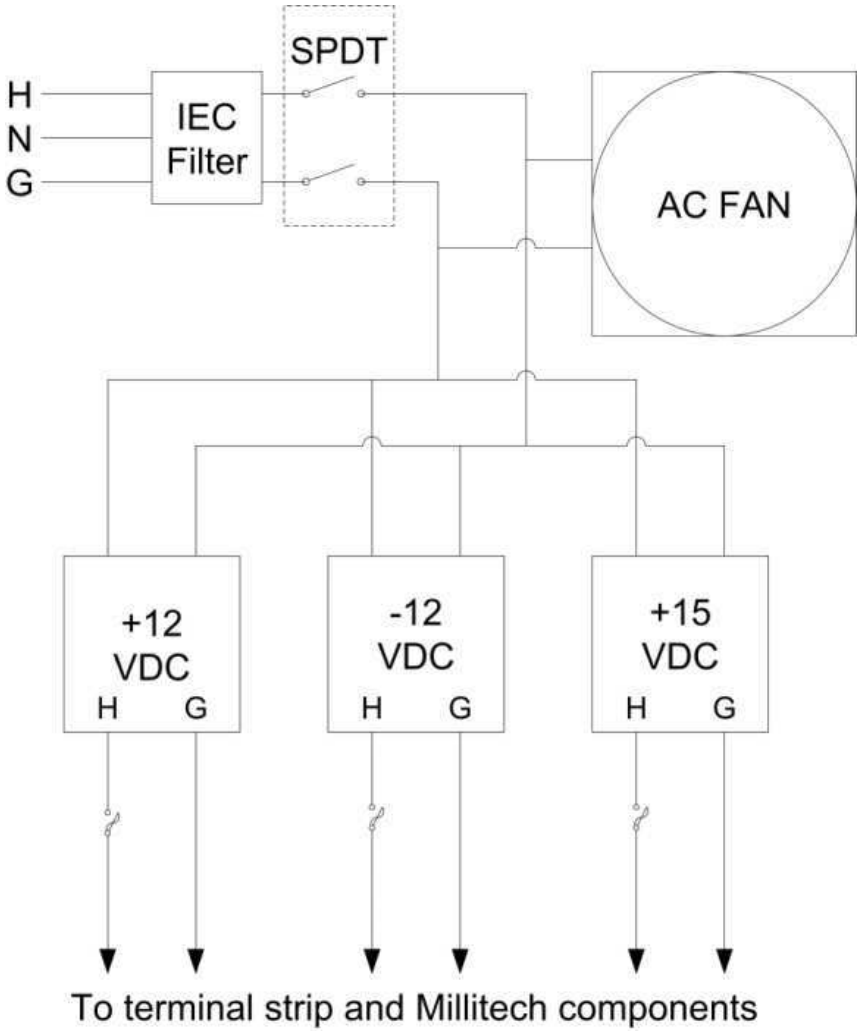

Figure 6.1. Millitech power supply

terminal is connected to the 24 VDC Return terminal on the 6K2. Power supply and additional terminal wiring connections on the 6K2 controller are found in Appendix B. To provide power to the individual limit sensors a 1.78 inch $\times$ 1.78 inch printed circuit board was fabricated in house for the six sensor cables. The layout of the printed circuit board is shown in Appendix B. The trigger lines for the sensors on Axis 2 were connected to a VM25 screw-terminal I/O component. The VM25 has 25-pin connectors and a 2 foot cable to connect to the LIMITS/HOME connector on the 6K2. A diagram of the VM25 and pin out connection is available in Appendix B.

The Gemini Digital Servo Drives support both 120 and 240 VAC power supplies. The Gemini drives are connected to 3-terminal AC input cables operating at 120 VAC. The drives feature no internal fuses, so 30 A fuses for both 120 VAC input lines are connected to the input prior to the Gemini's power terminals. The Gemini drives feature short circuit protection, high inrush current protection, over- and under-voltage protection and drive and motor over-temperature protection. Any of these cases will cut power to the Gemini drives and a LED on the drive will be activated red. The power supply wiring for the Gemini drives is found in Appendix B.

A diagram of the power supply built for the complex correlator electronics is shown in Figure 6.2. A single, 120 VAC input is used to produce output voltages of +5, -5, +2, +12 and +15 VDC, along with an adjustable voltage to control the voltage controlled oscillator in the correlator. The power supply also contains the 300 Hz signal circuitry used in the correlated signal demodulation. A circuit schematic for producing the 300 Hz signal is shown in Figure 6.3. The 120 VAC signal is attached to a line filter and DPST switch. The earth ground line is connected to the inside of the chassis. The input AC signal is connected to an AC fan in parallel before producing the various signals.

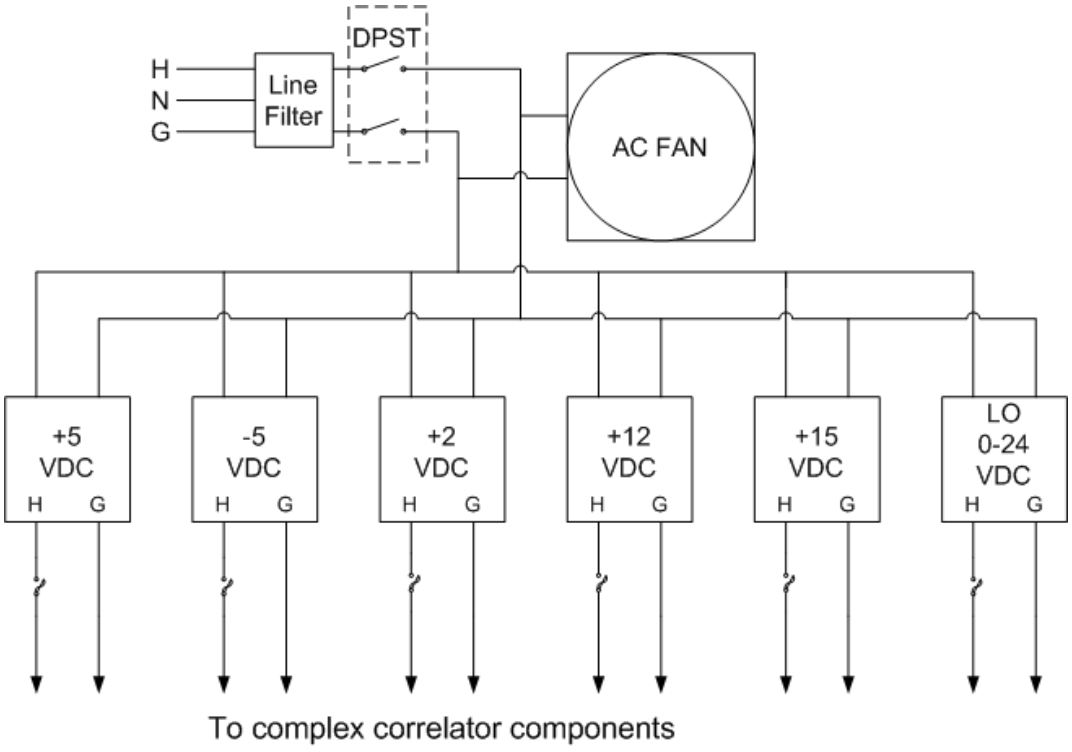

Figure 6.2. Complex correlator power supply

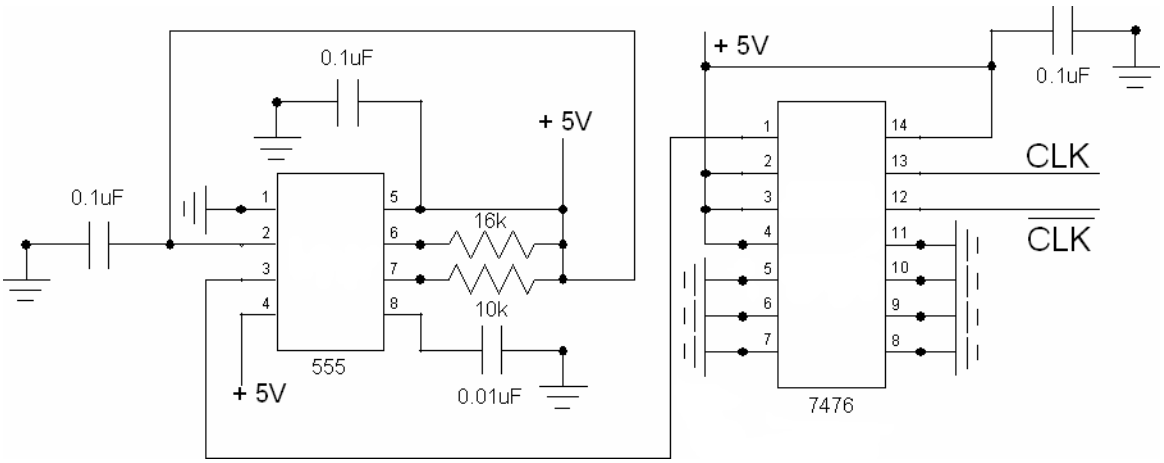

Figure 6.3. 300 Hz clock circuit for correlator demodulation

The radiometer and noise source power supply is housed in 17 inch × 13 inch rack-mounted enclosure. The component layout of the power supply is shown in Figure 6.4. The Cannon connectors, DPDT switch and AC fan are placed on the back panel of the enclosure. Each DC power supply is placed in the front end of the encasement with terminal strips for the various power inputs and outputs found in the back end.

A layout drawing of the complex correlator's packaging is shown in Figures 6.5. The entire correlator system including power supplies is contained in a 17 × 19.5 inch rack-mounted enclosure. The packaging is divided into two sections. The front end contains the analog correlator and A/D converter. The front panel has SMA connectors that are attached internally to the two correlator channel inputs. The RG402 cables carrying the measured noise signals from the radiometer are introduced at this interface. The output from the A/D converter is sent out of the back end through a USB cable and connected to the local computer. The enclosure back end contains all DC supplies and 300 Hz source for the front end electronics. All ground lines are connected to the inside chassis.

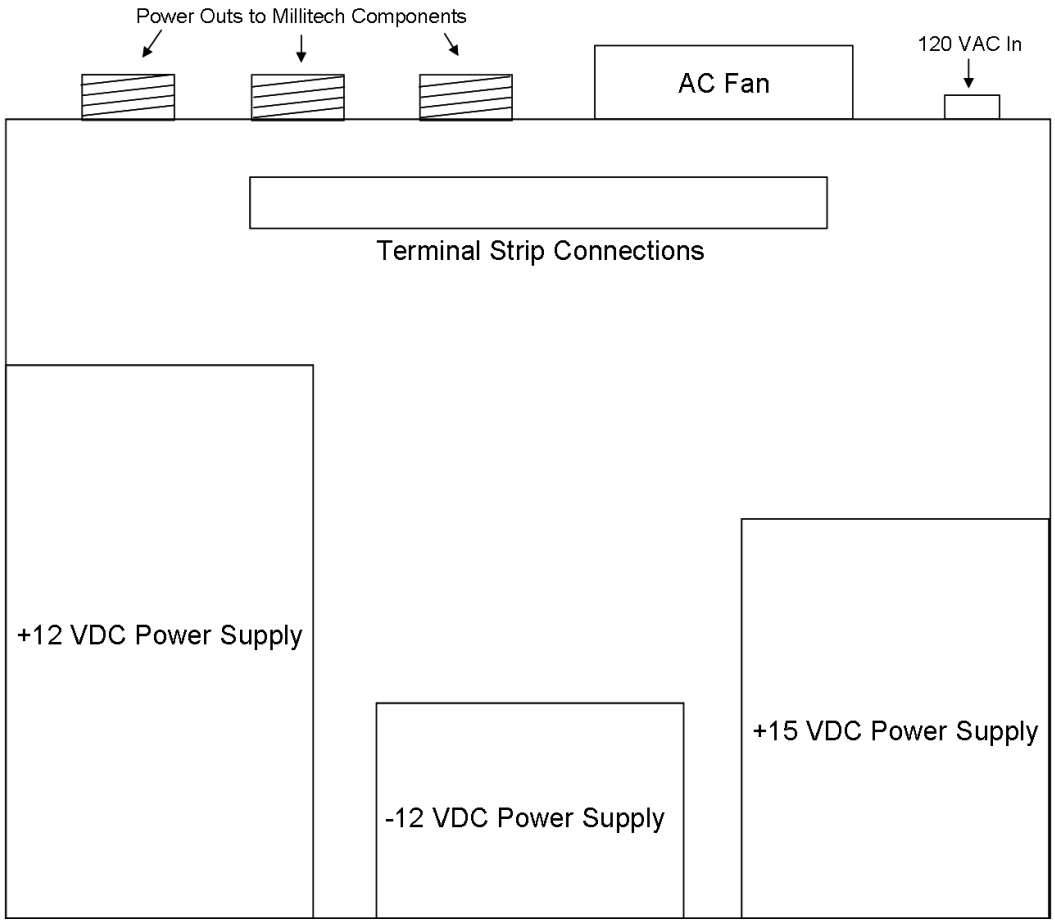

Figure 6.4. Top view enclosure layout of Millitech radiometer and noise source power supply

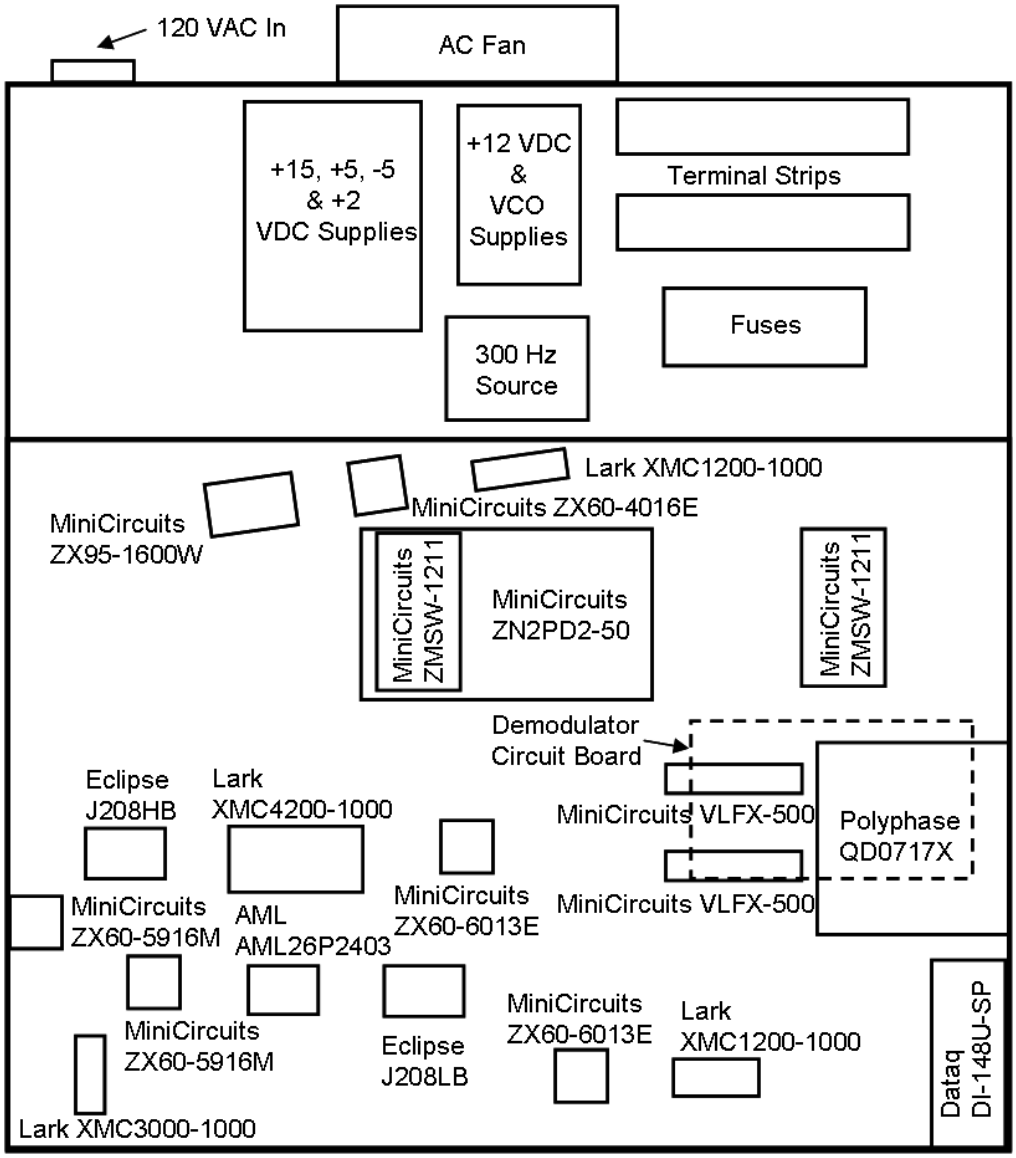

Figure 6.5. Top view enclosure layout of complex correlator and accompanying power supply

CHAPTER 7

RESULTS

Measurements were done to test the performance capabilities of the interferometer system. Narrowband measurements at 3 GHz were attempted under various conditions, the results of which will be discussed. The measurements at 3 GHz were taken using two microstrip patch antennas designed in-house that are resonant at 3 GHz. Dimensions for the patch antennas are shown in Figure 7.1. They were constructed on 31 mil Rogers 5880 Duroid, the patch and trace on 1 oz. copper and fed with a SMA end-launch connector. One patch antenna was connected to the stationary support structure and the other to the mobile support structure. The mobile patch antenna moved in discrete half-wavelength separations in the x- and y-plane across a synthesized 2 $\times$ 1 meter aperture. The entire measurement process time for this aperture size is over 2 hours. All measurements discussed were taken at the output of the passive RC low-pass filters, prior to any amplification. Output voltage levels at this stage were typically between $\pm$ 0.1 V.

An S-band pyramidal horn transmitted a 10 dBm 3 GHz narrowband signal produced by an Agilent E4437B signal generator and fed via a 1 meter RG402 cable. The horn was placed approximately 1.5 meters away from the patch antennas and placed so that the main beam was directed as close as possible at the x-axis. At this distance away, the radiating S-band horns are in the synthetic aperture's near field, so the additional focusing phase term discussed in Chapter 5 must be used in the image reproduction. The transmit horn was angled at 15 degrees so that the horn's maximum gain was directed toward the patch antennas. The horn was placed

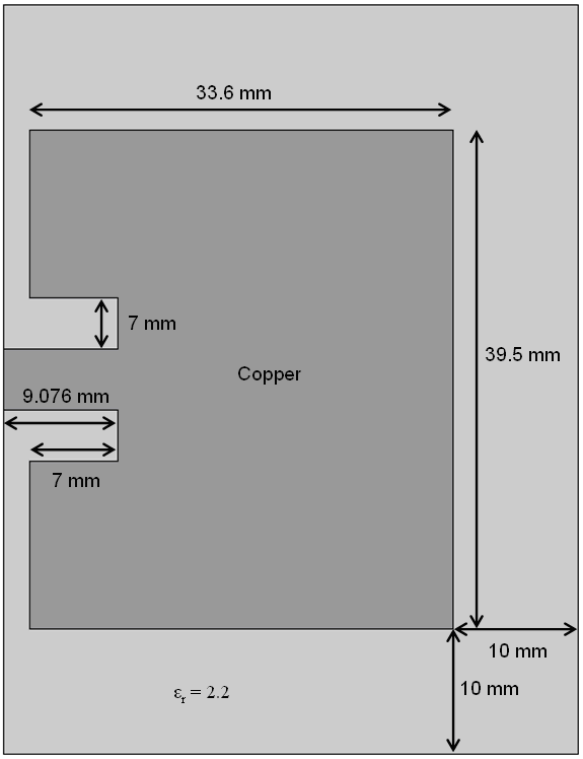

Figure 7.1. Dimensions of microstrip patch antenna used in 3 GHz narrowband correlation tests

approximately 0.2 meters below the top of the synthesized aperture. For this measurement, the synthetic aperture was 0.5×0.5 meters, resulting in a resolution of 0.3 meters. The mobile antenna was moved in discrete half-wavelength steps to fill the aperture. Under this measurement process, the S-band horns acts as a "hot-spot" in the image, as it is the only object radiating a large 3 GHz signal. The real and imaginary components of the visibility functions samples are shown in Figure 7.2 and the reproduced image is shown in Figure 7.3. The reproduced image is normalized and recognizes the strong 3 GHz signal being transmitted from the S-band horn, at approximately the correct location relative to the synthesized aperture.

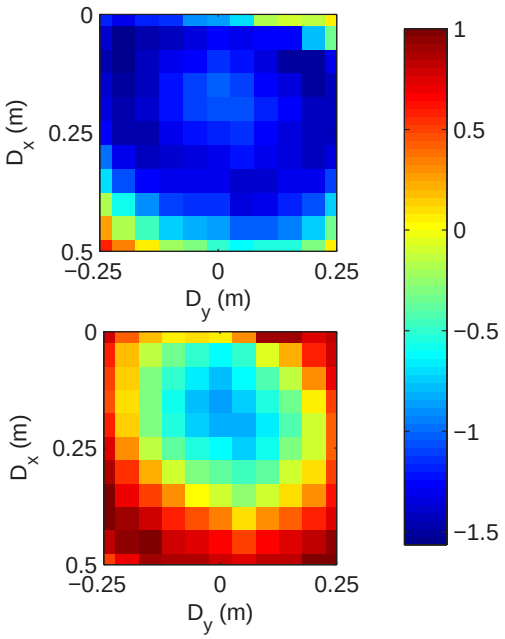

Figure 7.2. Visibility function samples (V_I top, V_Q bottom) from 0.5×0.5 meter synthetic aperture measurement with S-band horn

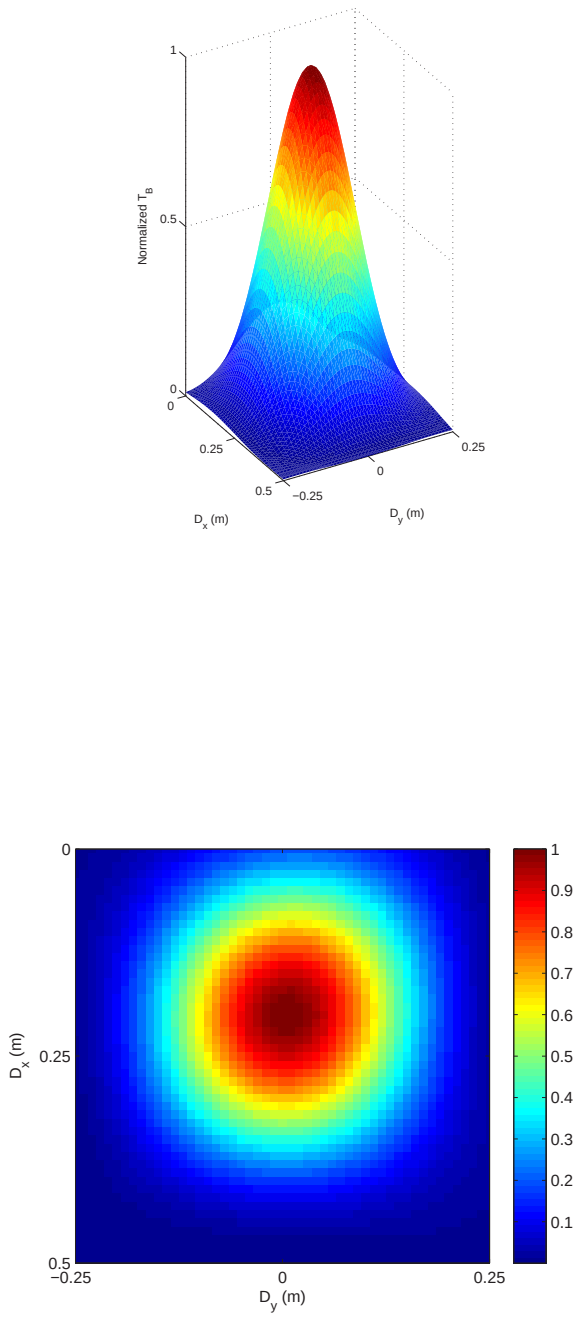

Figure 7.3. Image reconstruction of S-band horn at 3 GHz from 0.5 × 0.5 meter syntehtic aperture measurement

To test the full 2 × 1 meter synthesized aperture, two S-band pyramidal horns transmitted 3 GHz narrowband signals towards the aperture. A 10 dBm signal was evenly split through a 1:2 power divider and introduced to the antennas through 1 meter RG402 cables. The antennas were separated by approximately 1.2 meters in the horizontal and 0.5 meters in the vertical direction relative to the aperture plane. Antenna's 1 and 2 were located at approximate D_x and D_y positions (0.2, -0.6) and (0.7, 0.6) meters relative to the aperture dimensions. Both antennas were angled 15 degrees to directly face the synthetic aperture and placed a distance approximately 1.5 away from the aperture, which is in the synthetic aperture near field. The mobile antenna moved in half-wavelength intervals across the aperture, a total of 861 measurement points. The normalized real and imaginary visibility function samples for each unique D_x, D_y measurement location are shown in Figure 7.4. Reproduction of the measured scene is shown in Figure 7.5. The image reconstruction picks out the two 3 GHz radiating spots produced by the horn antennas at their respective locations. The reproduced data picked up signal strength difference between the two transmitting antennas. The power output from Antenna 1 output was roughly 2 dB less than Antenna 2.

Measurements were taken with different power-output levels from each of the transmitting horns. A 6 dB attenuation pad was placed on the input to Antenna 1 while the other maintained the original power output level. The measurement was repeated with Antenna 2 attenuated 6 dB and Antenna 1 transmitting the original power level. The visibility function samples and reproduced results are shown in Figures 7.6 and 7.7. The visibility function samples and reproduced results are shown in Figures 7.8 and 7.9. The hot spot locations are both observed and the attenuated signal appears with less intensity in each of the two measurement cases. The calculated attenuation on Antenna 1 in Figure 7.9 compared to the measured data shown in Figure 7.5 is 6.37 dB. The signal difference between Antenna's 1 and 2 when

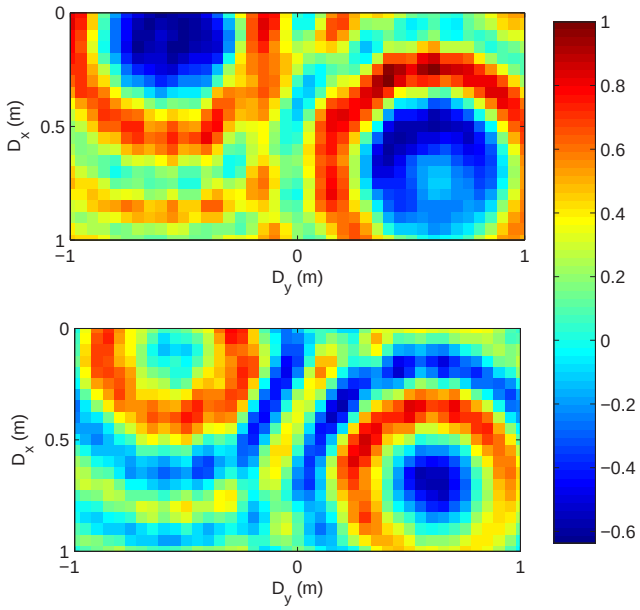

Figure 7.4. Visibility function samples (V_I top, V_Q bottom) of 2×1 meter synthetic aperture measurement with two offset S-band horns

Antenna 1 was attenuated is 8.22 dB and 4.2 dB when Antenna 2 was attenuated, due to the 2 dB signal difference between the two transmitting antennas mentioned earlier. The calculated attenuation on Antenna 2 in Figure 7.8 with respect to the measured data in Figure 7.5 is 6.47 dB.

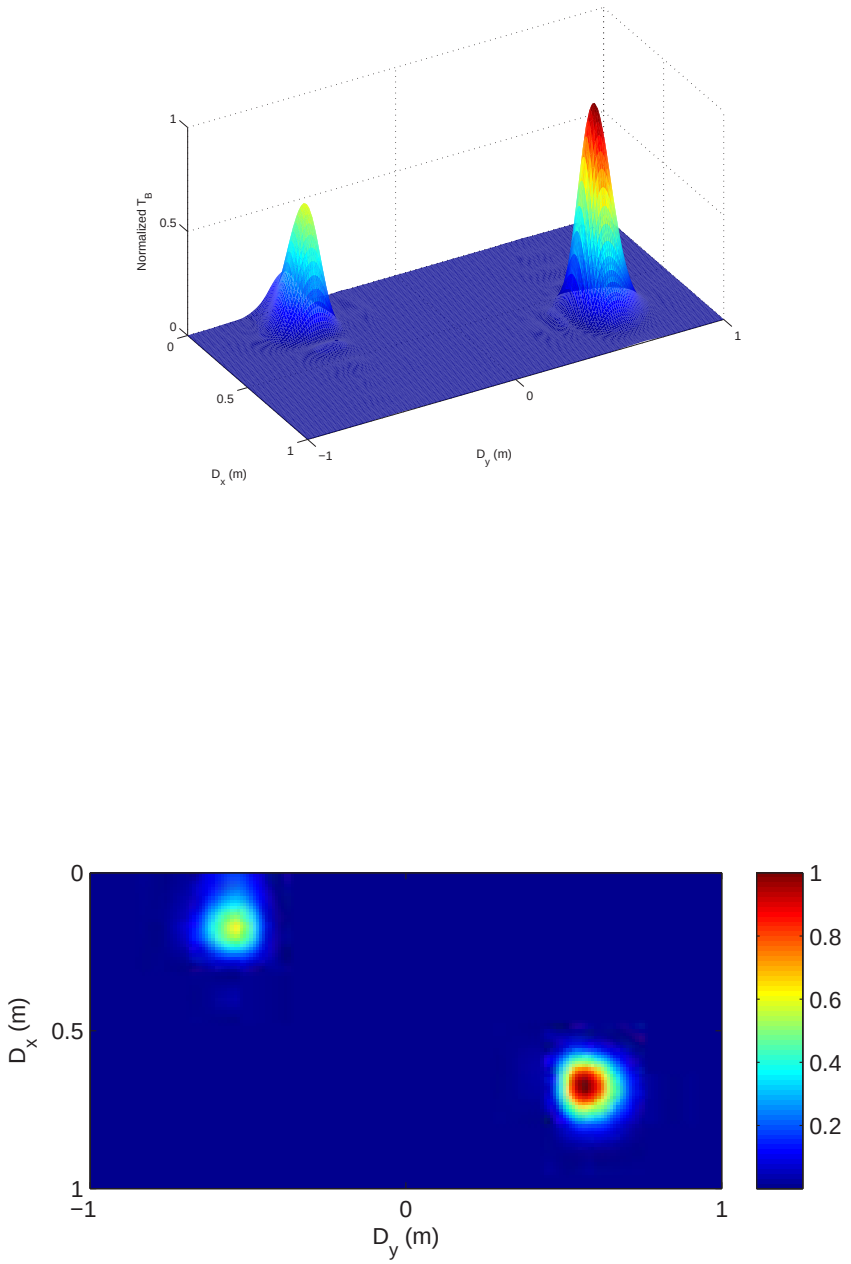

Figure 7.5. Image reconstruction of two offset S-band horns at 3 GHz from 2×1 meter syntehtic aperture measurement

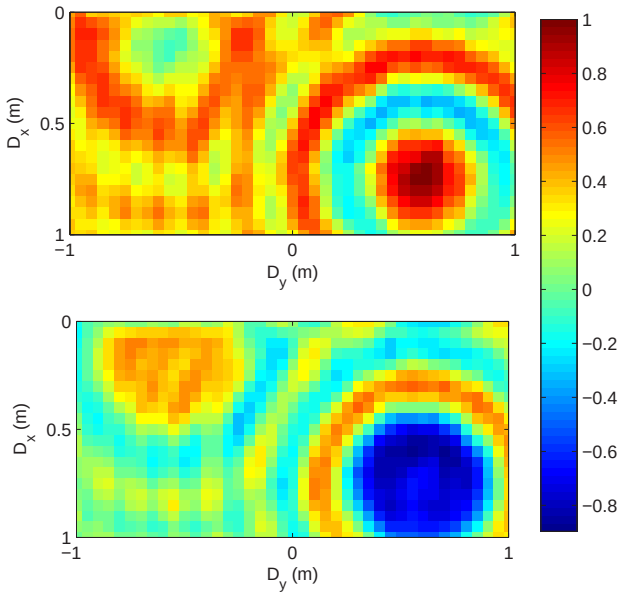

Figure 7.6. Visibility function samples (V_I top, V_Q bottom) of 2×1 meter synthetic aperture measurement with two offset S-band horns, Antenna 1 attenuated by 6 dB

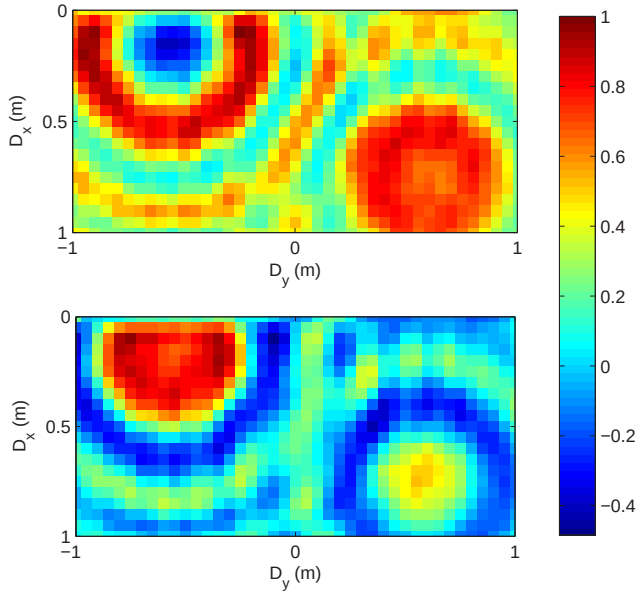

Figure 7.7. Visibility function samples (V_I top, V_Q bottom) of 2×1 meter synthetic aperture measurement with two offset S-band horns, Antenna 2 attenuated by 6 dB

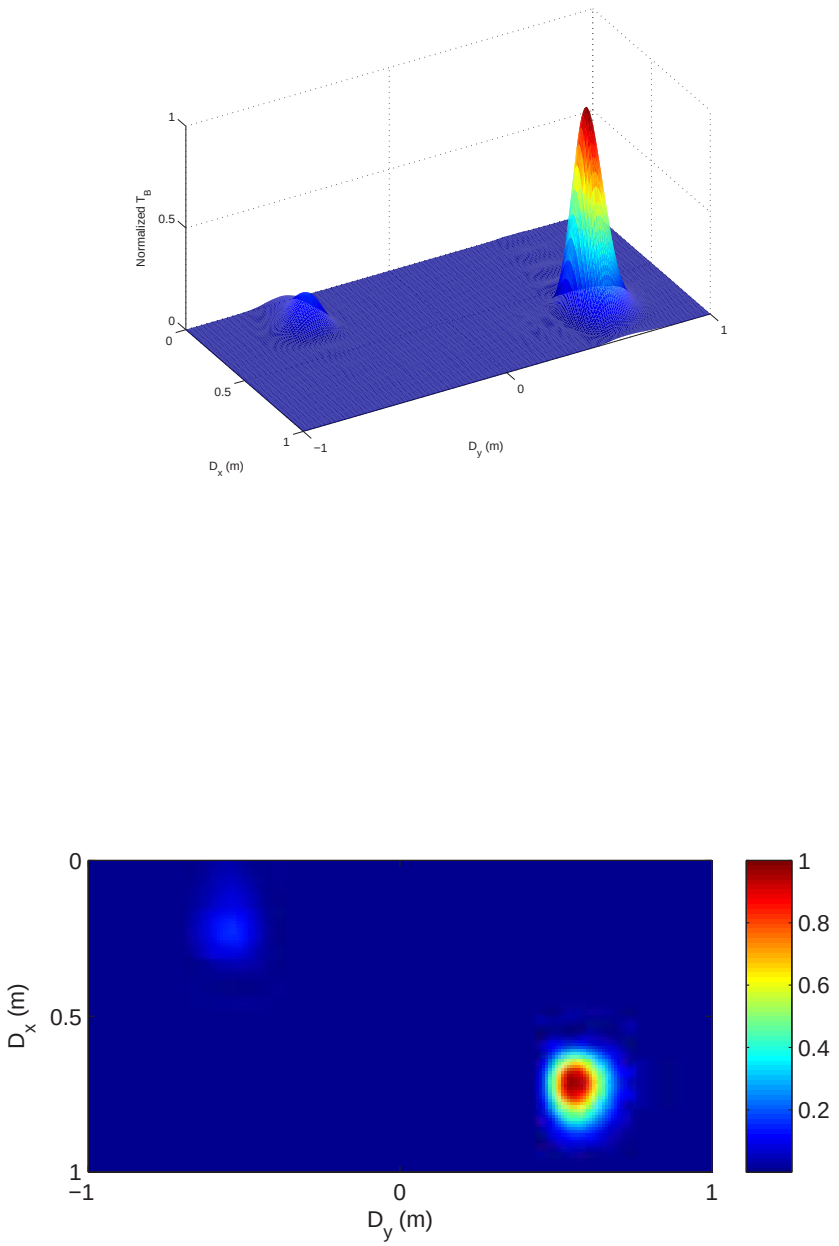

Figure 7.8. Image reconstruction of two offset S-band horns at 3 GHz from 2 × 1 meter syntehtic aperture measurement, Antenna 1 attenuated by 6 dB

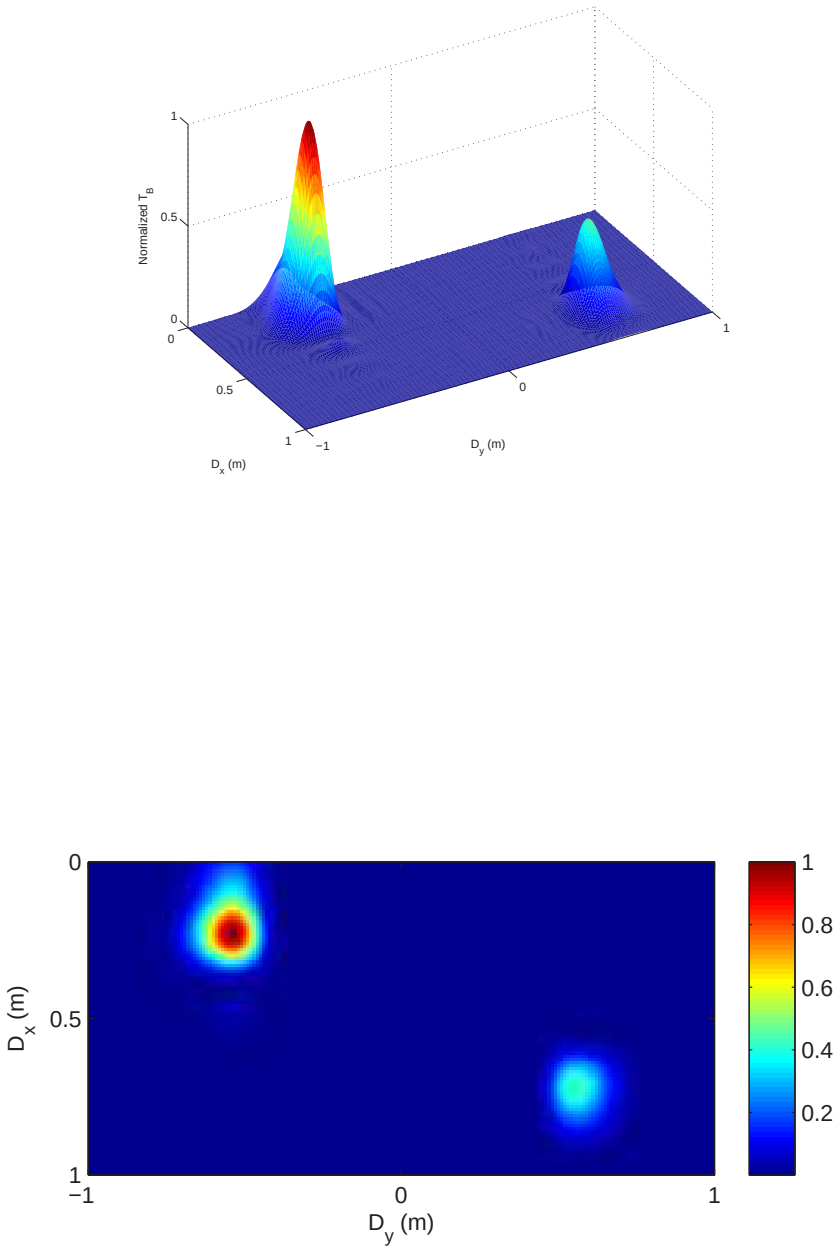

Figure 7.9. Image reconstruction of two offset S-band horns at 3 GHz from 2 × 1 meter syntehtic aperture measurement, Antenna 2 attenuated by 6 dB

The ambient scene was also measured using the two 3 GHz patch antenna configuration. This measurement should essentially determine the noise floor of the correlator system. The measured visibility function sample data for this case is shown in Figure 7.10. The output voltage variation for the in-phase and quadrature components are 3.1 and 4.5 millivolts at 0 VDC, respectively. Compared to the signal levels observed with the horn sources, these voltage levels correspond to 1.6% and 2.3% error in the in-phase and quadrature channels.

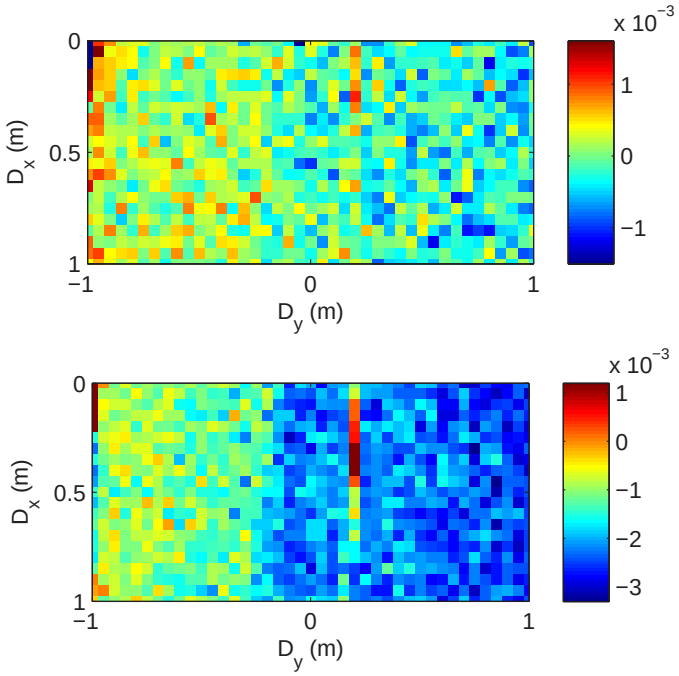

Figure 7.10. Visibility function (V_I top, V_Q bottom) of ambient scene measured by 3 GHz 2 × 1 meter synthetic aperture

When the 94.8 GHz radiometers and noise source were placed into the system for wideband testing, measured results were poor in comparison to the narrowband measurements. Voltage level outputs from the complex correlator were on the order of +/- 1 mV. Factoring in the large A/D converter DC bias to this resulted in measurements that could not be supported with confidence. The spectral correlated data

output from the 500 MHz low pass filters appears good, but the 300 Hz demodulating board appears unable to handle the wide baseband output.

CHAPTER 8

CONCLUSION AND RECOMMENDATIONS

Through narrowband 3 GHz IF testing the constructed correlator has been shown to successfully reproduce a radiating scene. The synthetic aperture created by two microstrip patch antennas demonstrated the potential of obtaining accurate image reconstruction of a measured scene's brightness temperature for high-frequency measurements. The method of measuring a stationary scene by movements executed by two linear drive tracks and collecting data from a complex correlator through an A/D converter was validated. Though the mixer implementation used for producing the correlation of the two received narrowband signals was successful, improvements to the system are still needed in order for wideband measurements at 94.8 GHz to be taken.

One improvement to the system would be the implementation of the square law method discussed in Section 4.1, whereby a power combiner and diode detector are instituted in place of the mixer and extra amplifier for the LO channel. So long as the power level of the combination of the two signals into the diode detector was within the square-law region, this method is preferred between the two as it wastes less power. Another method that has been used to produce these correlated signals is the direct multiplication of the two signals. A block diagram of this implementation is shown in Figure 8.1. Rather than upconvert one of the received signals, correlate the signals and finally demodulate down to a baseband signal, mixing to a baseband signal is done directly. Each signal is divided through a power splitter. One of the split signals is phase shifted 90 degrees. The I multiplier receives the signals from

receivers 1 and 2 that have not been phase shifted. The Q multiplier receives a signal from receiver 1 and a 90 degree phase shifted signal from receiver 2. The outputs from the I and Q channels are the baseband, in-phase and quadrature components of the complex correlated visibility function sample. Integration and DC bias removal stages, such as the 300 Hz modulation method used in this design, would follow the correlation stage. To implement this method requires wideband mixers that are currently unavailable. If such a product emerges, this is the recommended method for pursuing signal correlation because the other methods are wasteful with power.

It is also strongly recommended that alternate structures be created to support the linear drives and radiometers. The support structure presented in this thesis that held the linear drives is susceptible to vibrations and shaking that could be caused by movements executed by the linear drives or weather conditions. While strengthening was done to reduce these movements, the fundamental design of the support structure still results in unstable performance at times. It is also recommended that the support structure holding the stationary radiometer be replaced with a more stable structure. The hooked shape of the design could be removed altogether if a larger ground plane, in this case the maple butcher block, were extended upwards. This would allow for a structure much like the one used to hold the radiometer on the linear drives to be used instead.

The measurement system could also benefit from added electronic hardware with the intent of producing higher quality measurements. A null feedback design has been implemented in previous remote sensing instruments and is beneficial to the overall system performance. The null feedback circuit is used for the zeroth spacing signal correlation data, with the intent to remove receiver noise from the data. It is also recommended that a sophisticated temperature control system be included in the design in order to keep all electronic components at a constant temperature.

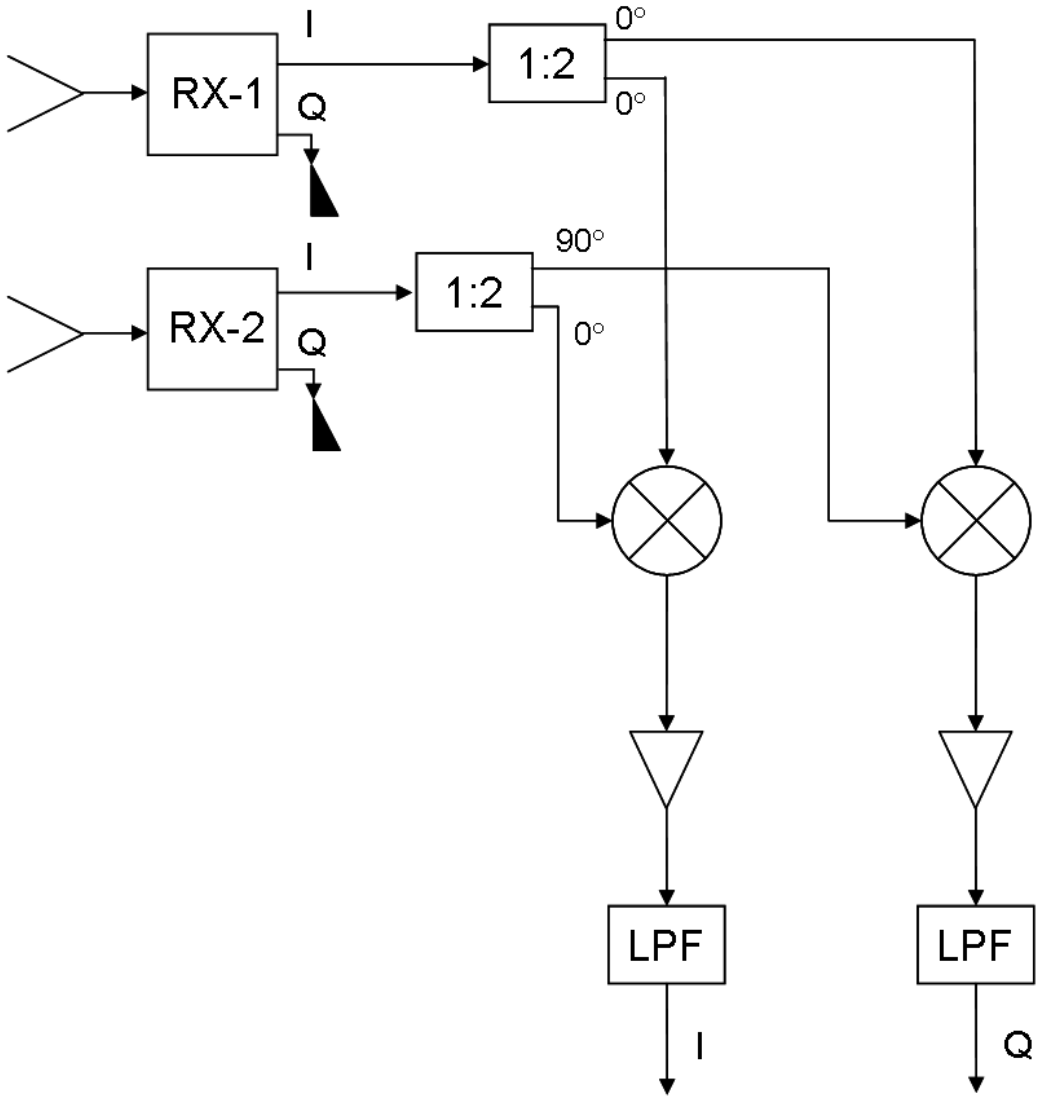

Figure 8.1. Analog complex correlator using direct multiplication

APPENDIX A

RADIOMETER AND NOISE SOURCE DATA SHEETS

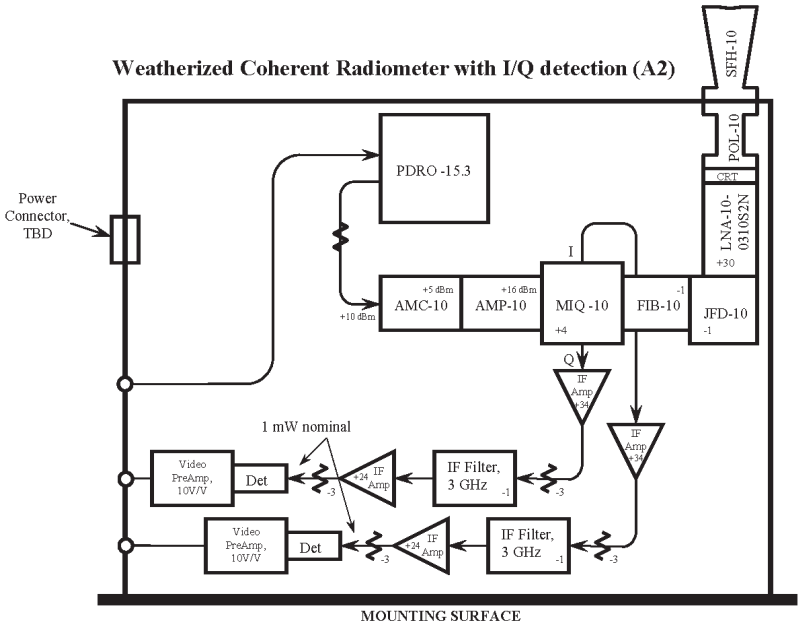

Figure A.1. Radiometer module RX-1 block diagram, provided by Millitech

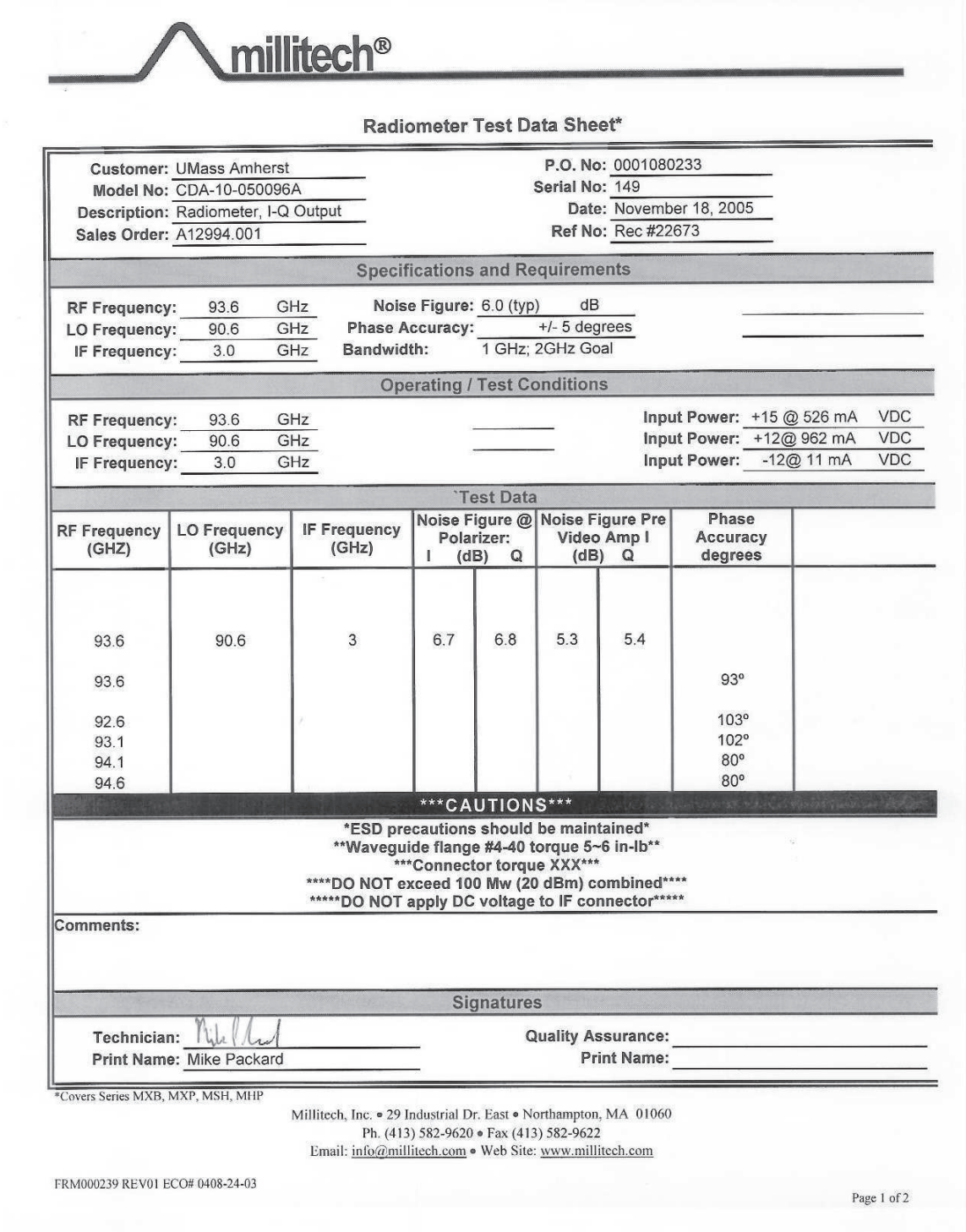

millitech®

Radiometer Test Data Sheet*

Customer:	UMass Amherst	**P.O. No:**	0001080233
Model No:	CDA-10-050096A	**Serial No:**	149
Description:	Radiometer, I-Q Output	**Date:**	November 18, 2005
Sales Order:	A12994.001	**Ref No:**	Rec #22673

Specifications and Requirements

RF Frequency:	93.6	GHz	**Noise Figure:**	6.0 (typ)	dB
LO Frequency:	90.6	GHz	**Phase Accuracy:**	+/- 5 degrees	
IF Frequency:	3.0	GHz	**Bandwidth:**	1 GHz; 2GHz Goal	

Operating / Test Conditions

RF Frequency:	93.6	GHz	**Input Power:**	+15 @ 526 mA	VDC
LO Frequency:	90.6	GHz	**Input Power:**	+12@ 962 mA	VDC
IF Frequency:	3.0	GHz	**Input Power:**	-12@ 11 mA	VDC

`Test Data

RF Frequency (GHZ)	LO Frequency (GHz)	IF Frequency (GHz)	Noise Figure @ Polarizer: I (dB)	Q	Noise Figure Pre Video Amp I (dB)	Q	Phase Accuracy degrees
93.6	90.6	3	6.7	6.8	5.3	5.4	
93.6							93°
92.6							103°
93.1							102°
94.1							80°
94.6							80°

*****CAUTIONS*****

ESD precautions should be maintained
****Waveguide flange #4-40 torque 5~6 in-lb****
*****Connector torque XXX*****
******DO NOT exceed 100 Mw (20 dBm) combined******
*******DO NOT apply DC voltage to IF connector*******

Comments:

Signatures

Technician:		**Quality Assurance:**	
Print Name:	Mike Packard	**Print Name:**	

*Covers Series MXB, MXP, MSH, MHP

Millitech, Inc. • 29 Industrial Dr. East • Northampton, MA 01060
Ph. (413) 582-9620 • Fax (413) 582-9622
Email: info@millitech.com • Web Site: www.millitech.com

Figure A.2. Radiometer module RX-1 test data sheet, provided by Millitech

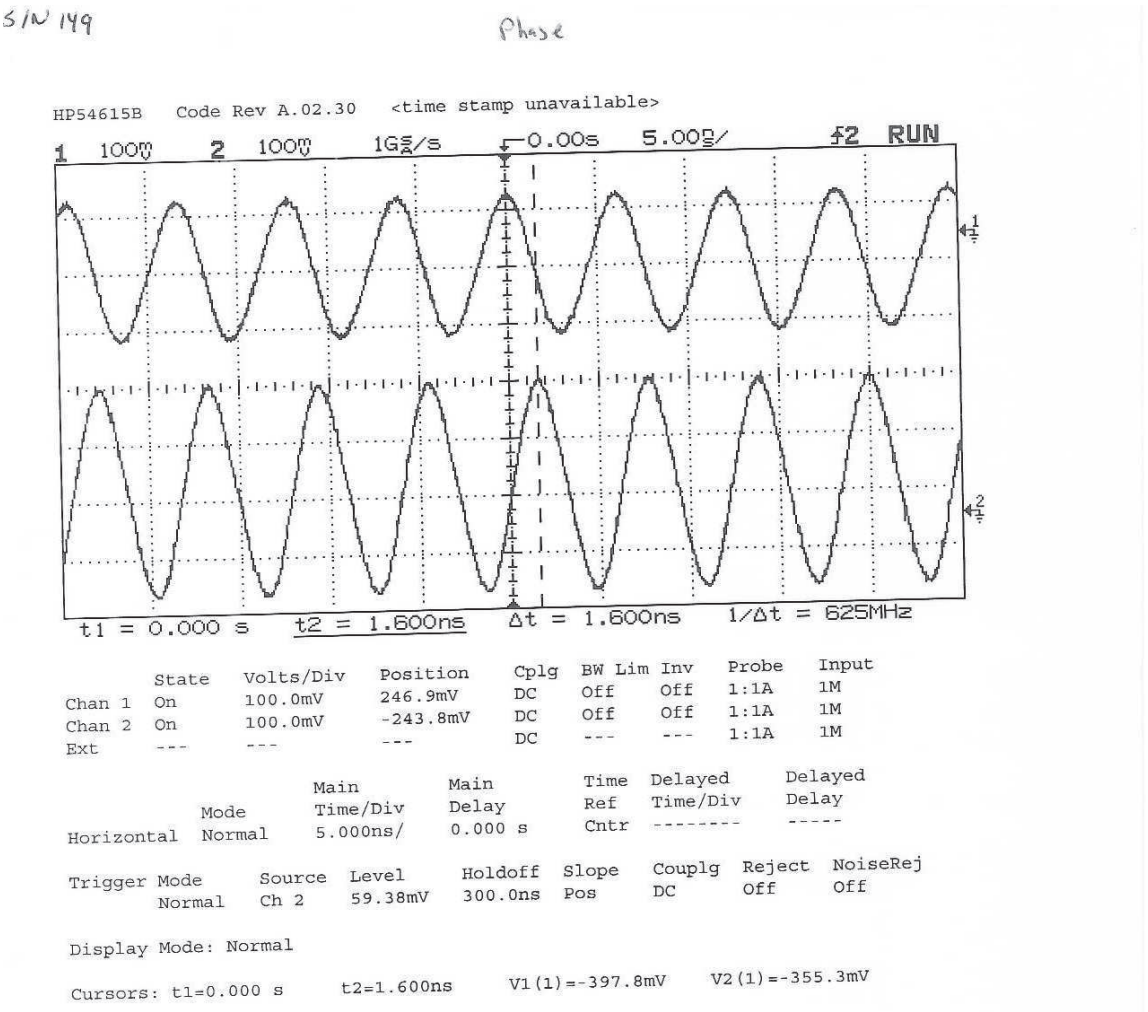

Figure A.3. Radiometer module RX-1 phase accuracy at 93.6 GHz, provided by Millitech

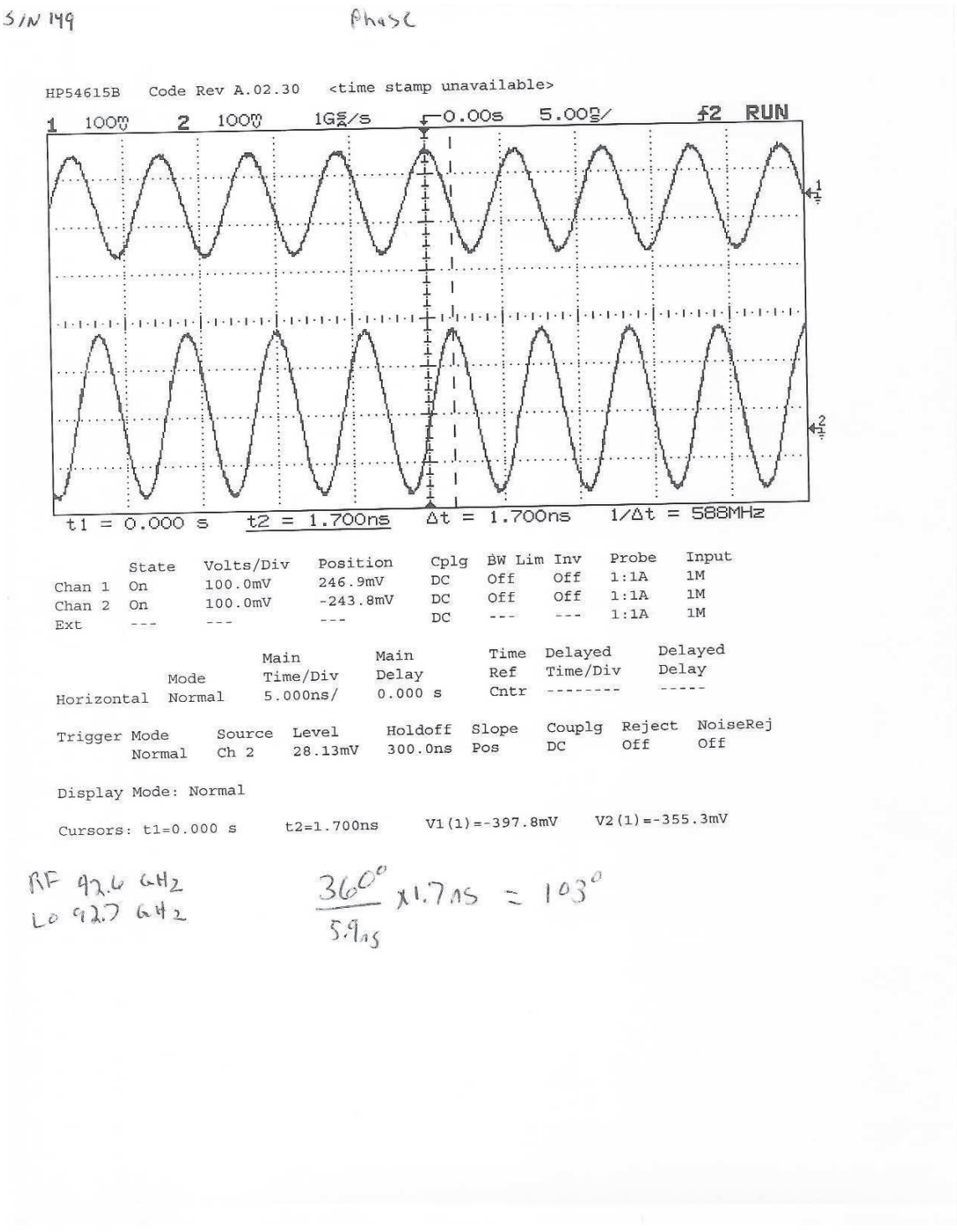

Figure A.4. Radiometer module RX-1 phase accuracy at 92.6 GHz, provided by Millitech

S/N M9

Phase

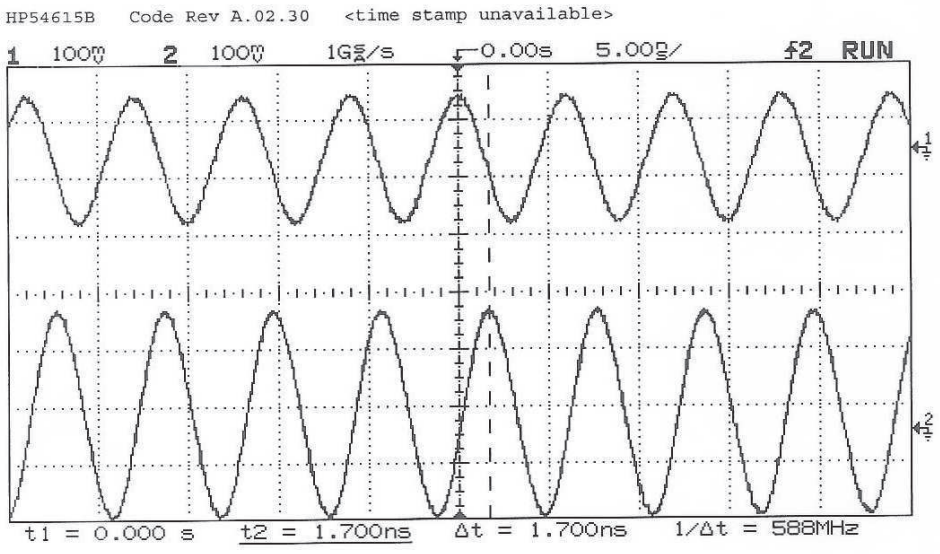

	State	Volts/Div	Position	Cplg	BW Lim	Inv	Probe	Input
Chan 1	On	100.0mV	246.9mV	DC	Off	Off	1:1A	1M
Chan 2	On	100.0mV	-243.8mV	DC	Off	Off	1:1A	1M
Ext	---	---	---	DC	---	---	1:1A	1M

	Mode	Main Time/Div	Main Delay	Time Ref	Delayed Time/Div	Delayed Delay
Horizontal	Normal	5.000ns/	0.000 s	Cntr	--------	-----

Trigger	Mode	Source	Level	Holdoff	Slope	Couplg	Reject	NoiseRej
	Normal	Ch 2	18.75mV	300.0ns	Pos	DC	Off	Off

Display Mode: Normal

Cursors: t1=0.000 s t2=1.700ns V1(1)=-397.8mV V2(1)=-355.3mV

RF 93.1 GHz

LO 93.2 GHz

$\frac{360^\circ}{1.7\,ns} \times 1.7\,ns \simeq 102^\circ$

Figure A.5. Radiometer module RX-1 phase accuracy at 93.1 GHz, provided by Millitech

S/N 149

Phase

HP54615B Code Rev A.02.30 <time stamp unavailable>

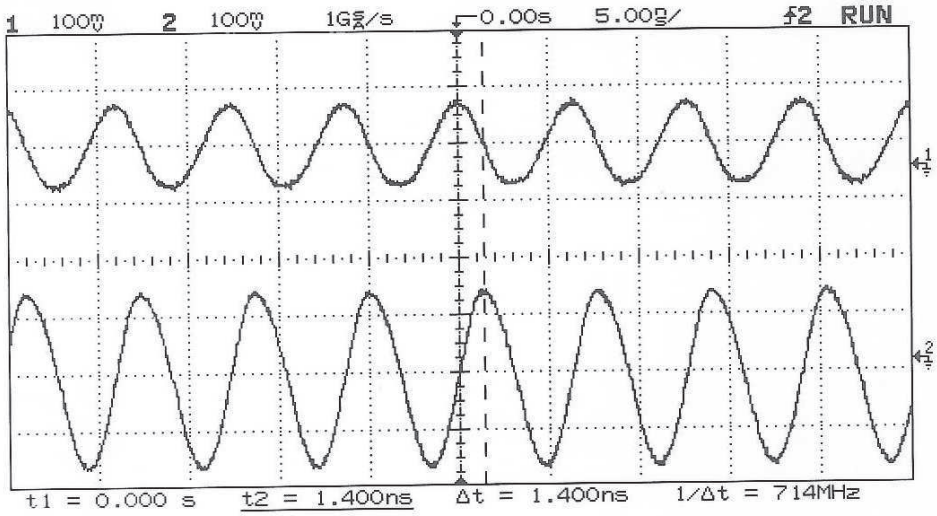

	State	Volts/Div	Position	Cplg	BW Lim	Inv	Probe	Input
Chan 1	On	100.0mV	156.3mV	DC	Off	Off	1:1A	1M
Chan 2	On	100.0mV	-181.3mV	DC	Off	Off	1:1A	1M
Ext	---	---	---	DC	---	---	1:1A	1M

	Mode	Main Time/Div	Main Delay	Time Ref	Delayed Time/Div	Delayed Delay
Horizontal	Normal	5.000ns/	0.000 s	Cntr	--------	-----

Trigger Mode	Source	Level	Holdoff	Slope	Couplg	Reject	NoiseRej
Normal	Ch 2	-3.125mV	300.0ns	Pos	DC	Off	Off

Display Mode: Normal

Cursors: t1=0.000 s t2=1.400ns V1(1)=-397.8mV V2(1)=-355.3mV

RF 94.16 Hz

LO 94.26 Hz

$\frac{360^\circ}{6.3ns} \times 1.4ns = 80^\circ$

Figure A.6. Radiometer module RX-1 phase accuracy at 94.1 GHz, provided by Millitech

S/N M9

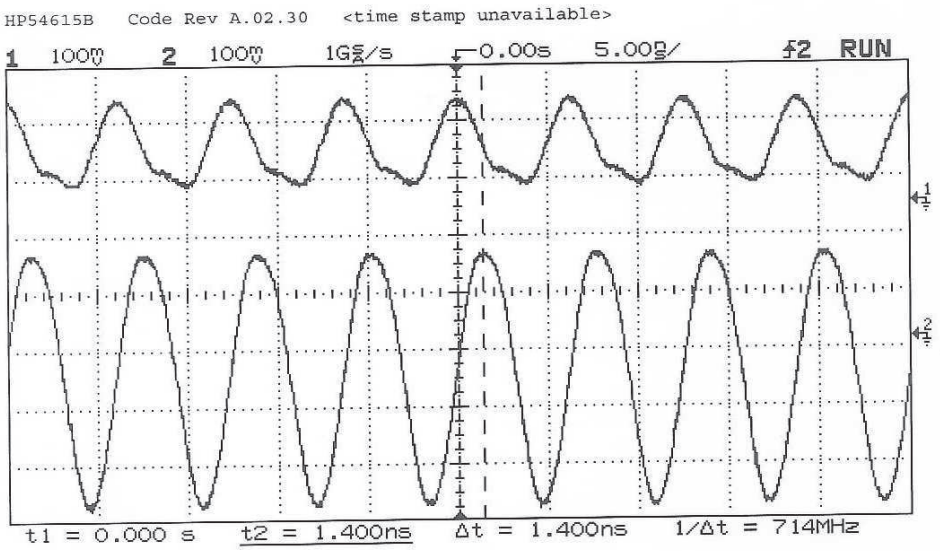

	State	Volts/Div	Position	Cplg	BW Lim	Inv	Probe	Input
Chan 1	On	100.0mV	156.3mV	DC	Off	Off	1:1A	1M
Chan 2	On	100.0mV	-81.25mV	DC	Off	Off	1:1A	1M
Ext	---	---	---	DC	---	---	1:1A	1M

	Mode	Main Time/Div	Main Delay	Time Ref	Delayed Time/Div	Delayed Delay
Horizontal	Normal	5.000ns/	0.000 s	Cntr	--------	-----

Trigger	Mode	Source	Level	Holdoff	Slope	Couplg	Reject	NoiseRej
	Normal	Ch 2	-3.125mV	300.0ns	Pos	DC	Off	Off

Display Mode: Normal

Cursors: t1=0.000 s t2=1.400ns V1(1)=-397.8mV V2(1)=-355.3mV

RF 94.6 GHz
LO 94.7 GHz

$\frac{360^\circ}{6.3\,ns} \times 1.4\,ns = 80^\circ$

Figure A.7. Radiometer module RX-1 phase accuracy at 94.6 GHz, provided by Millitech

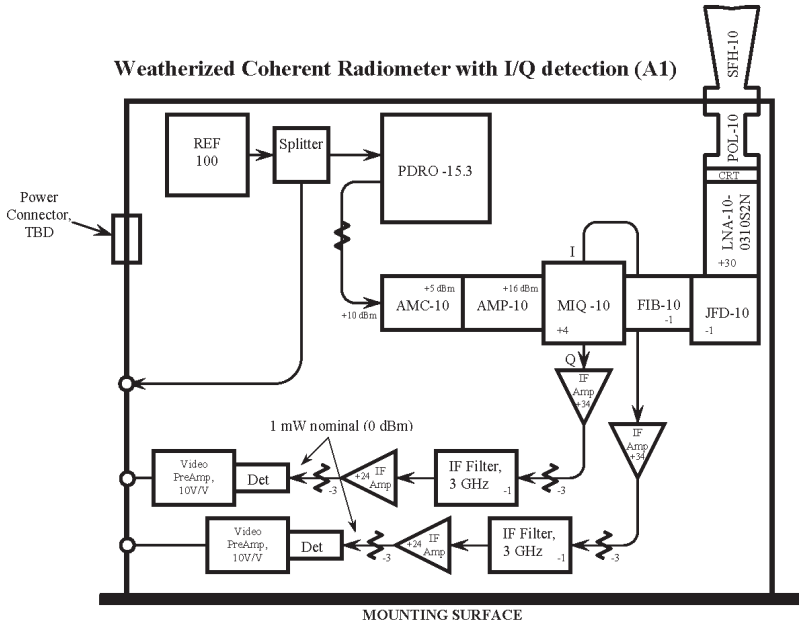

Figure A.8. Millitech radiometer module RX-2 block diagram, provided by Millitech

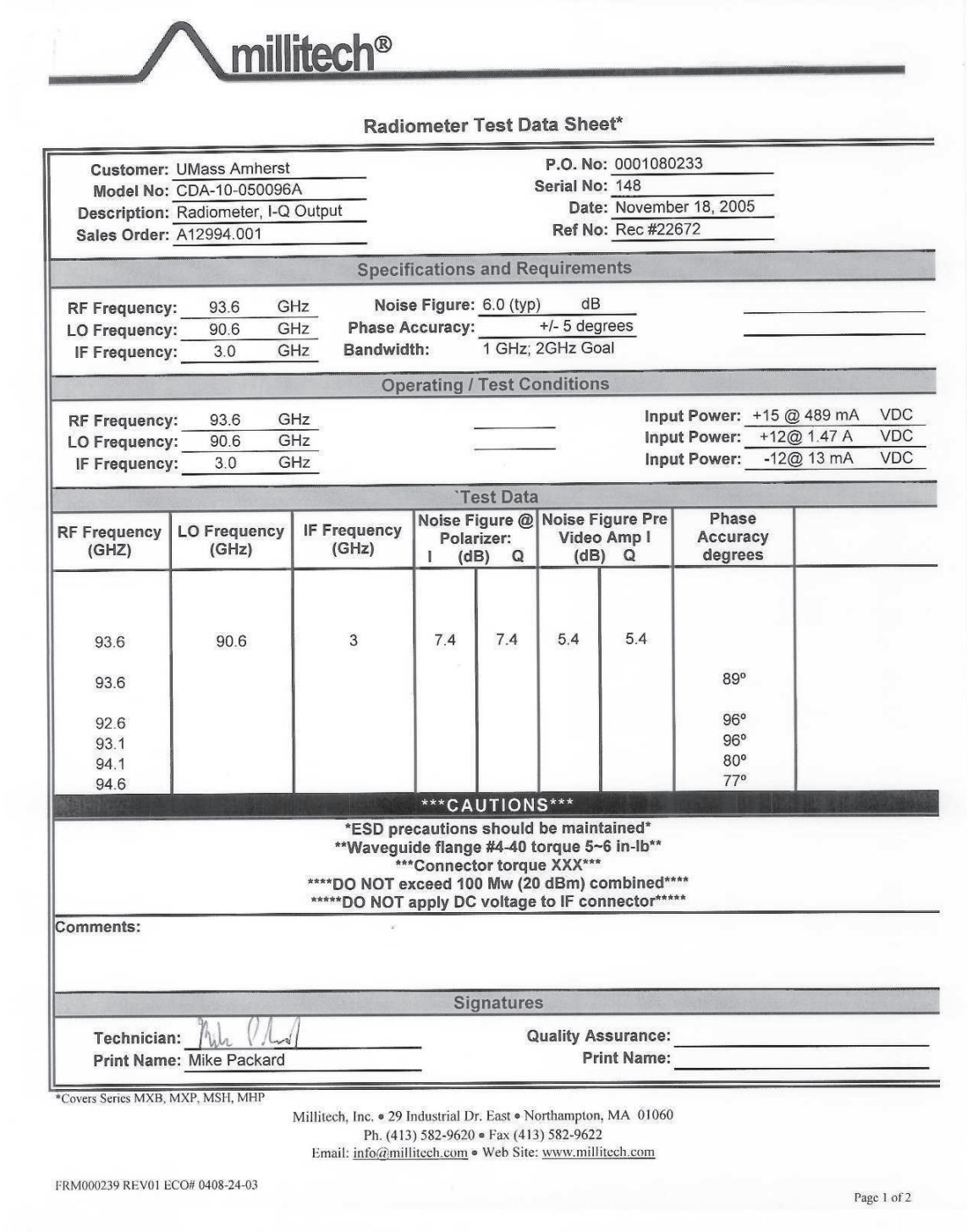

millitech®

Radiometer Test Data Sheet*

Customer:	UMass Amherst	**P.O. No:**	0001080233
Model No:	CDA-10-050096A	**Serial No:**	148
Description:	Radiometer, I-Q Output	**Date:**	November 18, 2005
Sales Order:	A12994.001	**Ref No:**	Rec #22672

Specifications and Requirements

RF Frequency:	93.6	GHz	**Noise Figure:**	6.0 (typ)	dB
LO Frequency:	90.6	GHz	**Phase Accuracy:**	+/- 5 degrees	
IF Frequency:	3.0	GHz	**Bandwidth:**	1 GHz; 2GHz Goal	

Operating / Test Conditions

RF Frequency:	93.6	GHz	**Input Power:**	+15 @ 489 mA	VDC
LO Frequency:	90.6	GHz	**Input Power:**	+12@ 1.47 A	VDC
IF Frequency:	3.0	GHz	**Input Power:**	-12@ 13 mA	VDC

`Test Data

RF Frequency (GHZ)	LO Frequency (GHz)	IF Frequency (GHz)	Noise Figure @ Polarizer: I (dB)	Q	Noise Figure Pre Video Amp I (dB)	Q	Phase Accuracy degrees
93.6	90.6	3	7.4	7.4	5.4	5.4	
93.6							89°
92.6							96°
93.1							96°
94.1							80°
94.6							77°

*****CAUTIONS*****

ESD precautions should be maintained
****Waveguide flange #4-40 torque 5~6 in-lb****
*****Connector torque XXX*****
******DO NOT exceed 100 Mw (20 dBm) combined******
*******DO NOT apply DC voltage to IF connector*******

Comments:

Signatures

Technician:	Mike Packard	**Quality Assurance:**	
Print Name:	Mike Packard	**Print Name:**	

*Covers Series MXB, MXP, MSH, MHP

Millitech, Inc. • 29 Industrial Dr. East • Northampton, MA 01060
Ph. (413) 582-9620 • Fax (413) 582-9622
Email: info@millitech.com • Web Site: www.millitech.com

Figure A.9. Radiometer module RX-2 test data sheet, provided by Millitech

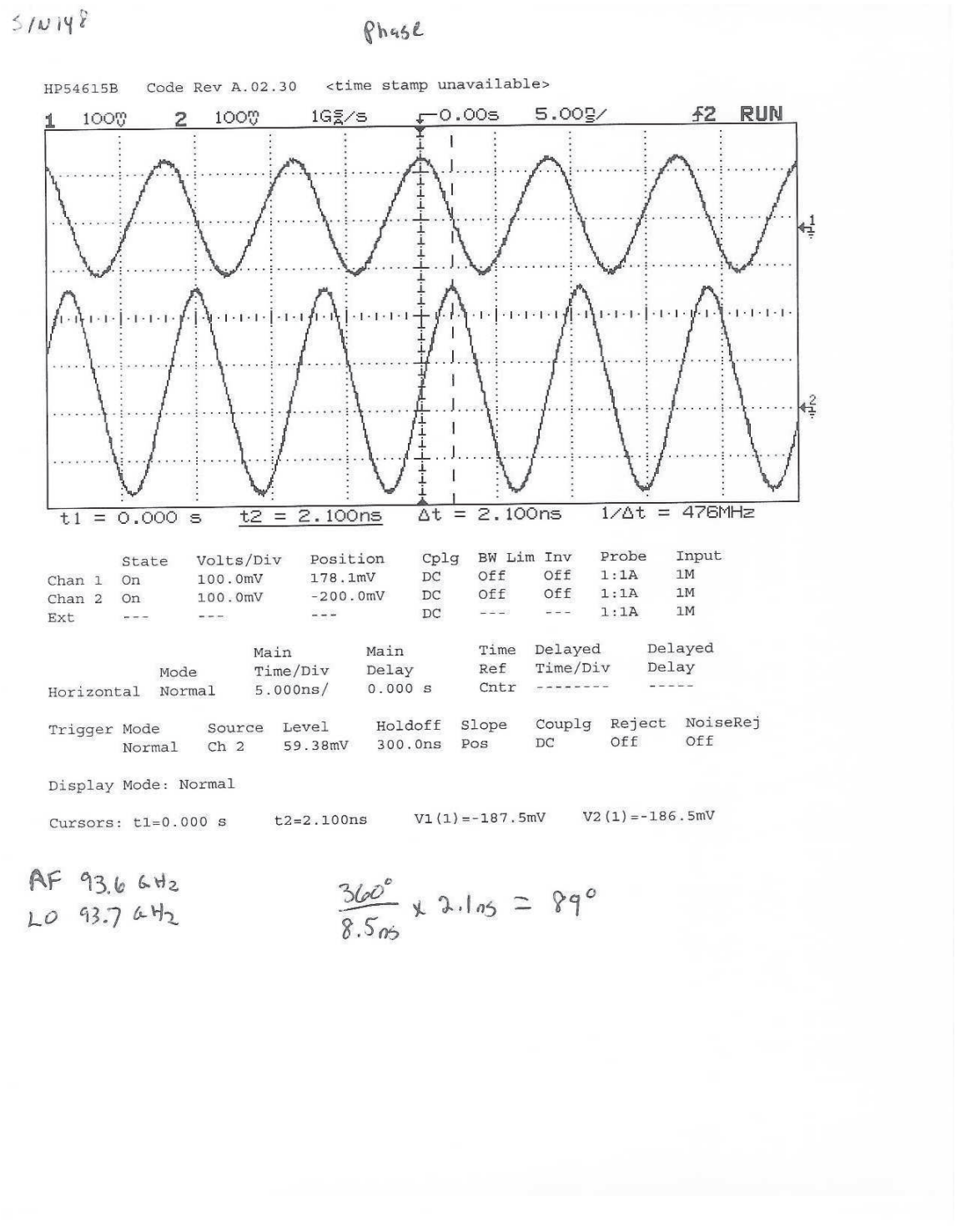

Figure A.10. Radiometer module RX-2 phase accuracy at 93.6 GHz, provided by Millitech

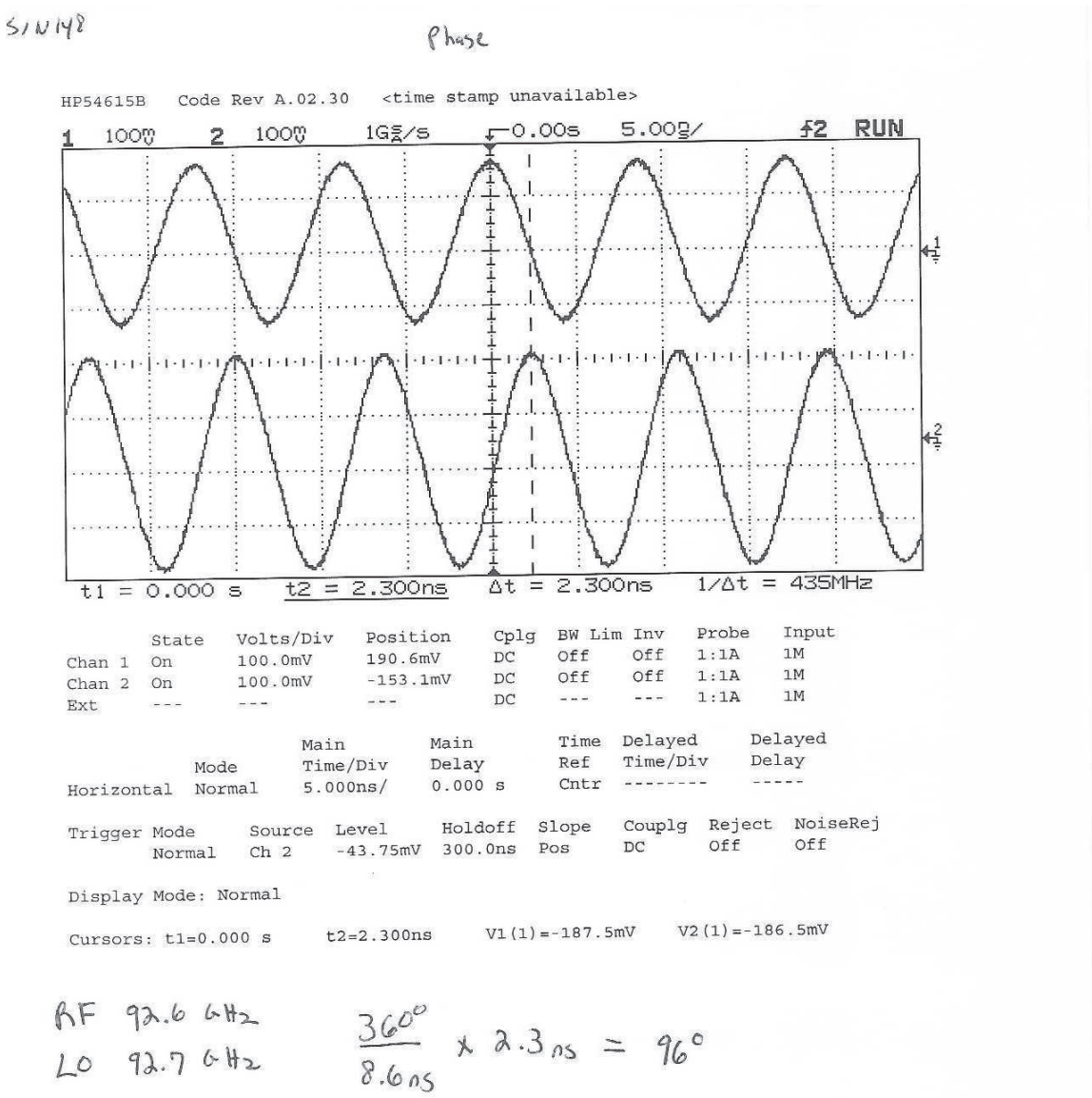

Figure A.11. Radiometer module RX-2 phase accuracy at 92.6 GHz, provided by Millitech

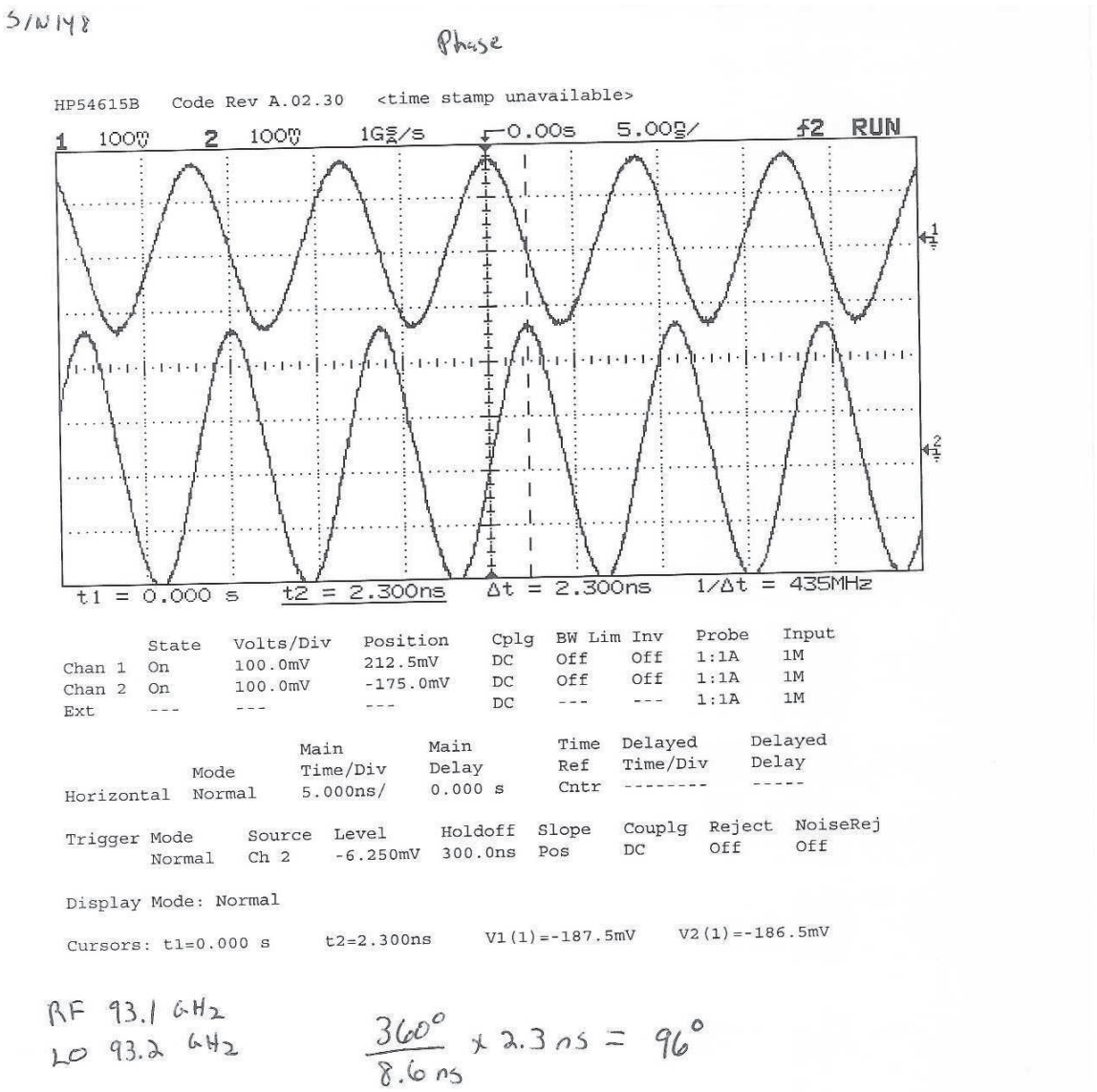

Figure A.12. Radiometer module RX-2 phase accuracy at 93.1 GHz, provided by Millitech

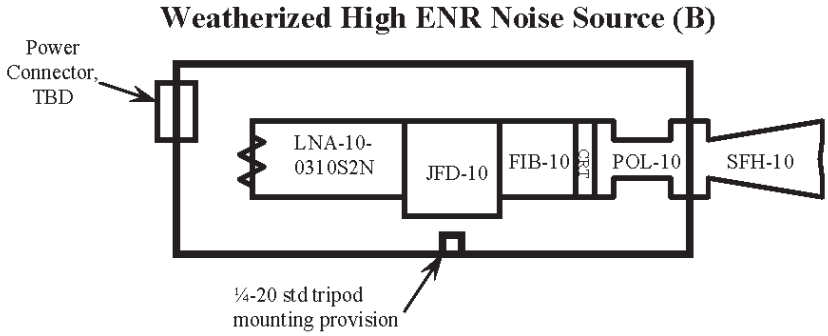

Figure A.13. Millitech noise source module block diagram, provided by Millitech

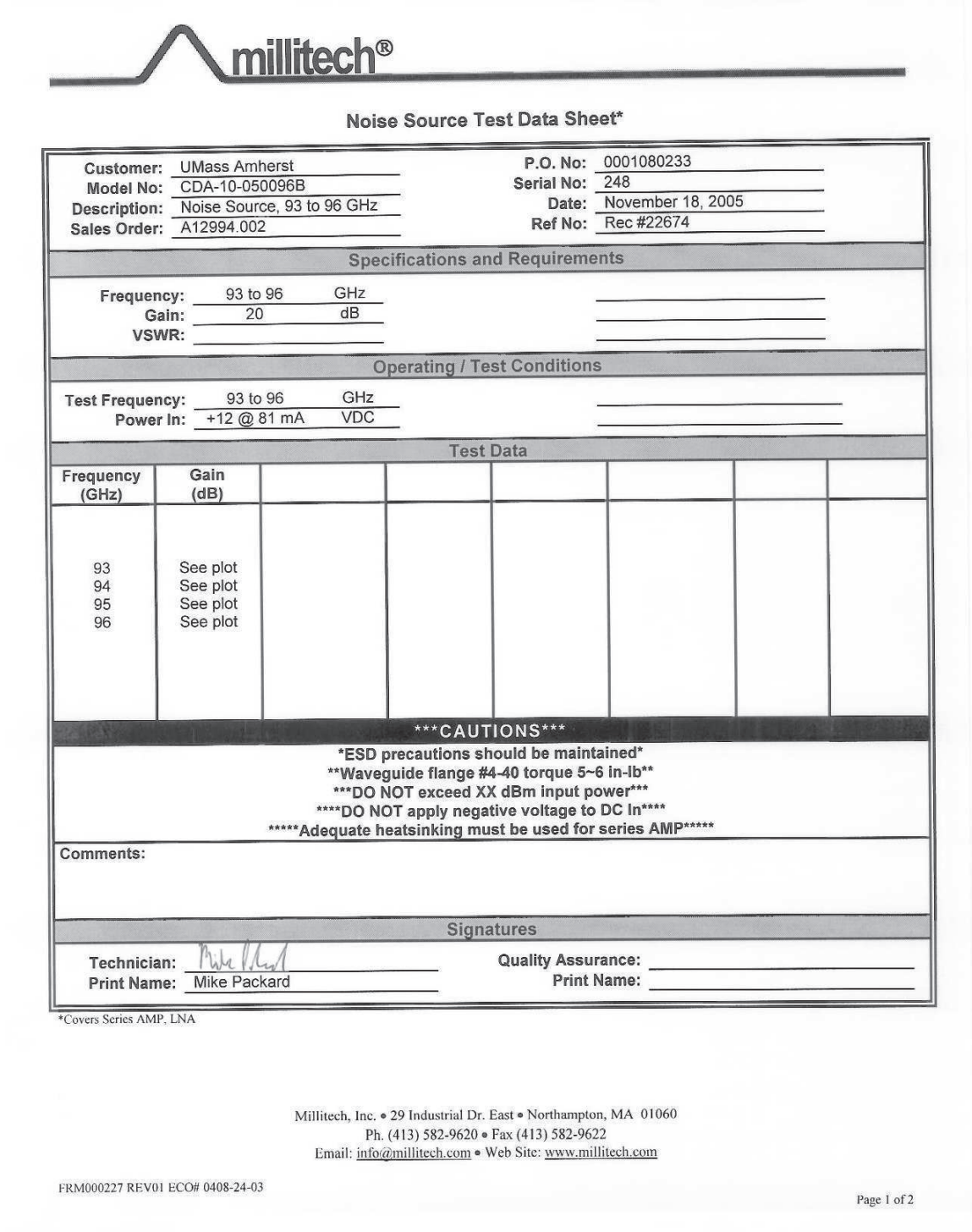

millitech®

Noise Source Test Data Sheet*

Customer:	UMass Amherst	**P.O. No:**	0001080233
Model No:	CDA-10-050096B	**Serial No:**	248
Description:	Noise Source, 93 to 96 GHz	**Date:**	November 18, 2005
Sales Order:	A12994.002	**Ref No:**	Rec #22674

Specifications and Requirements

Frequency:	93 to 96	GHz
Gain:	20	dB
VSWR:		

Operating / Test Conditions

Test Frequency:	93 to 96	GHz
Power In:	+12 @ 81 mA	VDC

Test Data

Frequency (GHz)	Gain (dB)						
93	See plot						
94	See plot						
95	See plot						
96	See plot						

*****CAUTIONS*****

ESD precautions should be maintained
****Waveguide flange #4-40 torque 5~6 in-lb****
*****DO NOT exceed XX dBm input power*****
******DO NOT apply negative voltage to DC In******
*******Adequate heatsinking must be used for series AMP*******

Comments:

Signatures

Technician:		**Quality Assurance:**	
Print Name:	Mike Packard	**Print Name:**	

*Covers Series AMP, LNA

Millitech, Inc. • 29 Industrial Dr. East • Northampton, MA 01060
Ph. (413) 582-9620 • Fax (413) 582-9622
Email: info@millitech.com • Web Site: www.millitech.com

FRM000227 REV01 ECO# 0408-24-03

Page 1 of 2

Figure A.14. Noise source test data sheet, provided by Millitech

S/N 148

Phase

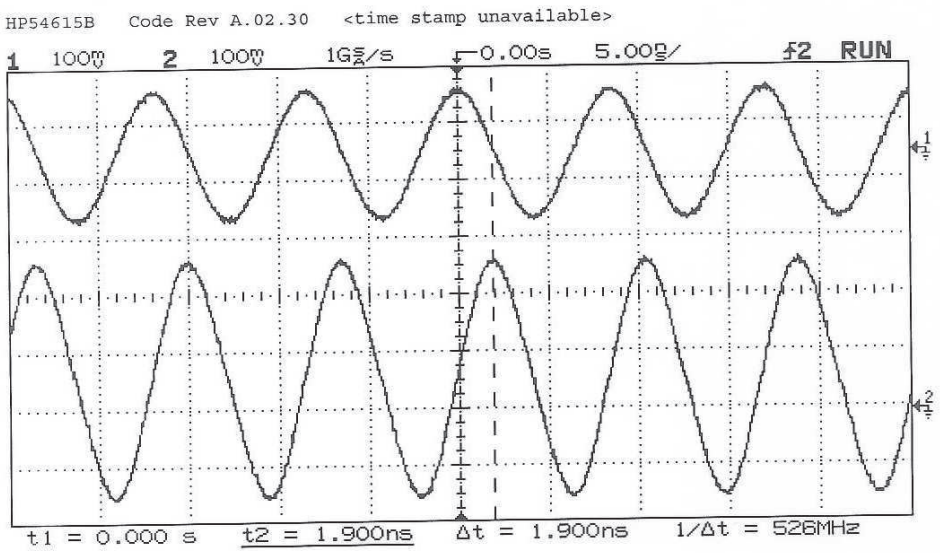

	State	Volts/Div	Position	Cplg	BW Lim	Inv	Probe	Input
Chan 1	On	100.0mV	246.9mV	DC	Off	Off	1:1A	1M
Chan 2	On	100.0mV	-206.3mV	DC	Off	Off	1:1A	1M
Ext	---	---	---	DC	---	---	1:1A	1M

	Mode	Main Time/Div	Main Delay	Time Ref	Delayed Time/Div	Delayed Delay
Horizontal	Normal	5.000ns/	0.000 s	Cntr	--------	-----

Trigger	Mode	Source	Level	Holdoff	Slope	Couplg	Reject	NoiseRej
	Normal	Ch 2	90.63mV	300.0ns	Pos	DC	Off	Off

Display Mode: Normal

Cursors: t1=0.000 s t2=1.900ns V1(1)=-187.5mV V2(1)=-186.5mV

RF 94.1 GHz
LO 94.2 GHz

$\frac{360^\circ}{8.5\text{ns}} \times 1.9\text{ns} \simeq 80^\circ$

Figure A.15. Noise source phase accuracy at 94.1 GHz, provided by Millitech

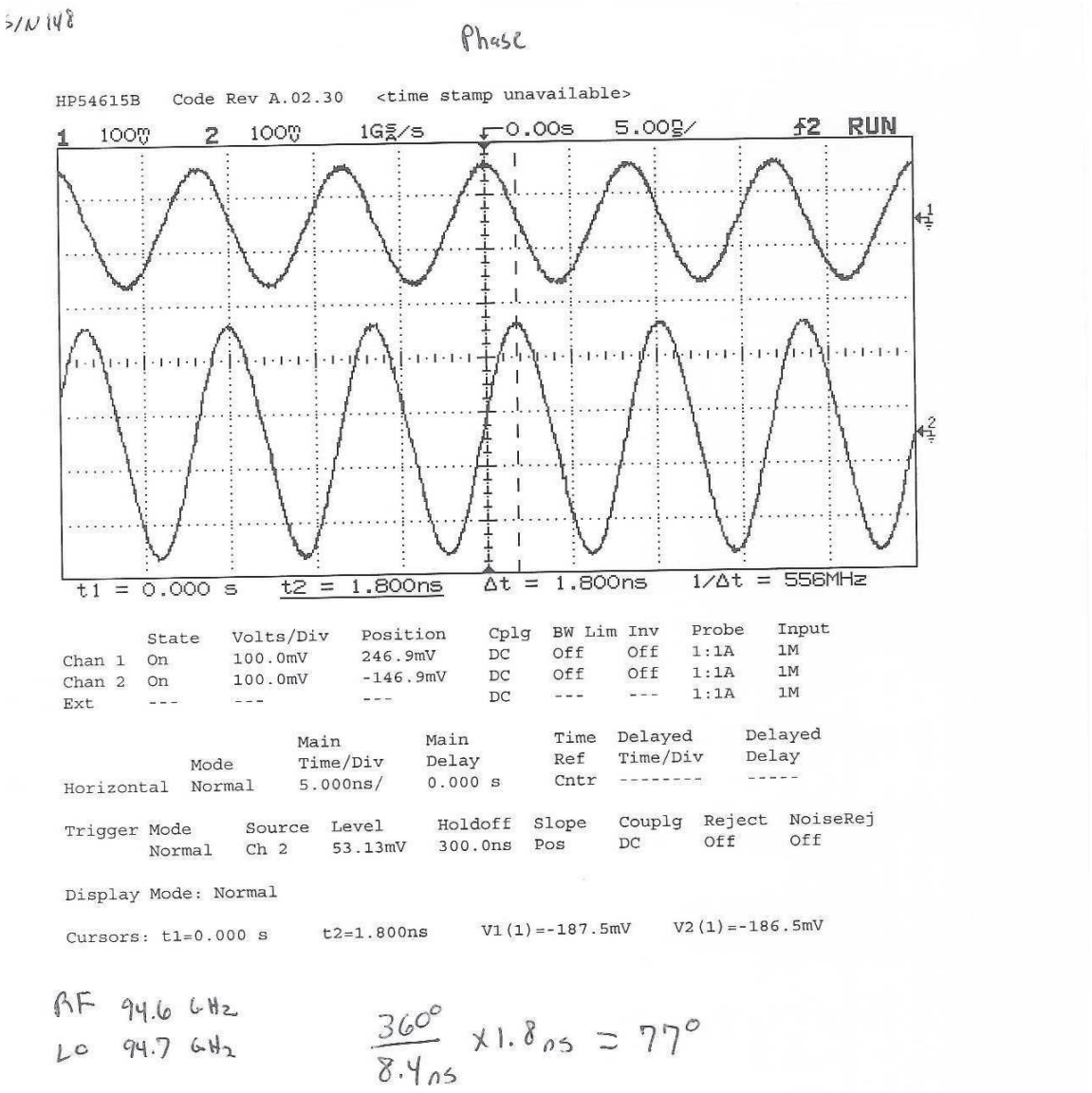

Figure A.16. Noise source phase accuracy at 94.7 GHz, provided by Millitech

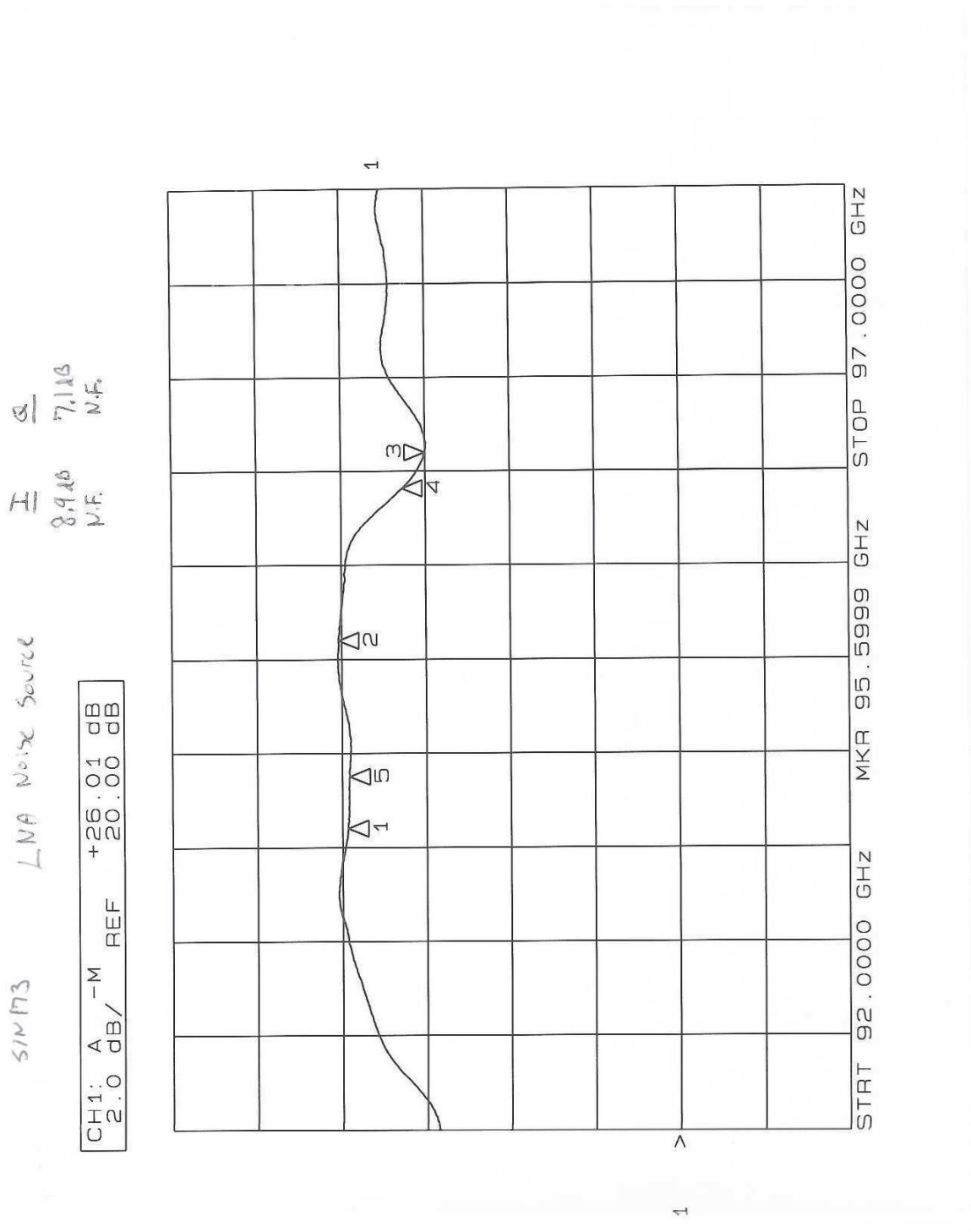

Figure A.17. Noise source gain, provided by Millitech

APPENDIX B

CORRELATOR COMPONENT SPECIFICATIONS AND LAYOUTS

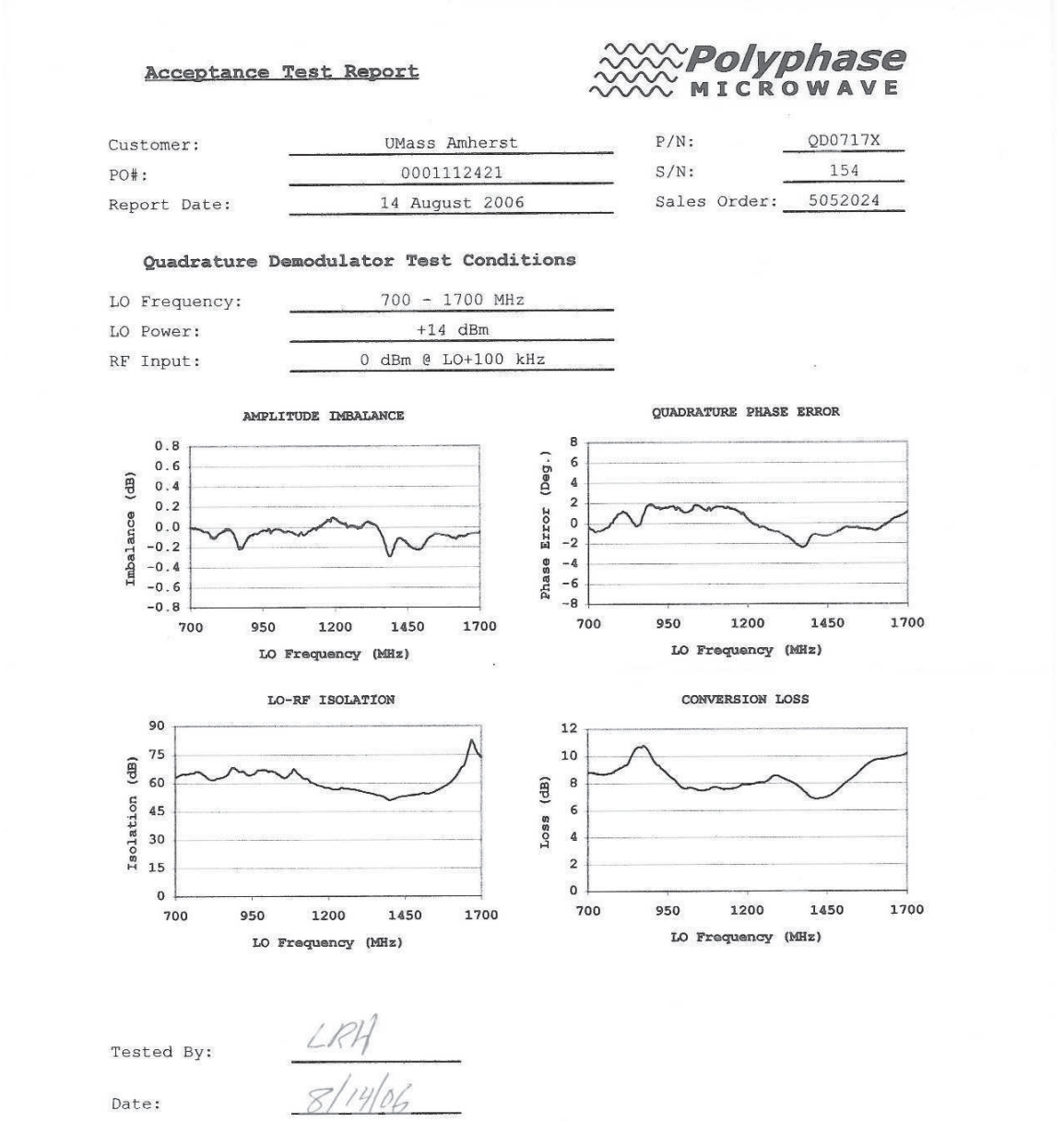

Figure B.1. QD0717XB quadrature demodulator diagram and specifications

Coaxial

Low Pass Filter

VLFX-500

DC to 500 MHz (40 dB Isolation up to 20 GHz)

Maximum Ratings

Operating Temperature	-55°C to 100°C
Storage Temperature	-55°C to 100°C
RF Power Input*	10W max. at 25°C

*Passband rating, derate linearly to 3.5W at 100°C ambient.

Features

- very good isolation, 40 dB up to 20 GHz
- 21 sections
- excellent power handling, 10W
- temperature stable LTCC internal structure
- re-entry frequency > 20 GHz
- rugged unibody construction
- protected by US patent 6,943,646

CASE STYLE: FF1118

Connectors	Model	Price	Qty.
SMA	VLFX-500-S	$39.95 ea.	(1-9)

Applications

- harmonic rejection
- transmitters/receivers
- lab use
- test instrumentation

Outline Drawing

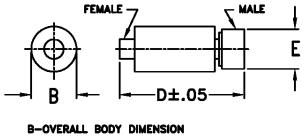

B—OVERALL BODY DIMENSION

Outline Dimensions (inch / mm)

B	D	E	wt.
.39	2.67	.312	grams
9.91	67.82	7.92	17.0

Low Pass Filter Electrical Specifications @ 25°C

MODEL NO.	PASSBAND (MHz) (Loss < 1.2dB) Max.	fco, MHz Nom (Loss 3 dB) Typ	STOPBAND (MHz) (Loss, dB) f20 Min.	STOPBAND (MHz) (Loss, dB) f40 Typ.	VSWR (:1) Stopband Typ.	VSWR (:1) Passband Typ.	NO. OF SECTIONS
VLFX-500	DC-500	750	900	1100-20000	10	1.15	21

Typical Performance Data @ 25°C

Frequency (MHz)	Insertion Loss (dB)	VSWR (:1)
50	0.29	1.06
150	0.38	1.11
375	0.71	1.10
500	0.94	1.03
575	1.17	1.13
650	1.53	1.29
750	2.70	1.39
820	7.04	1.70
900	25.98	6.19
1100	47.73	12.07
2000	73.43	33.59
3000	77.47	67.57
4000	82.46	74.00
5000	61.14	15.25
7500	70.97	19.22
10000	64.81	30.61
12500	66.48	3.65
15000	55.46	16.68
17500	69.61	10.20
20000	69.43	5.42

Functional Schematic

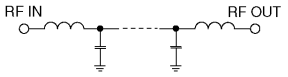

Typical Frequency Response

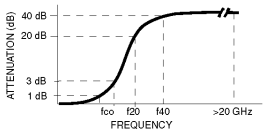

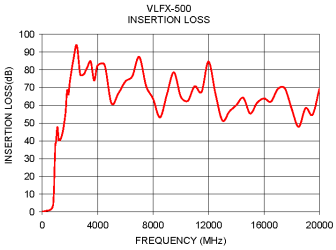

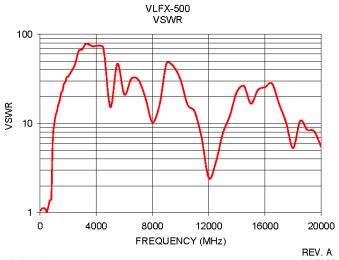

Mini-Circuits®

INTERNET http://www.minicircuits.com

P.O. Box 350166, Brooklyn, New York 11235-0003 (718) 934-4500 Fax (718) 332-4661

Distribution Centers NORTH AMERICA 800-654-7949 • 417-335-5935 • Fax 417-335-5945 • EUROPE 44-1252-832600 • Fax 44-1252-837010

Mini-Circuits ISO 9001 & ISO 14001 Certified

REV. A
M97025
VLFX-500
EDU-0399
ED-11930A/B
URJ/AD/CP
060605

Figure B.2. VLFX-500 low pass filter diagram and specifications

Coaxial

Switch

50Ω SPDT Pin Diode 10 to 2500 MHz

ZMSW-1211

CASE STYLE: JJ77

Connectors	Model	Price	Qty.
SMA	ZMSW-1211	$69.95	(1-9)

Maximum Ratings

Operating Temperature	-55°C to 100°C
Storage Temperature	-55°C to 100°C
Power	+20 dBm
Control Current	5mA

Coaxial/Pin Connections

RF IN	COM
RF OUT 1	RF-1
RF OUT 2	RF-2
CONTROL 1	1
CONTROL 2	2

Features

- wideband, 10 to 2500 MHz
- good isolation, 35 dB typ.

Applications

- VHF/UHF
- satellite communication
- antenna switching
- test set-ups

Switch Electrical Specifications

MODEL NO.	FREQ. (MHz)		INSERTION LOSS (dB)				IN-OUT ISOLATION (dB)					
			Low band lw		Upper band U		Frequency Band L		M		U	
	f_L	f_U	Typ.	Max.	Typ.	Max.	Typ.	Min.	Typ.	Min.	Typ.	Min.
ZMSW-1211	10	2500	1.1	1.9	1.9	2.7	50	45	35	28	28	22

L= low range(f_L to 10 f_L) M=mid range(10 f_L to f_U/2) lw=low band (f_L to f_U/2) U=upper range (f_U/2 to f_U)

Outline Drawing

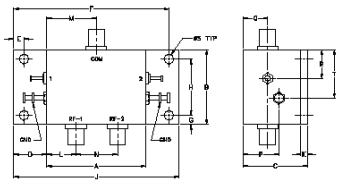

Outline Dimensions (inch / mm)

A	B	C	D	E	F	G	H	J
1.50	1.13	.97	.50	.155	2.345	.14	.850	2.50
38.10	28.70	24.64	12.70	3.94	59.56	3.56	21.59	63.50

K	L	M	N	P	Q	R	S	T	wt
.10	.44	.75	.63	.54	.37	.43	.150	.73	grams
2.54	11.18	19.05	16.00	13.72	9.40	10.92	3.81	18.54	50.0

Additional Specifications	
VSWR ("ON" STATE)	1.7 Max
SWITCHING TIME (μSEC) RISE TIME (μSEC)	4 Max. 2 Typ.
CONTROL VOLTAGE ON condition OFF condition	 +5V 0V
1 dB COMPRESSION 10 to 200 MHz Above 200 MHz	 +6 increasing to +19 dBm +19 dBm min.

LOGIC				
	CONTROL 1	CONTROL 2	RF-2	RF-1
State 1:	0V	+5V	ON	OFF
State 2:	+5V	0V	OFF	ON

Electrical Schematic

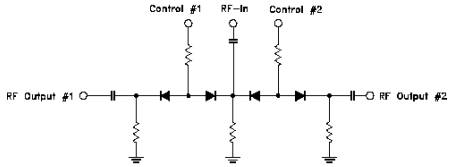

Mini-Circuits®
ISO 9001 ISO 14001 CERTIFIED

ALL-NEW minicircuits.com

P.O. Box 350166, Brooklyn, New York 11235-0003 (718) 934-4500 Fax (718) 332-4661 For detailed performance specs & shopping online see Mini-Circuits web site

The Design Engineers Search Engine Provides ACTUAL Data Instantly From MINI-CIRCUITS At: www.minicircuits.com

RF/IF MICROWAVE COMPONENTS

REV.OR
M97979
ZMSW-1211
WP/CP
070306
Page 1 of 2

Figure B.3. ZMSW-1211 SPDT switch diagram and specifications

Typical Performance Data

FREQ. (MHz)	ON INSERTION LOSS (dB) (Ctrl1 @ 0V, Ctrl 2 @5V) IN-OUT		AMP UNBALANCE (dB)		OFF ISOLATION (dB) (Ctrl1 @ 5V, Ctrl 2 @0V) IN-OUT		OFF ISOLATION (dB) DELTA		VSWR IN	VSWR OUT	VSWR OUT (RF1) OFF
	$\bar{X}$	σ	$\bar{X}$	σ	$\bar{X}$	σ	$\bar{X}$	σ	$\bar{X}$	$\bar{X}$	$\bar{X}$
10.00	1.29	0.19	0.13	0.12	88.14	5.32	5.52	5.48	1.20	1.20	27.17
20.00	1.22	0.14	0.09	0.06	80.95	3.49	5.99	5.45	1.12	1.12	25.49
50.00	1.10	0.10	0.07	0.06	66.03	2.18	0.79	0.77	1.06	1.06	26.18
100.00	1.07	0.09	0.07	0.06	56.13	2.48	0.63	1.00	1.05	1.04	24.91
200.00	1.08	0.09	0.06	0.05	47.23	1.83	0.85	0.71	1.07	1.07	24.71
409.45	1.15	0.08	0.07	0.05	40.05	1.43	0.45	0.39	1.15	1.15	23.36
500.00	1.16	0.08	0.06	0.04	38.02	1.28	0.50	0.28	1.17	1.18	22.80
672.45	1.22	0.08	0.06	0.04	35.50	1.05	0.49	0.36	1.21	1.22	21.45
863.73	1.29	0.08	0.06	0.04	33.51	0.92	0.71	0.29	1.23	1.24	19.28
1000.00	1.32	0.07	0.05	0.03	29.59	0.41	3.76	0.96	1.23	1.24	19.05
1126.73	1.30	0.08	0.06	0.05	30.50	0.46	2.81	0.52	1.22	1.25	17.59
1246.27	1.30	0.07	0.07	0.06	30.00	0.41	3.80	0.53	1.19	1.24	17.26
1389.73	1.67	0.09	0.41	0.09	29.58	0.43	1.32	1.45	1.08	1.28	15.74
1581.00	1.35	0.07	0.05	0.04	29.04	0.47	0.58	0.46	1.12	1.13	14.86
1772.27	1.39	0.08	0.05	0.05	27.59	0.59	1.64	0.77	1.08	1.09	13.60
1987.45	1.43	0.07	0.05	0.04	27.44	0.74	2.62	0.92	1.09	1.11	12.58
2178.73	1.42	0.08	0.06	0.04	27.34	0.87	3.10	1.03	1.12	1.14	14.41
2370.00	1.51	0.09	0.08	0.05	26.88	1.06	3.36	1.25	1.16	1.19	12.24
2441.73	1.51	0.08	0.07	0.04	27.35	1.15	3.49	1.39	1.16	1.20	10.69
2500.00	1.56	0.09	0.08	0.06	26.81	1.21	3.44	1.50	1.17	1.21	11.44

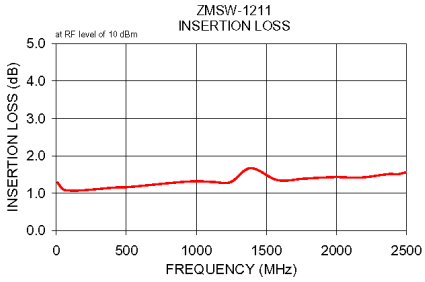

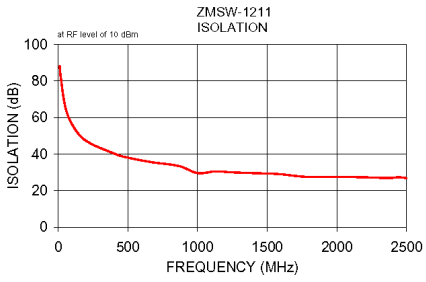

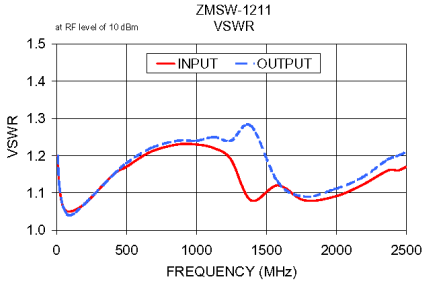

Figure B.4. ZMSW-1211 SPDT switch performance data

Coaxial

Power Splitter/Combiner

ZN2PD2-50+
ZN2PD2-50

2 Way-0° 50Ω 500 to 5000 MHz

CASE STYLE: VVV845

Connectors	Model	Price	Qty.
SMA	ZN2PD2-50-S	$74.95	(1-9)

+ RoHS compliant in accordance with EU Directive (2002/95/EC)

See our web site for RoHS Compliance methodologies and qualifications.

Maximum Ratings

Operating Temperature	-55°C to 100°C
Storage Temperature	-55°C to 100°C
Power Input (as a splitter)	10W max.
Internal Dissipation	0.25W max.

Coaxial Connections

SUM PORT	S
PORT 1	1
PORT 2	2

Features

- wideband, 500 to 5000 MHz
- excellent amplitude unbalance, 0.05 dB typ.
- excellent phase unbalance, 0.5 deg, typ.
- up to 10W power input as splitter

Applications

- UHF TV
- cellular/ISM/SMG/GSM
- satellite distribution
- GPS/L BAND (MARSAT)
- PCS/DCS/UMTS
- ISM
- MMDS
- SATCOM

Outline Drawing

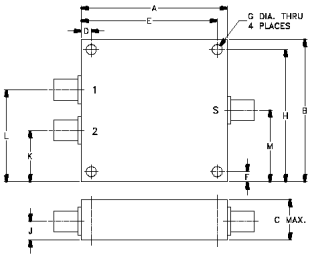

Outline Dimensions (inch / mm)

A	B	C	D	E	F	G
4.50	2.50	.67	.400	4.100	.125	.125
114.30	63.50	17.02	10.16	104.14	3.18	3.18

H	J	K	L	M	wt
2.375	.33	.75	1.75	1.25	grams
60.33	8.38	19.05	44.45	31.75	247

Splitter Electrical Specifications

FREQ. RANGE (MHz) f_L-f_U	ISOLATION (dB) Typ.	ISOLATION (dB) Min.	INSERTION LOSS (dB) ABOVE 3.0 dB Typ.	INSERTION LOSS (dB) ABOVE 3.0 dB Max.	PHASE UNBALANCE (Degrees) Max.	AMPLITUDE UNBALANCE (dB) Max.	VSWR (:1) S Typ.	VSWR (:1) OUT Typ.
500-5000	**25**	**15**	**0.8**	**1.4**	**4**	**0.5**	**1.2**	**1.1**
600-1600	24	17	0.7	1.1	2	0.3	1.2	1.1
1600-2700	26	18	0.8	1.2	3	0.3	1.2	1.1
2700-3600	28	19	0.9	1.3	3	0.4	1.2	1.1
3700-4800	22	18	0.9	1.4	4	0.5	1.2	1.1

Typical Performance Data

Frequency (MHz)	Insertion Loss (dB) S-1	Insertion Loss (dB) S-2	Amplitude Unbalance (dB)	Isolation (dB)	Phase Unbalance (deg.)	VSWR S	VSWR 1	VSWR 2
500.00	3.28	3.31	0.04	18.32	0.02	1.33	1.09	1.10
550.00	3.26	3.29	0.03	20.81	0.02	1.27	1.07	1.07
600.00	3.25	3.29	0.04	23.61	0.09	1.22	1.07	1.07
700.00	3.26	3.29	0.03	26.64	0.12	1.18	1.10	1.10
800.00	3.31	3.35	0.04	23.51	0.07	1.22	1.14	1.14
900.00	3.35	3.39	0.04	21.06	0.04	1.29	1.16	1.16
1000.00	3.70	3.74	0.03	20.52	0.12	1.33	1.14	1.15
1500.00	3.71	3.72	0.01	31.72	0.23	1.20	1.15	1.13
2000.00	3.76	3.81	0.05	24.24	0.19	1.28	1.10	1.10
2500.00	3.73	3.78	0.06	29.88	0.36	1.07	1.04	1.02
3000.00	3.79	3.83	0.04	29.70	0.48	1.16	1.10	1.11
3500.00	3.87	3.90	0.02	26.49	0.58	1.20	1.10	1.09
4000.00	3.88	3.90	0.03	27.25	0.54	1.15	1.07	1.06
4500.00	3.93	3.94	0.01	23.23	0.81	1.13	1.06	1.01
5000.00	3.66	3.62	0.04	21.19	1.03	1.09	1.26	1.15

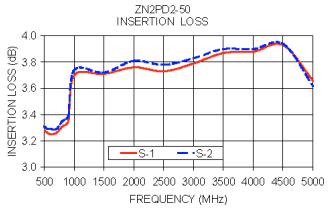

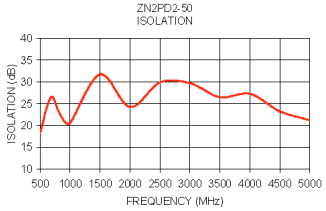

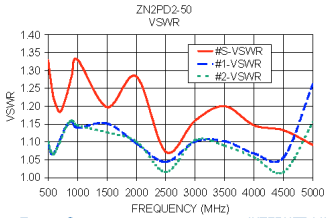

electrical schematic

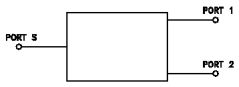

Mini-Circuits®
Distribution Centers NORTH AMERICA 800-654-7949 • 417-335-5935 • Fax 417-335-5945 • EUROPE 44-1252-832600 • Fax 44-1252-837010
INTERNET http://www.minicircuits.com
P.O. Box 350166, Brooklyn, New York 11235-0003 (718) 934-4500 Fax (718) 332-4661
Mini-Circuits ISO 9001 & ISO 14001 Certified

REV. B
M98898
ZN2PD-9G
ED-7451/1
LC/TD/CP
060209

Figure B.5. ZN2PD2-50 power divider diagram and specifications

ECLIPSE MICROWAVE

Double Balanced Mixers
J SERIES
10 MHz to 26.0 GHz

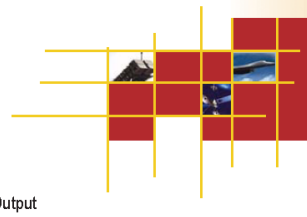

FEATURES

- Multi-Octave Bandwidth
- Broad Frequency: Input and Output
- Wide DC to IF Frequency Response
- Low Conversion Loss
- High Port-to-Port Isolations

Maximum Input Power: 250mW CW
Operating Temperature Range: -55°C to +125°C
Storage Temperature Range: -65°C to +150°C
Specification @ +25°C

Model No.	RF Frequency GHz	LO Frequency GHz	IF Frequency GHz	LO Power dBm Nom.	Conversion Loss dB Typ./Max.	L-R Isolation dB Typ./Min.	L-I Isolation dB Typ./Min.	Input 1-dB Comp. Pt. dBm Typ.	Input TOIP dBm Typ.
J0020L	.01 - 1.5	.01 - 1.5	DC - 0.6	+7	7.0/8.5	40/30	33/26	+1	+11
J0020M	.01 - 1.5	.01 - 1.5	DC - 0.6	+10	7.0/8.5	40/30	33/26	+4	+14
J0020N	.01 - 1.5	.01 - 1.5	DC - 0.6	+13	7.0/8.5	40/30	33/26	+7	+17
J0020H	.01 - 1.5	.01 - 1.5	DC - 0.6	+16	7.0/8.5	40/30	33/26	+10	+19
J1020L	1.0 - 2.0	1.0 - 2.0	DC - 1.0	+7	6.5/7.5	33/28	28/20	+1	+11
J1020M	1.0 - 2.0	1.0 - 2.0	DC - 1.0	+10	6.5/7.5	33/28	28/20	+4	+14
J1020N	1.0 - 2.0	1.0 - 2.0	DC - 1.0	+13	6.5/7.5	33/28	28/20	+7	+17
J1020H	1.0 - 2.0	1.0 - 2.0	DC - 1.0	+16	6.5/7.5	33/28	28/20	+10	+19
J2080L	2.0 - 8.0	2.0 - 8.0	DC - 2.0	+7	5.5/7.0	35/25	25/18	+1	+11
J2080M	2.0 - 8.0	2.0 - 8.0	DC - 2.0	+10	5.5/7.0	35/25	25/18	+4	+14
J2080N	2.0 - 8.0	2.0 - 8.0	DC - 2.0	+13	5.5/7.0	35/25	25/18	+7	+17
J2080H	2.0 - 8.0	2.0 - 8.0	DC - 2.0	+16	5.5/7.0	35/25	25/18	+10	+19
J2012L	2.0 - 12.0	2.0 - 12.0	DC - 2.0	+7	5.5/7.5	35/25	25/18	+1	+11
J2012M	2.0 - 12.0	2.0 - 12.0	DC - 2.0	+10	5.5/7.5	35/25	25/18	+4	+14
J2012N	2.0 - 12.0	2.0 - 12.0	DC - 2.0	+13	5.5/7.5	35/25	25/18	+7	+17
J2012H	2.0 - 12.0	2.0 - 12.0	DC - 2.0	+16	5.5/7.5	35/25	25/18	+10	+19
J2118L	2.0 - 18.0	1.8 - 18.2	DC - 0.2	+7	6.0/8.0	28/20	25/18	+1	+10
J2118M	2.0 - 18.0	1.8 - 18.2	DC - 0.2	+10	6.0/8.0	28/20	25/18	+4	+14
J2018L	2.0 - 18.0	2.0 - 18.0	DC - 0.7	+7	6.5/8.5	28/20	25/18	+1	+10
J2018M	2.0 - 18.0	2.0 - 18.0	DC - 0.7	+10	6.5/8.5	28/20	25/18	+4	+14

1. To indicate package style, add prefix to the end of the model number. (Example: Model No. J2018LB - Package "B").
2. Connectors and Spacers are standard to the parts and spacers are optional.
3. Custom operating frequency bands & power levels are available upon request.

tel 888.672.6961 fax 408.321.0160 3

Figure B.6. J2080HB and J2080LB double balanced mixer specifications

Connectorized

Amplifier

ZX60-3018G

50Ω, 20 MHz to 3 GHz

Features

- Wide Bandwidth, 20 MHz to 3 GHz
- Low Noise Figure, 2.7 dB Typ.
- Output Power,Up to 12.8 dBm Typ.
- Protected by US Patent 6,790,049

Applications

- Buffer Amplifier
- Cellular
- PCS
- Lab
- Instrumentation
- Test Equipment

CASE STYLE: GC957

Connectors	Model	Price	Qty.
SMA	ZX60-3018G-S	$49.95 ea.	(1-9)

Electrical Specifications at T_{AMB} = 25°C

MODEL NO.	FREQ. (GHz)	DC VOLTAGE @ Pin V+ (V)	GAIN over frequency in GHz Typ (dB)					MAXIMUM POWER (dBm) Output (1 dB Comp.) Typ.		DYNAMIC RANGE		VSWR (:1) Typ.		ACTIVE DIRECTIVITY (dB) Isolation-Gain	DC OPERATING CURRENT @ Pin V+ (mA)	
			0.1	1.0	2.0	3.0	Min.at 2 GHz			NF (dB)	IP3 (dBm)					
	f_L - f_U							f_L	f_U	Typ.	Typ.	In	Out	Typ.	Typ.	Max.
ZX60-3018G	0.02-3	12.0	22.8	21.9	20.3	18.8	18.0	12.8	10.2	2.7	25.0	1.3	1.4	2-6	34	45

Maximum Ratings

Operating Temperature	-45°C to 85°C
Storage Temperature	-55°C to 100°C
DC Voltage	12.5V
Input Power(no Damage)	13dBm
Power	0.7W

Outline Drawing

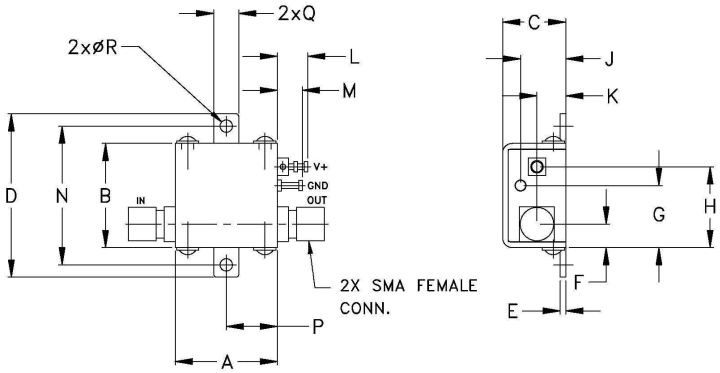

Outline Dimensions (inch / mm)

A	B	C	D	E	F	G	H	J	K	L	M	N	P	Q	R	wt.
.74	.75	.46	1.18	.04	.17	.45	.59	.33	.21	.22	.18	1.00	0.37	.18	.09	grams
18.8	19.1	11.6	30.0	1.0	4.3	11.4	14.9	8.3	5.3	5.6	4.6	25.4	9.4	4.6	2.3	23.0

Mini-Circuits®
Distribution Centers NORTH AMERICA 800-654-7949 • 417-335-5935 • Fax 417-335-5945 • EUROPE 44-1252-832600 • Fax 44-1252-837010
INTERNET http://www.minicircuits.com
P.O. Box 350166, Brooklyn, New York 11235-0003 (718) 934-4500 Fax (718) 332-4661
Mini-Circuits ISO 9001 & ISO 14001 Certified

REV.OR
M97089
EDR-6178/4
ZX60-3018G
RAV
060122
page 1 of 2

Figure B.7. ZX60-3018G amplifier diagram and specifications

Typical Performance Data & Curves at 25°C ZX60-3018G

FREQUENCY (MHz)	GAIN (dB)	DIRECTIVITY (dB)	VSWR IN (:1)	VSWR OUT (:1)	POWER OUT @1dB COMPRESSION (dBm)	IP3 (dBm)	NF (dB)
20	22.58	2.30	1.16	1.32	12.80	25.61	2.92
50	22.75	2.12	1.15	1.27	13.05	25.87	2.66
100	22.76	2.00	1.15	1.25	12.94	25.89	2.61
351	22.61	2.22	1.18	1.27	12.92	25.39	2.69
500	22.42	2.36	1.21	1.29	12.94	25.26	2.72
663	22.28	2.61	1.25	1.33	12.88	25.39	2.66
866	21.83	3.17	1.30	1.33	12.73	25.67	2.69
1000	21.83	3.03	1.31	1.39	12.76	25.66	2.64
1168	21.52	3.35	1.34	1.42	12.69	25.66	2.60
1378	21.16	3.74	1.38	1.46	12.51	25.64	2.59
1500	20.97	3.85	1.40	1.47	12.41	25.45	2.59
1671	20.60	4.23	1.41	1.47	12.15	25.80	2.60
1863	20.39	4.54	1.40	1.50	12.16	25.64	2.62
2000	20.22	4.66	1.40	1.51	11.89	25.08	2.63
2174	20.04	4.83	1.40	1.51	11.72	24.67	2.62
2376	19.76	5.15	1.39	1.49	11.39	23.90	2.61
2500	19.56	5.46	1.38	1.48	11.25	23.54	2.58
2668	19.26	5.50	1.37	1.48	10.65	22.94	2.60
2879	18.97	5.83	1.35	1.46	10.42	22.62	2.61
3000	18.78	6.14	1.34	1.45	10.09	22.36	2.64

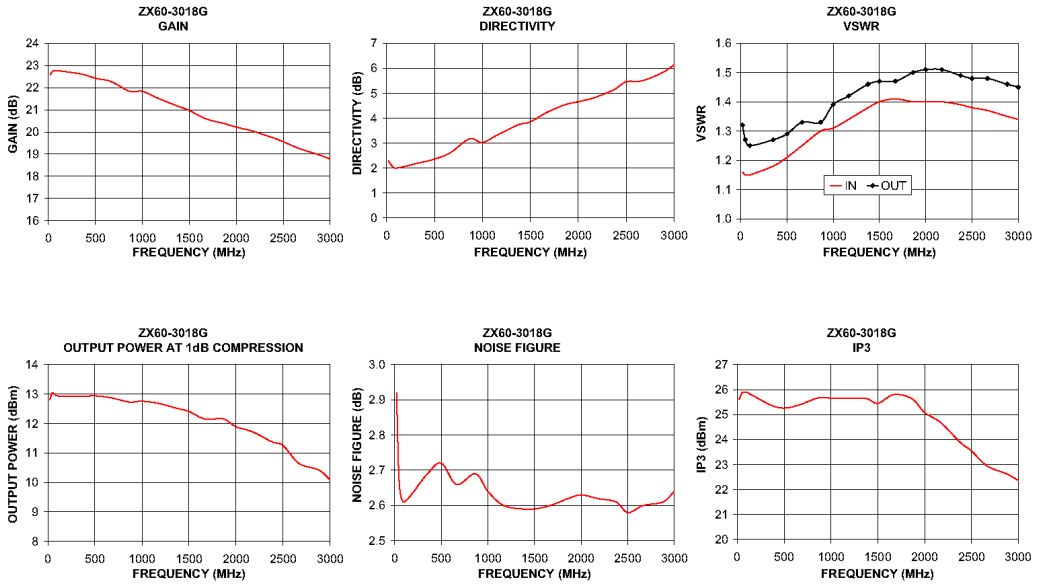

Figure B.8. ZX60-3018G amplifier performance data

Connectorized

Amplifier

ZX60-4016E+

50Ω, 20 MHz to 4 GHz

Features

- Wide Bandwidth, 20 MHz to 4 GHz
- Low Noise Figure, 3.9 dB Typ.
- Output Power,Up to 17.4 dBm Typ.
- Protected by US Patent 6,790,049

Applications

- Cellular
- PCS
- Communication Receivers & Transmitters
- Lab
- Instrumentation
- Test Equipment

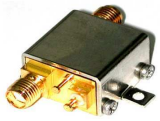

CASE STYLE: GC957

Connectors	Model	Price	Qty.
SMA	ZX60-4016E-S+	$49.95 ea.	(1-9)

+ RoHS compliant in accordance with EU Directive (2002/95/EC)

The +suffix has been added in order to identify RoHS Compliance. See our web site for RoHS Compliance methodologies and qualifications.

Electrical Specifications at T_{AMB} = 25°C

MODEL NO.	FREQ. (GHz) f_L - f_U	DC VOLTAGE @ Pin V+ (V)	GAIN over frequency in GHz Typ (dB) 0.1	1.0	2.0	3.0	4.0	Min.at 2 GHz	MAXIMUM POWER (dBm) Output (1 dB Comp.) Typ. f_L	f_U	DYNAMIC RANGE NF (dB) Typ.	IP3 (dBm) Typ.	VSWR (:1) Typ. In f_L-3 GHz	3-f_U GHz	Out f_L-3 GHz	3-f_U GHz	ACTIVE DIRECTIVITY (dB) Isolation-Gain Typ.	DC OPERATING CURRENT @ Pin V+ (mA) Typ.	Max.
ZX60-4016E+	0.02 - 4	12.0	20.1	19.5	18.2	16.5	14.9	15.7	17.4	14.5	3.9	30.0	1.25	1.3	1.3	1.2	3-6	64	75

Maximum Ratings

Operating Temperature	-45°C to 80°C case
Storage Temperature	-55°C to 100°C
DC Voltage	12.5V
Input Power(no Damage)	13dBm
Power	950mW

Outline Drawing

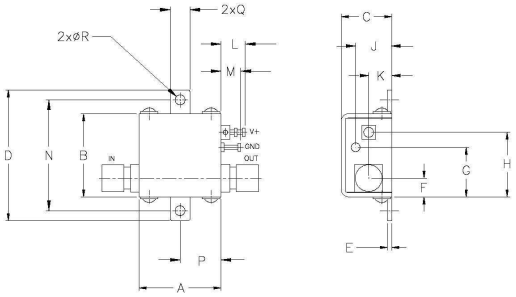

Outline Dimensions (inch / mm)

A	B	C	D	E	F	G	H	J	K	L	M	N	P	Q	R	wt.
.74	.75	.46	1.18	.04	.17	.45	.59	.33	.21	.22	.18	1.00	.37	.18	.09	grams
18.80	19.05	11.68	29.97	1.02	4.32	11.43	14.99	8.38	5.33	5.59	4.57	25.40	9.40	4.57	2.29	23.0

Mini-Circuits®
ISO 9001 ISO 14001 CERTIFIED
ALL NEW minicircuits.com
P.O. Box 350166, Brooklyn, New York 11235-0003 (718) 934-4500 Fax (718) 332-4661 For detailed performance specs & shopping online see Mini-Circuits web site
The Design Engineers Search Engine Provides ACTUAL Data Instantly From MINI-CIRCUITS At: www.minicircuits.com
RF/IF MICROWAVE COMPONENTS
REV. A
M108294
EDR-6177/2
ZX60-4016E+
RAV/URJ
070613
page 1 of 2

Figure B.9. ZX60-4016E amplifier diagram and specifications

Typical Performance Data & Curves at 25°C ZX60-4016E+

FREQUENCY (MHz)	GAIN (dB)	DIRECTIVITY (dB)	VSWR IN (:1)	VSWR OUT (:1)	POWER OUT @1dB COMPRESSION (dBm)	IP3 (dBm)	NF (dB)
20	19.93	3.47	1.31	1.41	17.64	31.98	3.78
50	20.09	3.11	1.28	1.34	17.89	32.36	3.64
100	20.14	2.99	1.28	1.31	17.93	32.64	3.51
250	20.10	3.04	1.29	1.30	17.97	32.89	3.65
500	19.94	3.13	1.27	1.28	17.94	32.28	3.73
750	19.83	3.21	1.26	1.27	17.84	32.03	3.81
1000	19.54	3.35	1.22	1.24	17.95	32.66	3.82
1250	19.34	3.57	1.19	1.20	17.61	31.91	3.66
1500	18.96	3.59	1.18	1.18	17.68	31.35	3.86
1750	18.56	3.80	1.18	1.16	17.83	31.57	3.78
2000	18.24	4.02	1.21	1.11	17.68	31.24	3.97
2250	17.85	4.38	1.25	1.07	17.56	31.10	3.93
2500	17.42	4.75	1.30	1.04	17.40	30.48	4.01
2750	16.94	4.97	1.35	1.02	16.95	29.71	3.96
3000	16.51	5.37	1.40	1.04	16.20	29.86	4.09
3250	15.94	5.45	1.43	1.05	15.82	28.85	4.29
3500	15.68	5.86	1.47	1.08	15.45	27.57	4.36
3700	15.34	6.00	1.48	1.09	14.94	28.90	4.41
3900	15.07	6.03	1.46	1.10	14.53	27.18	4.46
4000	14.93	5.98	1.48	1.09	14.35	27.84	4.45

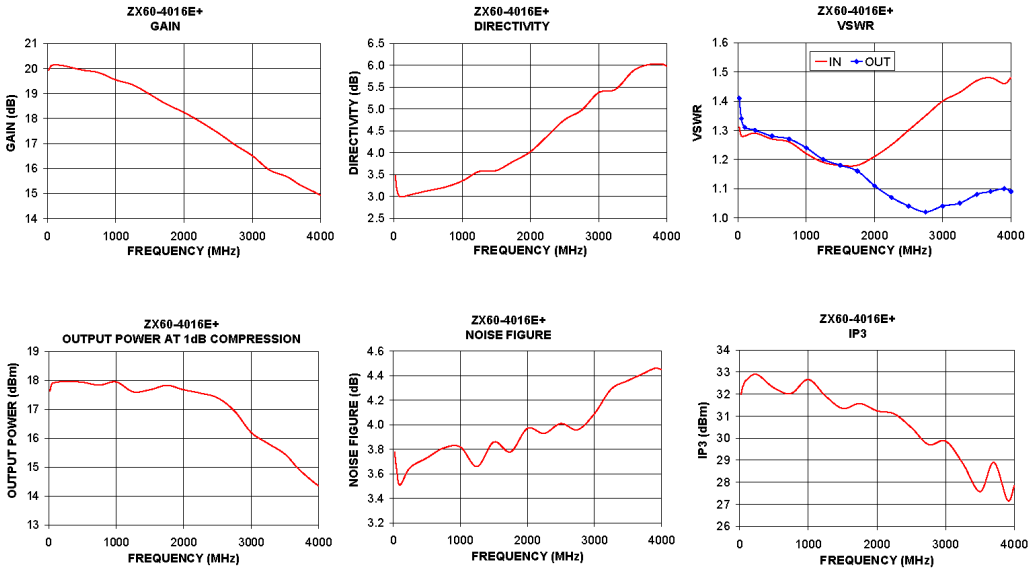

Figure B.10. ZX60-4016E amplifier performance data

Coaxial

Amplifier

ZX60-5916M+

50Ω High Isolation 1.5 to 5.9 GHz

CASE STYLE: GC957

Connectors	Model	Price	Qty.
SMA	ZX60-5916M-S+	$59.95 ea.	(1-9)

+ RoHS compliant in accordance with EU Directive (2002/95/EC)

The +Suffix has been added in order to identify RoHS Compliance. See our web site for RoHS Compliance methodologies and qualifications.

Features

- from 2.8V to 5V operation
- wide bandwidth, 1.5 to 5.9 GHz
- high active directivity, 25 dB typ.
- output power, up to 14.5 dBm typ.
- protected by US patent 6,790,049

Applications

- buffer amplifier
- LO amplifiers for mixers
- cellular
- PCN

Electrical Specifications T_{AMB}=25°C

MODEL NO.	FREQ. (GHz)		DC VOLTS (V)	GAIN, dB Typical over frequency, GHz						MAXIMUM POWER (dBm) Output (1 dB Comp.) Typ.			DYNAMIC RANGE NF (dB) Typ.		IP3 (dBm) Typ.		VSWR (:1) Typ.		ACTIVE DIRECTIVITY (dB) (Isolation-Gain)	DC OPERATING CURRENT @ Pin V+ (mA)	
				1.5	2.0	3.5	5.0	5.9	Min. at 2 GHz			Input (no damage)	at 2 GHz		at 2 GHz	at 5.9 GHz	In	Out		Typ	Max.
	f_L	f_U								f_L	f_U								Typ		
ZX60-5916M+	1.5	5.9	5.0	17.0	17.7	17.2	18.0	13.8	15.5	14.5	15.7	10	6.4	28.3	28.9		2.2	1.2	20	73	96
			2.8	13.6	14.6	14.7	16.5	11.5	—	11.5	12.8	10	7.0	23.5	23.5		2.5	1.4	25	66	—

Maximum Ratings

Operating Temperature	-40°C to 85°C case
Storage Temperature	-55°C to 100°C
DC Voltage	7V
Input Power(no damage)	10 dBm
Power	500mW

Outline Drawing

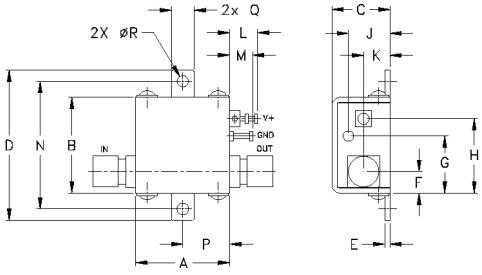

Outline Dimensions (inch / mm)

A	B	C	D	E	F	G	H	J	K	L	M	N	P	Q	R	wt
.74	.75	.46	1.18	.04	.17	.45	.59	.33	.21	.22	.18	1.00	.37	.18	.09	grams
18.80	19.05	11.68	29.97	1.02	4.32	11.43	14.99	8.38	5.33	5.59	4.57	25.40	9.40	4.57	2.29	23.0

REV. B
M98898
ZX60-5916M
EDR-6128
RVN/TD/CP/AM
070330

Figure B.11. ZX60-5916M amplifier diagram and specifications

FREQUENCY (MHz)	GAIN (dB)		DIRECTIVITY (dB)		VSWR IN (:1)		VSWR OUT (:1)		NOISE FIGURE (dB)		POUT at 1 dB COMPR. (dBm)	
	2.8V	5V	2.8V	5V	2.8V	5V	2.8V	5V	2.8V	5V	2.8V	5V
1500.00	13.96	17.17	56.17	43.10	4.75	4.59	1.54	1.44	8.59	7.95	10.65	14.88
2000.00	14.62	17.57	35.49	34.05	3.07	2.81	1.58	1.34	7.15	6.49	11.19	14.69
2500.00	14.52	17.17	29.52	27.98	2.51	2.30	1.52	1.22	6.77	6.09	10.47	14.40
3000.00	14.58	16.96	25.18	24.90	2.27	2.13	1.46	1.19	6.12	5.53	10.98	14.19
3500.00	14.72	17.05	22.78	22.37	2.15	2.11	1.38	1.17	6.18	5.62	10.71	13.82
4000.00	14.85	17.27	20.93	20.39	2.06	2.11	1.29	1.14	5.87	5.44	10.50	13.47
4400.00	15.50	17.75	19.31	19.04	1.97	2.05	1.23	1.14	5.40	5.02	10.55	13.15
5000.00	16.48	18.04	17.36	17.44	2.02	2.00	1.24	1.15	5.44	5.21	11.39	13.79
5600.00	14.10	15.78	18.86	18.78	1.83	1.70	1.24	1.33	5.04	4.91	12.10	14.60
5900.00	11.72	13.97	21.38	20.13	1.74	1.61	1.25	1.33	5.82	5.29	11.27	14.99

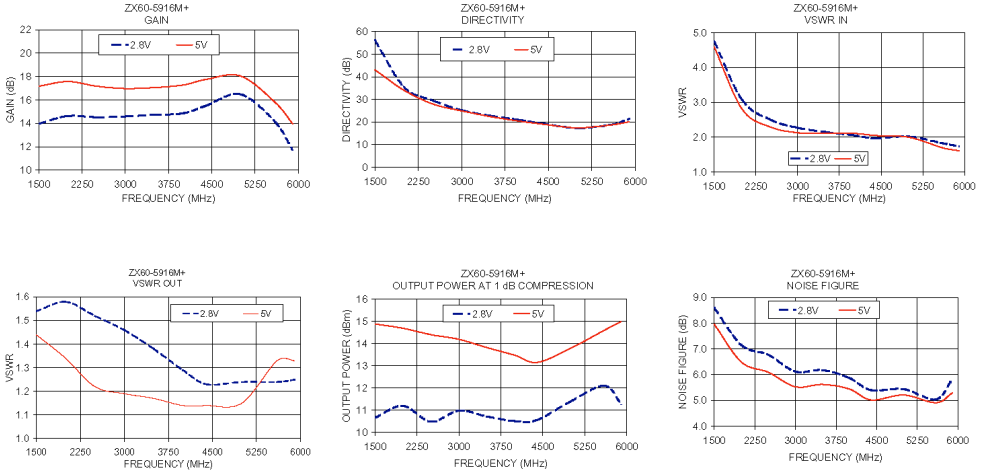

Figure B.12. ZX60-5916M amplifier performance data

Connectorized

Amplifier

ZX60-6013E+
ZX60-6013E

50Ω, 20 MHz to 6 GHz

CASE STYLE: GC957

Features
- Wide Bandwidth, 20 MHz to 6 GHz
- Low Noise Figure, 3.3 dB Typ.
- Protected by US Patent 6,790,049

Applications
- Buffer Amplifier
- Cellular
- PCS
- Lab
- Instrumentation
- Test Equipment

Connectors	Model	Price	Qty.
SMA	ZX60-6013E-S+	$49.95 ea.	(1-9)
SMA	ZX60-6013E-S	$49.95 ea.	(1-9)

+ RoHS compliant in accordance with EU Directive (2002/95/EC)

The + suffix identifies RoHS Compliance. See our web site for RoHS Compliance methodologies and qualifications.

Electrical Specifications at T_{AMB} = 25°C

MODEL NO.	FREQ. (GHz) f_L- f_U	DC VOLTAGE @ Pin V+ (V)	GAIN over frequency in GHz Typ (dB) 0.1	1.0	2.0	3.0	4.0	5.0	6.0	Min.at 2 GHz	MAXIMUM POWER (dBm) Output (1 dB Comp.) Typ. f_L	f_U	DYNAMIC RANGE NF (dB) Typ.	IP3 (dBm) Typ.	VSWR (:1) Typ. In f_L-3 GHz	In 3-f_U GHz	Out f_L-3 GHz	Out 3-f_U GHz	ACTIVE DIRECTIVITY (dB) Isolation-Gain Typ.	DC OPERATING CURRENT @ Pin V+ (mA) Typ.	Max.
ZX60-6013E(+)	0.02-6	12.0	16.2	15.9	15.2	14.3	13.4	12.7	12.1	13.0	13.4	5.8	3.3	28.7	1.4	1.6	1.2	1.2	3-9	39	50

Maximum Ratings

Operating Temperature	-45°C to 85°C
Storage Temperature	-55°C to 100°C
DC Voltage	12.5V
Input Power(no Damage)	15dBm
Power	650mW

Outline Drawing

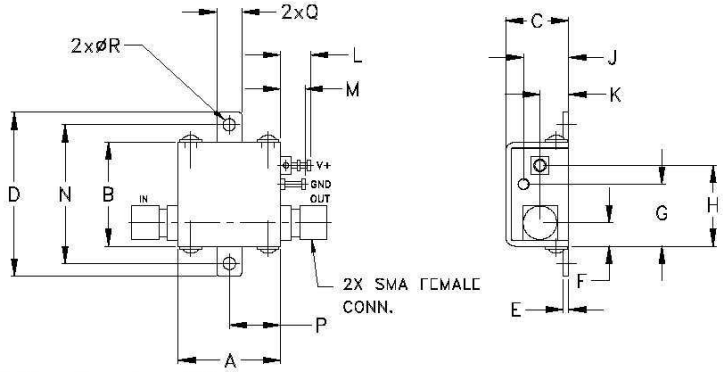

Outline Dimensions (inch / mm)

A	B	C	D	E	F	G	H	J	K	L	M	N	P	Q	R	wt.
.74	.75	.46	1.18	.04	.17	.45	.59	.33	.21	.22	.18	1.00	0.37	.18	.09	grams
18.8	19.1	11.6	30.0	1.0	4.3	11.4	14.9	8.3	5.3	5.6	4.6	25.4	9.4	4.6	2.3	23.0

Mini-Circuits®
Distribution Centers NORTH AMERICA 800-654-7949 • 417-335-5935 • Fax 417-335-5945 • EUROPE 44-1252-832600 • Fax 44-1252-837010
INTERNET http://www.minicircuits.com
P.O. Box 350166, Brooklyn, New York 11235-0003 (718) 934-4500 Fax (718) 332-4661
Mini-Circuits ISO 9001 & ISO 14001 Certified
REV B
M98888
EDR-6286
ZX60-6013E
RAV/URJ
060702
page 1 of 2

Figure B.13. ZX60-6013E amplifier diagram and specifications

Typical Performance Data & Curves at 25°C

ZX60-6013E+
ZX60-6013E

FREQUENCY (MHz)	GAIN (dB)	DIRECTIVITY (dB)	VSWR IN (:1)	VSWR OUT (:1)	POWER OUT @1dB COMPRESSION (dBm)	IP3 (dBm)	NF (dB)
20	16.09	3.60	1.24	1.03	13.24	29.97	3.33
50	16.28	3.33	1.21	1.08	13.28	29.96	3.27
100	16.31	3.24	1.20	1.10	13.35	29.95	3.20
500	16.20	3.40	1.22	1.11	13.61	29.73	3.26
1000	15.94	3.73	1.27	1.12	13.50	29.20	3.16
1500	15.60	4.12	1.38	1.14	13.22	28.42	3.27
2000	15.22	4.54	1.48	1.18	12.87	27.42	3.35
2500	14.76	5.59	1.57	1.21	12.45	26.23	3.20
3000	14.24	6.08	1.59	1.22	11.90	24.91	3.11
3220	14.11	6.22	1.57	1.25	11.60	24.28	3.32
3500	13.85	6.78	1.54	1.22	11.16	23.48	3.42
3670	13.72	6.91	1.55	1.22	10.86	22.97	3.36
3850	13.52	7.28	1.53	1.23	10.51	22.43	3.25
4000	13.37	7.13	1.51	1.22	10.21	21.98	3.21
4200	13.15	7.35	1.69	1.15	9.78	21.37	3.10
4500	13.05	7.95	1.68	1.13	9.10	20.45	3.04
5000	12.62	8.79	1.60	1.05	7.93	18.92	3.16
5500	12.33	8.81	1.51	1.07	6.81	17.44	3.19
5750	12.18	9.27	1.45	1.12	6.30	16.72	3.22
6000	12.06	9.18	1.39	1.19	5.81	16.04	3.21

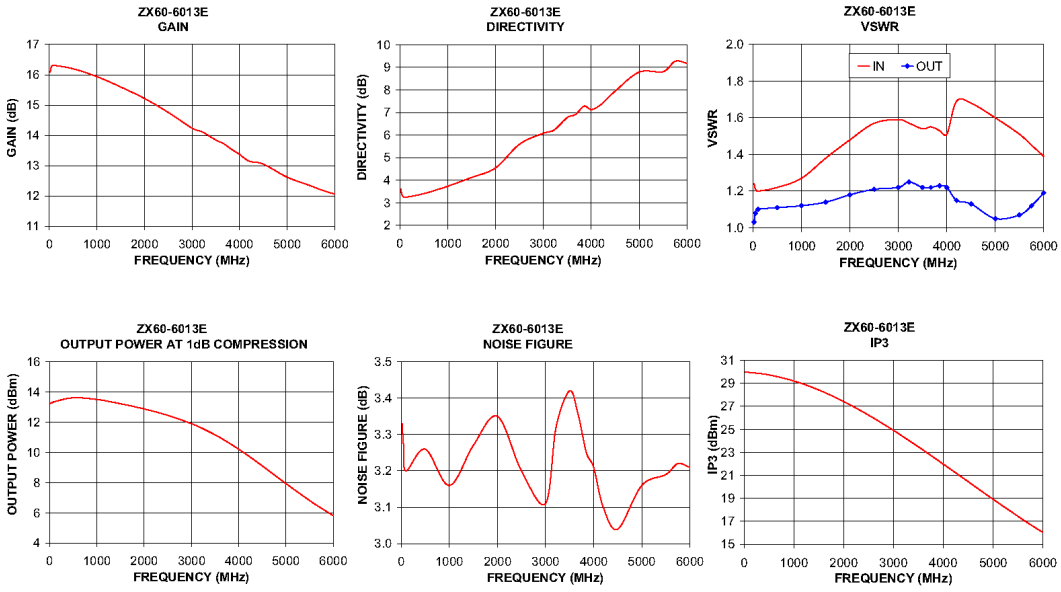

Figure B.14. ZX60-6013E amplifier performance data

Coaxial

Voltage Controlled Oscillator ZX95-1600W

Linear Tuning 800 to 1600 MHz

Features

- Low Phase Noise
- Wide Bandwidth
- Low Pushing
- Protected by US Patent 6,790,049

Applications

- R & D
- Lab
- Instrumentation
- Test Equipment

CASE STYLE: GB956

Connectors	Model	Price	Qty.
SMA	ZX95-1600W-S	$44.95 ea.	(1-9)

Electrical Specifications

MODEL NO.	FREQ. (MHz)		POWER OUTPUT (dBm)	PHASE NOISE dBc/Hz SSB at offset frequencies,KHz Typ.				TUNING					NON HARMONIC SPURIOUS (dBc)	HARMONICS (dBc)		PULLING pk-pk @ 12 dBr (MHz)	PUSHING (MHz/V)	DC OPERATING POWER	
								VOLTAGE RANGE (V)		SENSI-TIVITY (MHz/V)	PORT CAP (pF)	3 dB MODULATION BANDWIDTH (MHz)						Vcc (volts)	Current (mA) Max.
	Min.	Max.	Typ.	1	10	100	1000	Min.	Max.	Typ.	Typ.	Typ.	Typ.	Typ.	Max.	Typ.	Typ.		
ZX95-1600W	800	1600	9.0	-72	-99	-122	-143	0.5	24.0	35.0-58.0	210	90.0	-90	-22.0	-15.0	10.0	0.3	11.5	35

Maximum Ratings

Operating Temperature	-55°C to 85°C
Storage Temperature	-55°C to 100°C
Absolute Max. Supply Voltage (Vcc)	12V
Absolute Max. Tuning Voltage (Vtune)	24V
All specifications	50 ohm system

Outline Drawing

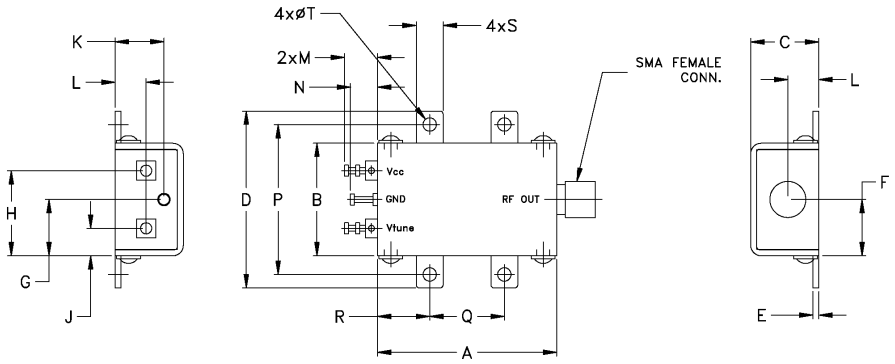

Outline Dimensions (inch / mm)

A	B	C	D	E	F	G	H	J	K	L	M	N	P	Q	R	S	T	wt.
1.20	.75	.46	1.18	.04	.38	.45	.57	.18	.33	.21	.22	.18	1.00	.50	.35	.18	.09	grams
30.50	19.10	11.6	30.0	1.0	9.6	11.4	14.5	4.7	8.3	5.3	5.6	4.6	25.4	12.7	8.9	4.6	2.3	35.0

Mini-Circuits®
Distribution Centers NORTH AMERICA 800-654-7949 • 417-335-5935 • Fax 417-335-5945 • EUROPE 44-1252-832600 • Fax 44-1252-837010
INTERNET http://www.minicircuits.com
P.O. Box 350166, Brooklyn, New York 11235-0003 (718) 934-4500 Fax (718) 332-4661
Mini-Circuits ISO 9001 & ISO 14001 Certified
REV. OR
M96760
ED/R 7307/3
ZX95-1600W
RAV/URJ
060220
page 1 of 2

Figure B.15. ZX95-1600W voltage controlled oscillator diagram and specifications

Performance Data & Curves*

ZX95-1600W

V TUNE	TUNING SENS (MHz/V)	FREQUENCY (MHz)			POWER OUTPUT (dBm)			Icc (mA)	HARMONICS (dBc)			FREQ. PUSHING (MHz/V)	FREQ. PULLING (MHz)	PHASE NOISE (dBc/Hz) at offsets				FREQ OFFSET (kHz)	PHASE NOISE at 1200 MHz (dBc/Hz)
		-55°C	+25°C	+85°C	-55°C	+25°C	+85°C		F2	F3	F4			1 kHz	10 kHz	100 kHz	1 MHz		
0.0	74.6	645.6	627.3	607.1	9.8	9.5	9.3	26	-36.7	-26.1	-35.5	0.19	9.36	-70.9	-93.9	-114.2	-134.1	1.00	-70.6
1.0	57.9	712.9	697.1	680.3	9.7	9.4	9.2	26	-37.8	-25.2	-36.2	0.28	9.86	-73.3	-95.6	-116.3	-136.2	2.00	-80.4
2.0	51.2	768.0	752.8	737.4	9.7	9.4	8.9	26	-30.7	-24.4	-39.3	0.28	7.48	-73.6	-97.5	-117.7	-138.1	3.50	-87.0
3.0	49.5	818.7	803.6	788.2	9.8	9.3	8.9	26	-28.1	-24.4	-44.6	0.31	4.04	-74.0	-98.0	-118.7	-138.5	6.00	-92.8
6.0	50.5	967.4	951.1	935.6	10.0	9.4	8.9	26	-22.4	-24.4	-48.5	0.25	6.96	-73.7	-100.5	-121.0	-141.3	8.50	-96.2
7.0	53.7	1019.3	1002.3	986.5	10.2	9.5	9.0	26	-21.5	-25.8	-46.1	0.26	4.60	-71.8	-98.9	-121.2	-141.6	10.00	-98.2
8.0	56.2	1073.6	1056.0	1039.9	10.0	9.5	8.9	26	-21.0	-28.9	-43.2	0.31	11.82	-72.3	-99.5	-122.1	-142.7	20.80	-105.4
10.0	58.2	1188.8	1170.3	1154.1	10.2	9.4	8.8	26	-20.7	-34.6	-39.1	0.22	4.90	-69.6	-97.9	-122.2	-143.5	35.50	-112.4
12.0	52.7	1300.1	1282.7	1267.6	9.9	9.1	8.3	26	-20.6	-32.4	-38.2	0.16	4.98	-69.3	-97.5	-122.1	-144.2	60.70	-116.9
13.0	49.4	1350.5	1334.4	1320.5	9.8	8.8	8.3	26	-21.0	-31.3	-42.1	0.27	4.15	-69.9	-98.1	-122.4	-144.4	86.70	-120.9
15.0	43.2	1443.5	1429.0	1416.2	9.0	8.3	7.6	26	-21.4	-30.8	-41.1	0.28	6.53	-71.1	-98.8	-122.9	-145.2	100.00	-122.0
16.0	41.9	1486.4	1472.0	1459.5	8.9	8.0	7.4	26	-21.8	-30.5	-43.1	0.25	6.92	-72.2	-98.9	-123.3	-145.3	211.60	-129.5
18.0	37.9	1565.8	1551.9	1539.7	8.2	7.5	7.0	26	-22.7	-30.0	-46.7	0.17	6.33	-75.3	-100.1	-123.6	-144.8	361.50	-134.6
19.0	35.2	1602.7	1589.3	1577.1	8.0	7.3	6.7	26	-24.3	-29.9	-48.1	0.11	6.85	-72.2	-99.8	-123.2	-145.2	507.50	-137.7
21.0	30.7	1669.7	1656.2	1644.3	7.6	6.8	6.5	26	-27.0	-30.0	-47.1	0.04	7.26	-71.6	-99.6	-123.3	-144.6	600.00	-139.2
22.0	29.1	1699.9	1686.7	1674.6	7.3	6.6	6.3	26	-28.2	-30.2	-46.4	0.01	8.49	-72.4	-100.3	-123.5	-144.4	851.60	-142.4
24.0	25.9	1754.6	1741.4	1729.6	6.8	6.3	5.8	26	-30.2	-32.3	-47.6	0.02	8.26	-74.2	-101.0	-123.5	-144.2	1000.00	-143.6

*at 25°C unless mentioned otherwise

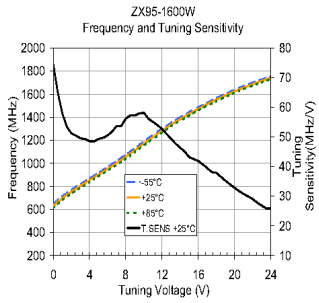

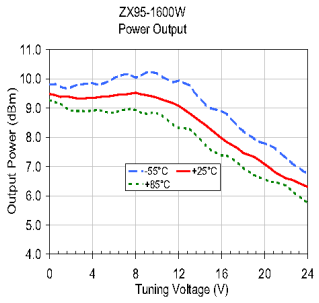

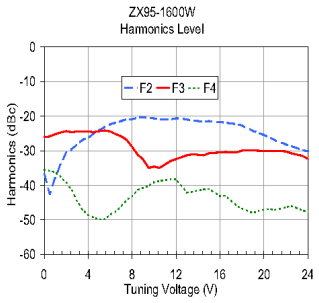

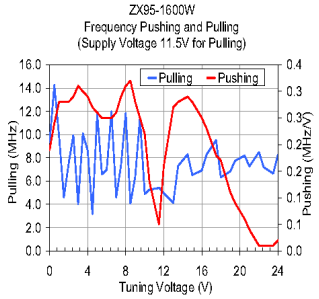

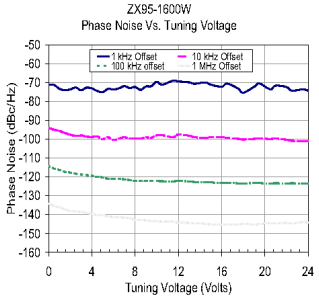

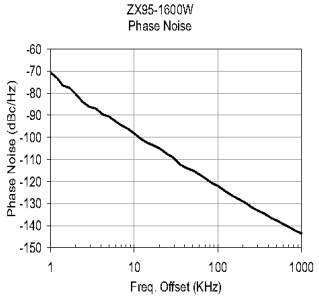

Mini-Circuits®
INTERNET http://www.minicircuits.com
P.O. Box 350166, Brooklyn, New York 11235-0003 (718) 934-4500 Fax (718) 332-4661
Distribution Centers NORTH AMERICA 800-654-7949 • 417-335-5935 • Fax 417-335-5945 • EUROPE 44-1252-832600 • Fax 44-1252-837010
Mini-Circuits ISO 9001 & ISO 14001 Certified

Figure B.16. ZX95-1600W voltage controlled oscillator performance datas

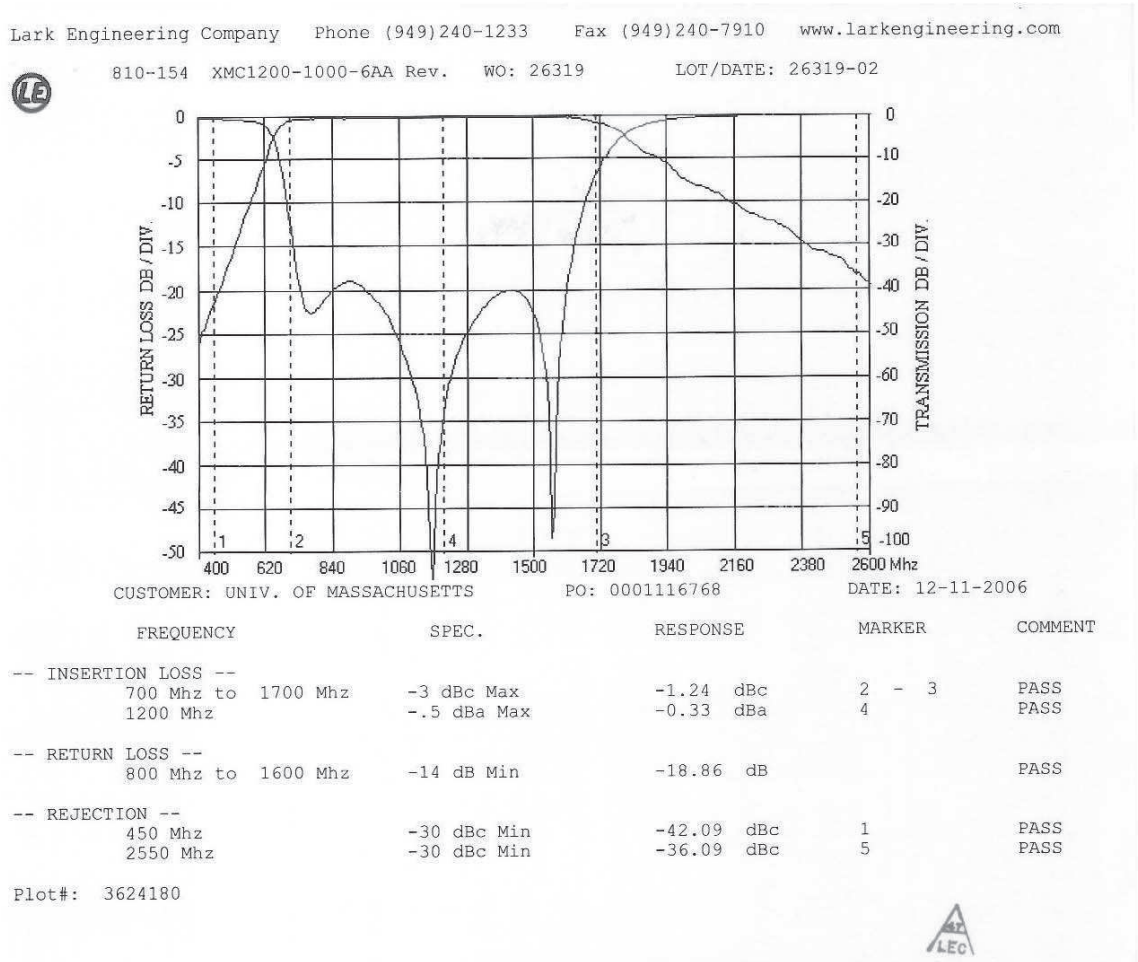

Figure B.17. Return loss and instertion loss of 1.2 GHz bandpass filter

Lark Engineering Company Phone (949)240-1233 Fax (949)240-7910 www.larkengineering.com

810-155 XMC3000-1000-3AA Rev. -- WO: 26320 LOT/DATE: 26320-02

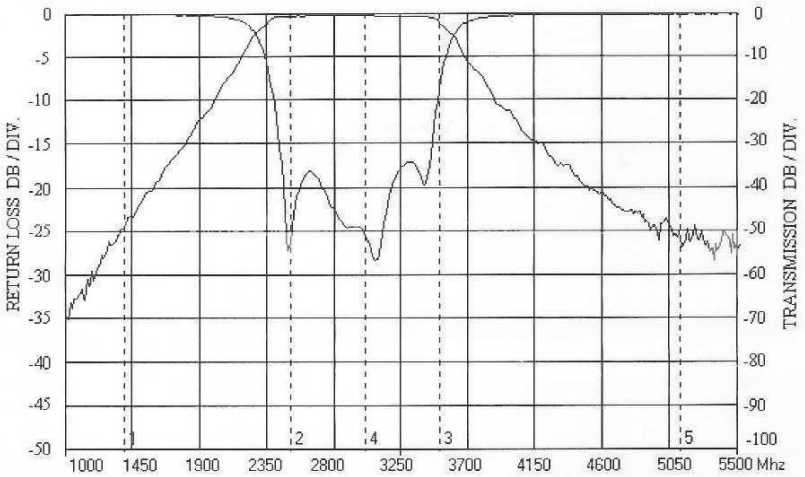

CUSTOMER: UNIV. OF MASSACHUSETTS PO: 0001116768 DATE: 12-07-2006

FREQUENCY	SPEC.	RESPONSE	MARKER	COMMENT
-- INSERTION LOSS --				
2500 Mhz to 3500 Mhz	-3 dBc Max	-1.23 dBc	2 - 3	PASS
3000 Mhz	-.6 dBa Max	-0.43 dBa	4	PASS
-- RETURN LOSS --				
2650 Mhz to 3350 Mhz	-14 dB Min	-17.05 dB		PASS
-- REJECTION --				
1400 Mhz	-30 dBc Min	-47.79 dBc	1	PASS
5100 Mhz	-30 dBc Min	-50.37 dBc	5	PASS

Plot#: 3621028

Figure B.18. Return loss and instertion loss of 3.0 GHz bandpass filter

Lark Engineering Company Phone (949)240-1233 Fax (949)240-7910 www.larkengineering.com

810-156 X3B4200-1000-3AA Rev. -- WO: 26321 LOT/DATE: 26321-02

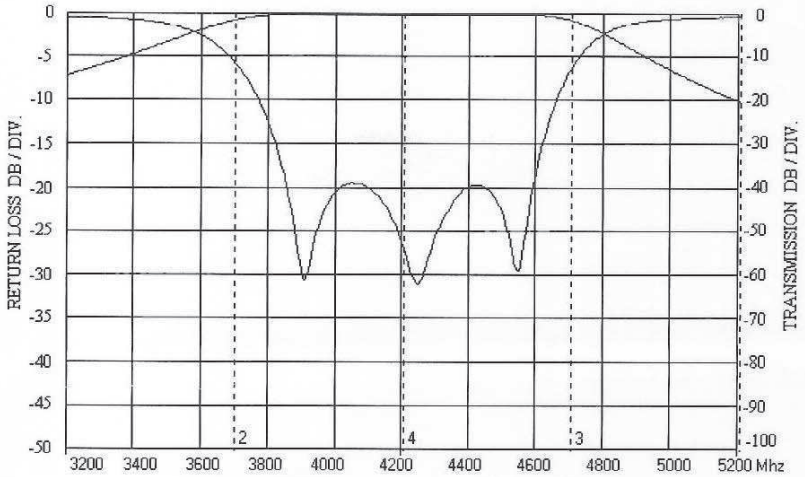

CUSTOMER: UNIV. OF MASSACHUSETTS PO: 0001116768 DATE: 12-13-2006

FREQUENCY	SPEC.	RESPONSE	MARKER	COMMENT
-- INSERTION LOSS --				
3700 Mhz to 4700 Mhz	-3 dBc Max	-1.45 dBc	2 - 3	PASS
4200 Mhz	-.5 dBa Max	-0.22 dBa	4	PASS
-- RETURN LOSS --				
3850 Mhz to 4550 Mhz	-14 dB Min	-19.41 dB		PASS
-- REJECTION --				
800 Mhz	-30 dBc Min	-37.96 dBc	1	PASS
6200 Mhz	-30 dBc Min	-41.61 dBc	5	PASS

Plot#: 3626558

Figure B.19. Return loss and instertion loss of 4.2 GHz bandpass filter

National Semiconductor

August 2003

LMH6609
900MHz Voltage Feedback Op Amp

General Description

The LMH6609 is an ultra wideband, unity gain stable, low power, voltage feedback op amp that offers 900MHz bandwidth at a gain of 1, 1400V/µs slew rate and 90mA of linear output current.

The LMH6609 is designed with voltage feedback architecture for maximum flexibility especially for active filters and integrators. The LMH6609 has balanced, symmetrical inputs with well-matched bias currents and minimal offset voltage.

With Differential Gain of .01 and Differential Phase of .026 the LMH6609 is suited for video applications. The 90mA of linear output current makes the LMH6609 suitable for multiple video loads and cable driving applications as well.

The recommended supply voltage range of 6V to 12V and is specified at 6.6 and 10V. A low supply current of 7mA (at 10V supply) makes the LMH6609 useful in a wide variety of platforms, including portable or remote equipment that must run from battery power.

The LMH6609 is available in the industry standard 8-pin SOIC package and in the space-saving 5-pin SOT package. The LMH6609 is specified for operation over the -40˚C to +85˚C temperature range. The LMH6609 is manufactured in National Semiconductor's state-of-the-art VIP10™ technology for high performance.

Features

- 900MHz −3dB bandwidth (A_V = 1)
- Large signal bandwidth and slew rate 100% tested
- 280MHz −3dB bandwidth (A_V = +2, V_{OUT} = $2V_{PP}$)
- 90mA linear output current
- 1400V/µs slew rate
- Unity gain stable
- <1mV input Offset voltage
- 7mA Supply current (no load)
- 6V to 12V supply voltage range
- .01/ .026 differential gain/phase PAL
- 3.1nV/ $\sqrt{Hz}$ voltage noise
- Improved replacement for CLC440, 420, 426

Applications

- Test equipment
- IF/RF amplifier
- A/D Input driver
- Active filter
- Integrator
- DAC output buffer
- Transimpedance amplifier

Typical Application

$$K = 1 + \frac{R_F}{R_G} \quad Q = \frac{m}{1+m^2} \quad \omega_O = \frac{1}{mRC}$$

Q, K ARE UNITLESS
ω_O IS IN UNITS OF RADIANS/SEC.
DIVIDE ω_O BY 2π TO GET IT IN Hz

20079037

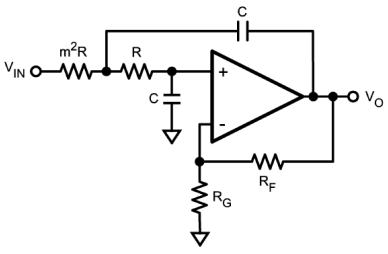

20079038

Sallen Key Low Pass Filter

Figure B.20. LMH6609 wideband amplifier features and general description

LMH6609

Absolute Maximum Ratings (Note 1)

If Military/Aerospace specified devices are required, please contact the National Semiconductor Sales Office/ Distributors for availability and specifications.

V_S (V^+ - V^-)	±6.6V
I_{OUT}	(Note 3)
Common Mode Input Voltage	V+ to V–
Maximum Junction Temperature	+150˚C
Storage Temperature Range	–65˚C to +150˚C
Lead Temperature Range	+300˚C
ESD Tolerance (Note 4)	
Human Body Model	2000V
Machine Model	200V

Operating Ratings (Note 3)

Thermal Resistance		
Package	(θ_{JC})	(θ_{JA})
8-Pin SOIC	65˚C/W	145˚C/W
5-Pin SOT23	120˚C/W	187˚C/W
Operating Temperature	–40˚C	+85˚C
Nominal Supply Voltage (Note 6)	±3.3V	±6V

±5V Electrical Characteristics

Unless specified, A_V = +2, R_F = 250Ω: V_S = ±5V, R_L = 100Ω; unless otherwise specified. **Boldface** limits apply over temperature Range. (Note 2)

Symbol	Parameter	Conditions	Min	Typ	Max	Units
Frequency Domain Response						
SSBW	–3dB Bandwidth	V_{OUT} = 0.5V_{PP}		260		MHz
LSBW	–3dB Bandwidth	V_{OUT} = 4.0V_{PP}	150	170		MHz
SSBWG1	–3dB Bandwidth A_V = 1	V_{OUT} = 0.25V_{PP}		900		MHz
GFP	.1dB Bandwidth	Gain is Flat to .1dB		130		MHz
DG	Differential Gain	R_L = 150Ω, 4.43MHz		0.01		%
DP	Differential Phase	R_L = 150Ω, 4.43MHz		0.026		deg
Time Domain Response						
TRS	Rise and Fall Time	1V Step		1.6		ns
TRL		4V Step		2.6		ns
t_s	Settling Time to 0.05%	2V Step		15		ns
SR	Slew Rate	4V Step (Note 5)	1200	1400		V/µs
Distortion and Noise Response						
HD2	2nd Harmonic Distortion	2V_{PP}, 20MHz		–63		dBc
HD3	3rd Harmonic Distortion	2V_{PP}, 20MHz		–57		dBc
	Equivalent Input Noise					
VN	Voltage Noise	>1MHz		3.1		nV/$\sqrt{Hz}$
CN	Current Noise	>1MHz		1.6		pA/$\sqrt{Hz}$
Static, DC Performance						
V_{IO}	Input Offset Voltage			±0.8	±2.5 **±3.5**	mV
I_{BN}	Input Bias Current			–2	±5 **±8**	µA
I_{BI}	Input Offset Current			.1	±1.5 **±3**	µA
PSRR	Power Supply Rejection Ratio	DC, 1V Step	67 **65**	73		dB
CMRR	Common Mode Rejection Ratio	DC, 2V Step	67 **65**	73		dB
I_{CC}	Supply Current	R_L = ∞		7.0	7.8 **8.5**	mA
Miscellaneous Performance						
R_{IN}	Input Resistance			1		MΩ
C_{IN}	Input Capacitance			1.2		pF
R_{OUT}	Output Resistance	Closed Loop		0.3		Ω

www.national.com

Figure B.21. LMH6609 wideband amplifier electrical characteristics

±5V Electrical Characteristics (Continued)

Unless specified, A_V = +2, R_F = 250Ω: V_S = ±5V, R_L = 100Ω; unless otherwise specified. **Boldface** limits apply over temperature Range. (Note 2)

Symbol	Parameter	Conditions	Min	Typ	Max	Units
V_O	Output Voltage Range	R_L = ∞	±3.6 **±3.3**	±3.9		V
V_{OL}		R_L = 100Ω	±3.2 **±3.0**	±3.5		V
CMIR	Input Voltage Range	Common Mode, CMRR > 60dB	±2.8 **±2.5**	±3.0		V
I_O	Linear Output Current	V_{OUT}	±60 **±50**	±90		mA

±3.3V Electrical Characteristics

Unless specified, A_V = +2, R_F = 250Ω: V_S = ±3.3V, R_L = 100Ω; unless otherwise specified. **Boldface** limits apply over temperature Range. (Note 2)

Symbol	Parameter	Conditions	Min	Typ	Max	Units
Frequency Domain Response						
SSBW	−3dB Bandwidth	V_{OUT} = 0.5V_{PP}		180		MHz
LSBW	−3dB Bandwidth	V_{OUT} = 3.0V_{PP}		110		MHz
SSBWG1	−3dB Bandwidth A_V = 1	V_{OUT} = 0.25V_{PP}		450		MHz
GFP	.1dB Bandwidth	V_{OUT} = 1V_{PP}		40		MHz
DG	Differential Gain	R_L = 150Ω, 4.43MHz		.01		%
DP	Differential Phase	R_L = 150Ω, 4.43MHz		.06		deg
Time Domain Response						
TRL		1V Step		2.2		ns
SR	Slew Rate	2V Step (Note 5)		800		V/µs
Distortion and Noise Response						
HD2	2nd Harmonic Distortion	2V_{PP}, 20MHz		−63		dBc
HD3	3rd Harmonic Distortion	2V_{PP}, 20MHz		−43		dBc
	Equivalent Input Noise					
VN	Voltage Noise	>1MHz		3.7		nV/ $\sqrt{Hz}$
CN	Current Noise	>1MHz		1.1		pA/ $\sqrt{Hz}$
Static, DC Performance						
V_{IO}	Input Offset Voltage			0.8	±2.5 **±3.5**	mV
I_{BN}	Input Bias Current			−1	±3 **±6**	µA
I_{BI}	Input Offset Current			0	±1.5 **±3**	µA
PSRR	Power Supply Rejection Ratio	DC, .5V Step	67	73		dB
CMRR	Common Mode Rejection Ratio	DC, 1V Step	67	75		dB
I_{CC}	Supply Current	R_L = ∞		3.6	5 **6**	mA
Miscellaneous Performance						
R_{OUT}	Input Resistance	Close Loop		.05		Ω
V_O	Output Voltage Range	R_L = ∞	±2.1	±2.3		V
V_{OL}		R_L = 100Ω	±1.9	±2.0		V
CMIR	Input Voltage Range	Common Mode		±1.3		V
I_O	Linear Output Current	V_{OUT}	±30	±45		mA

Figure B.22. LMH6609 wideband amplifier electrical characteristics, continued

±3.3V Electrical Characteristics (Continued)

Note 1: Absolute Maximum Ratings indicate limits beyond which damage to the device may occur. Operating Ratings indicate conditions for which the device is intended to be functional, but specific performance is not guaranteed. For guaranteed specifications, see the Electrical Characteristics tables.

Note 2: Electrical Table values apply only for factory testing conditions at the temperature indicated. Factory testing conditions result in very limited self-heating of the device such that $T_J = T_A$. No guarantee of parametric performance is indicated in the electrical tables under conditions of internal self heating where $T_J > T_A$. See Applications Section for information on temperature derating of this device. Min/Max ratings are based on product characterization and simulation. Individual parameters are tested as noted.

Note 3: The maximum output current (I_{OUT}) is determined by device power dissipation limitations. See the Power Dissipation section of the Application Section for more details.

Note 4: Human body model, 1.5kΩ in series with 100pF. Machine model, 0Ω In series with 200pF.

Note 5: rate is Average of Rising and Falling 40-60% slew rates.

Note 6: Nominal Supply voltage range is for supplies with regulation of 10% or better.

Connection Diagrams

5-Pin SOT23

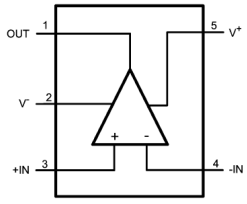

Top View

8-Pin SOIC

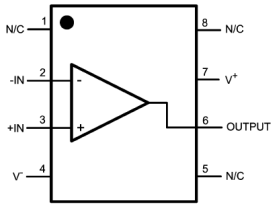

Top View

Ordering Information

Package	Part Number	Package Marking	Transport Media	NSC Drawing
8-Pin SOIC	LMH6609MA	LMH6609MA	95 Units/Rails	M08A
	LMH6609MAX		2.5k Units Tape and Reel	
5-SOT23	LMH6609MF	A89A	1k Units Tape and Reel	MF05A
	LMH6609MFX		2.5k Units Tape and Reel	

Figure B.23. LMH6609 wideband amplifier pin configuration

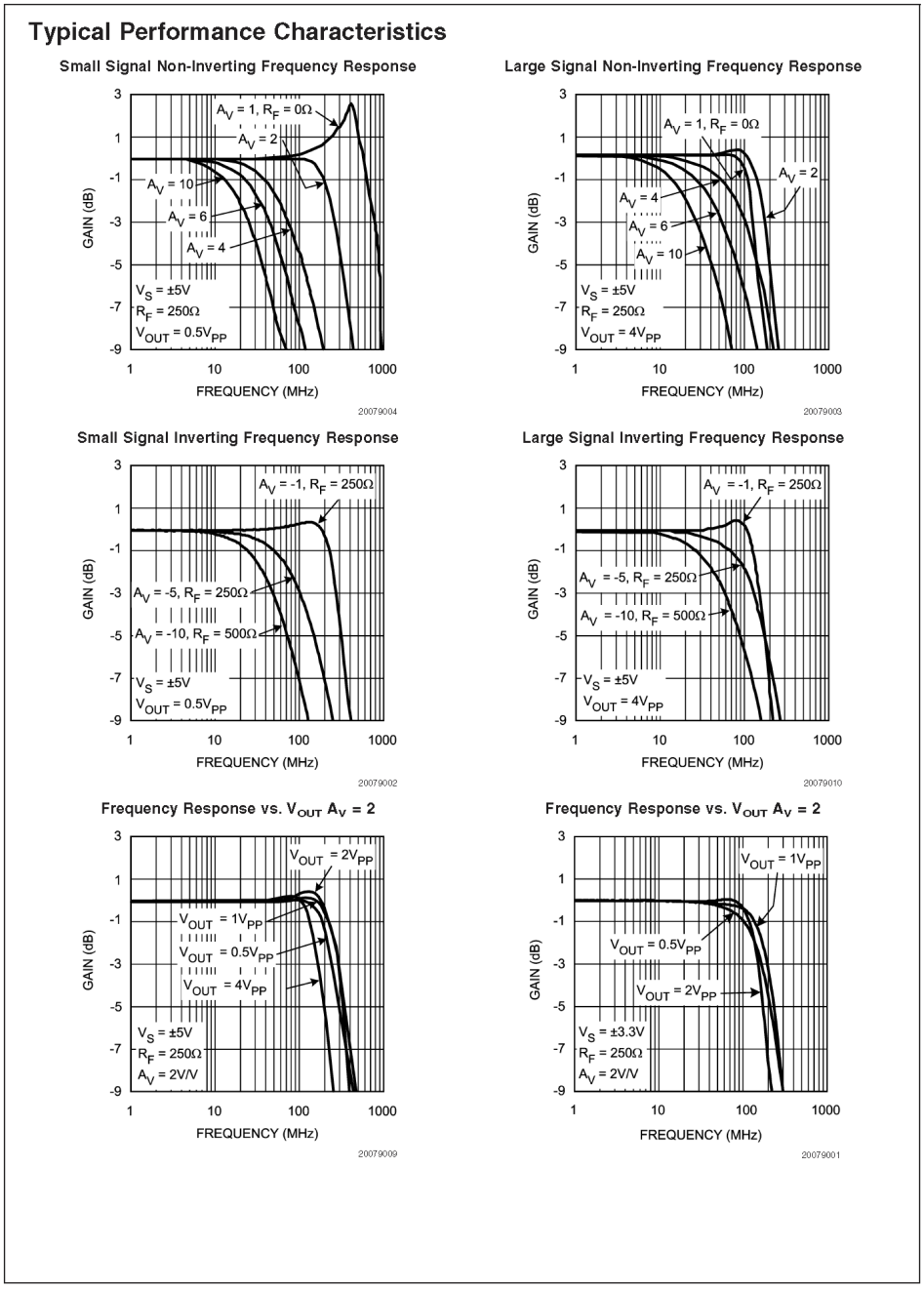

Figure B.24. LMH6609 wideband amplifier performance characteristics

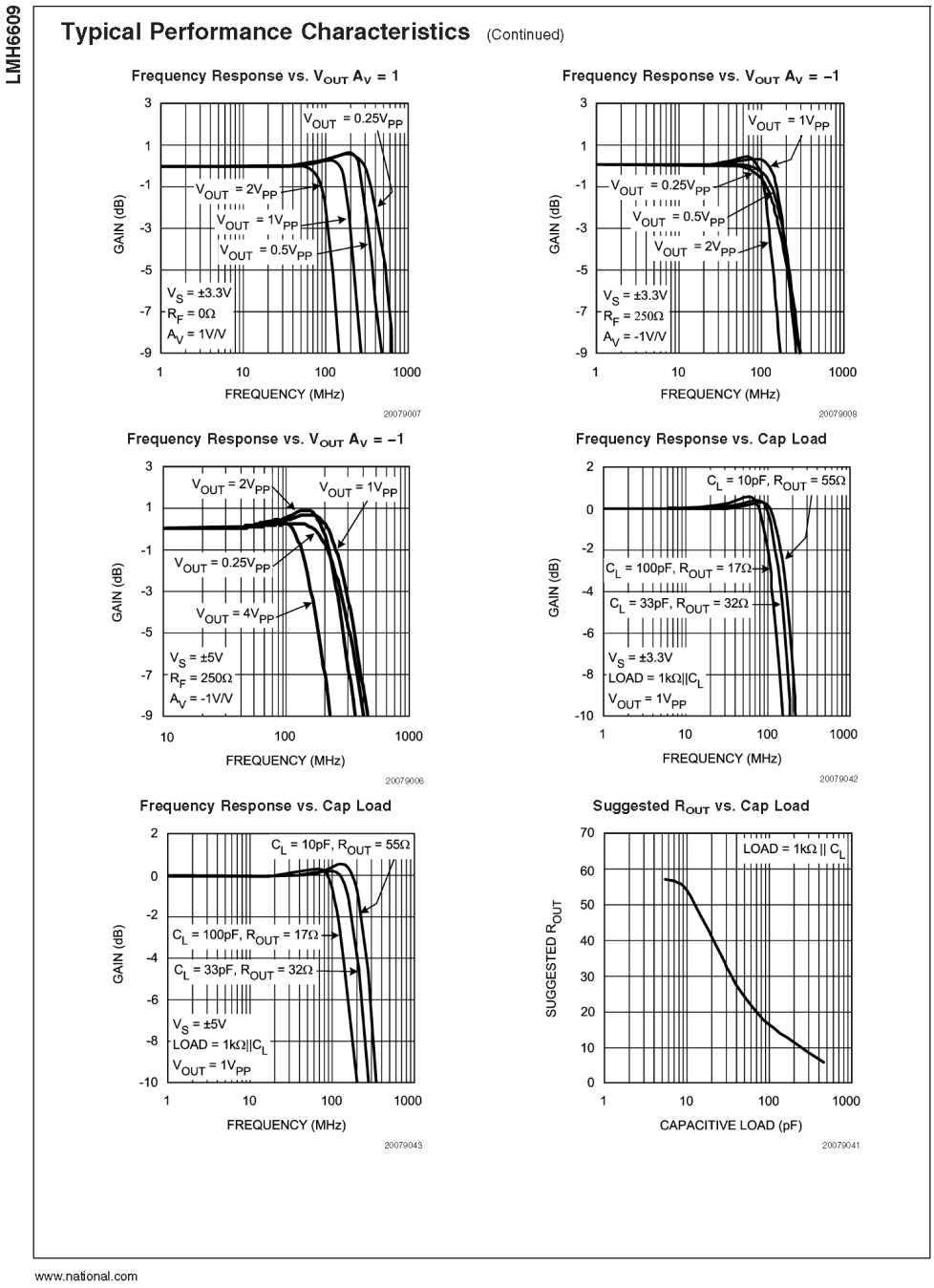

Figure B.25. LMH6609 wideband amplifier performance characteristics

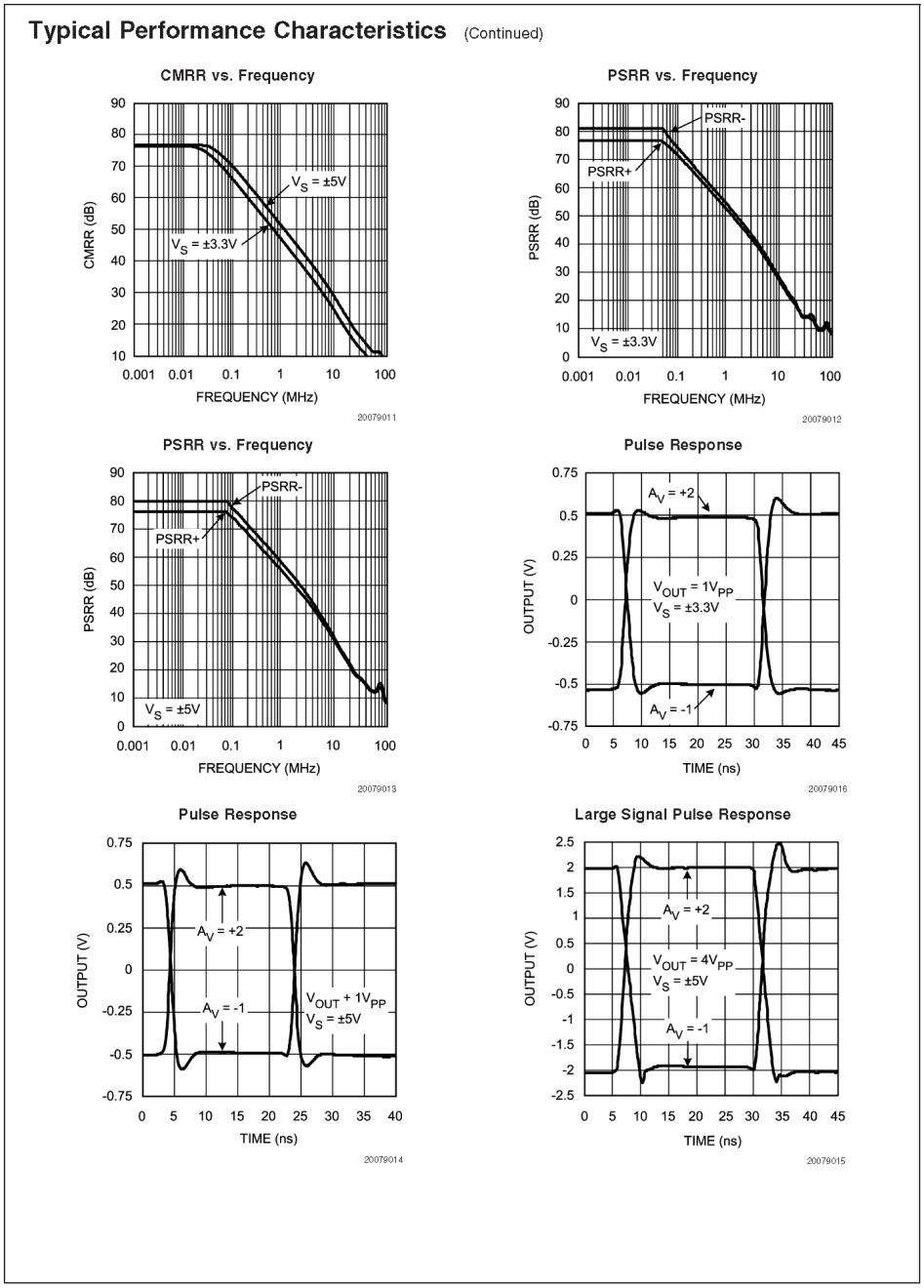

Figure B.26. LMH6609 wideband amplifier performance characteristics, continued

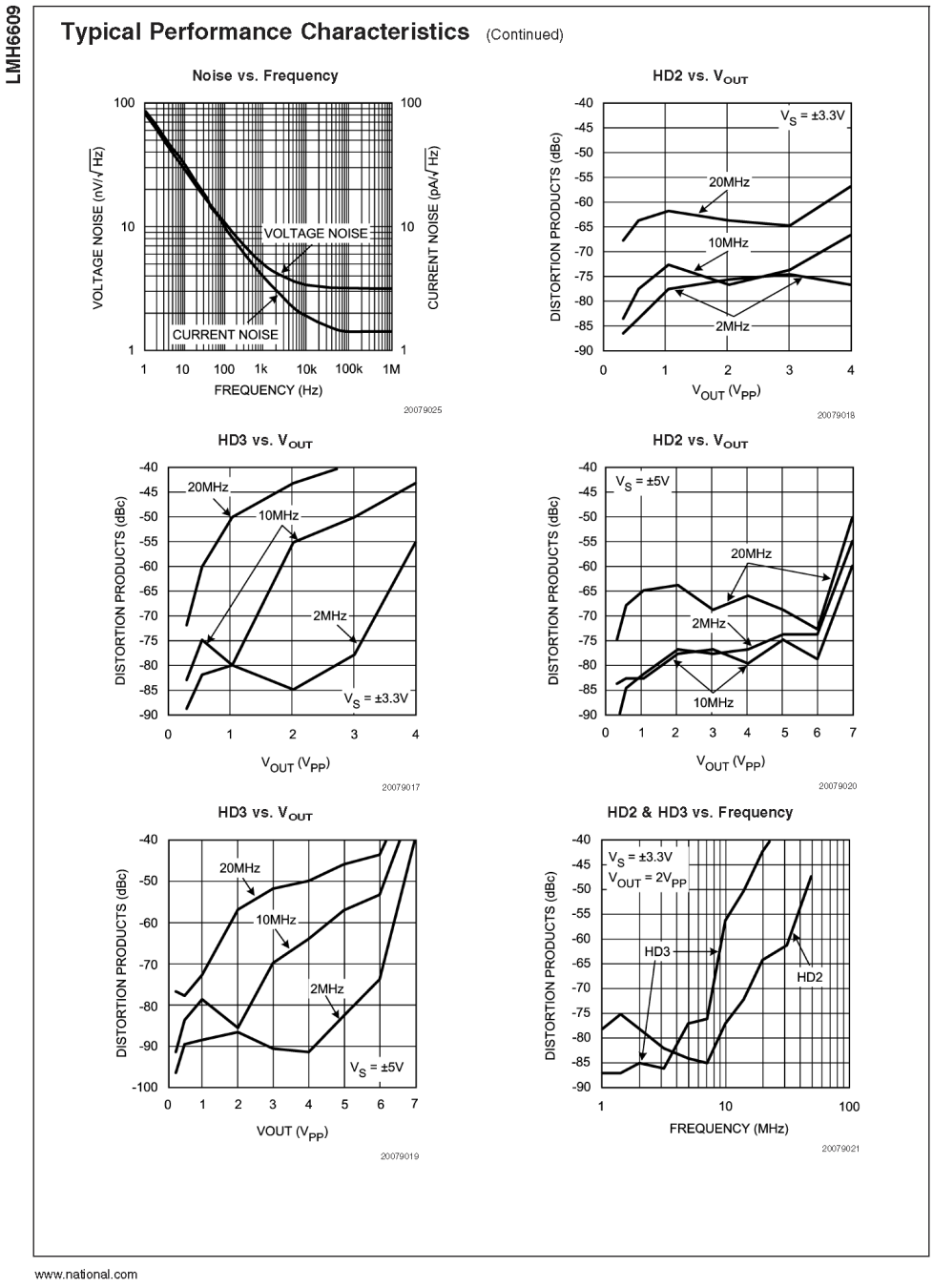

Figure B.27. LMH6609 wideband amplifier performance characteristics, continued

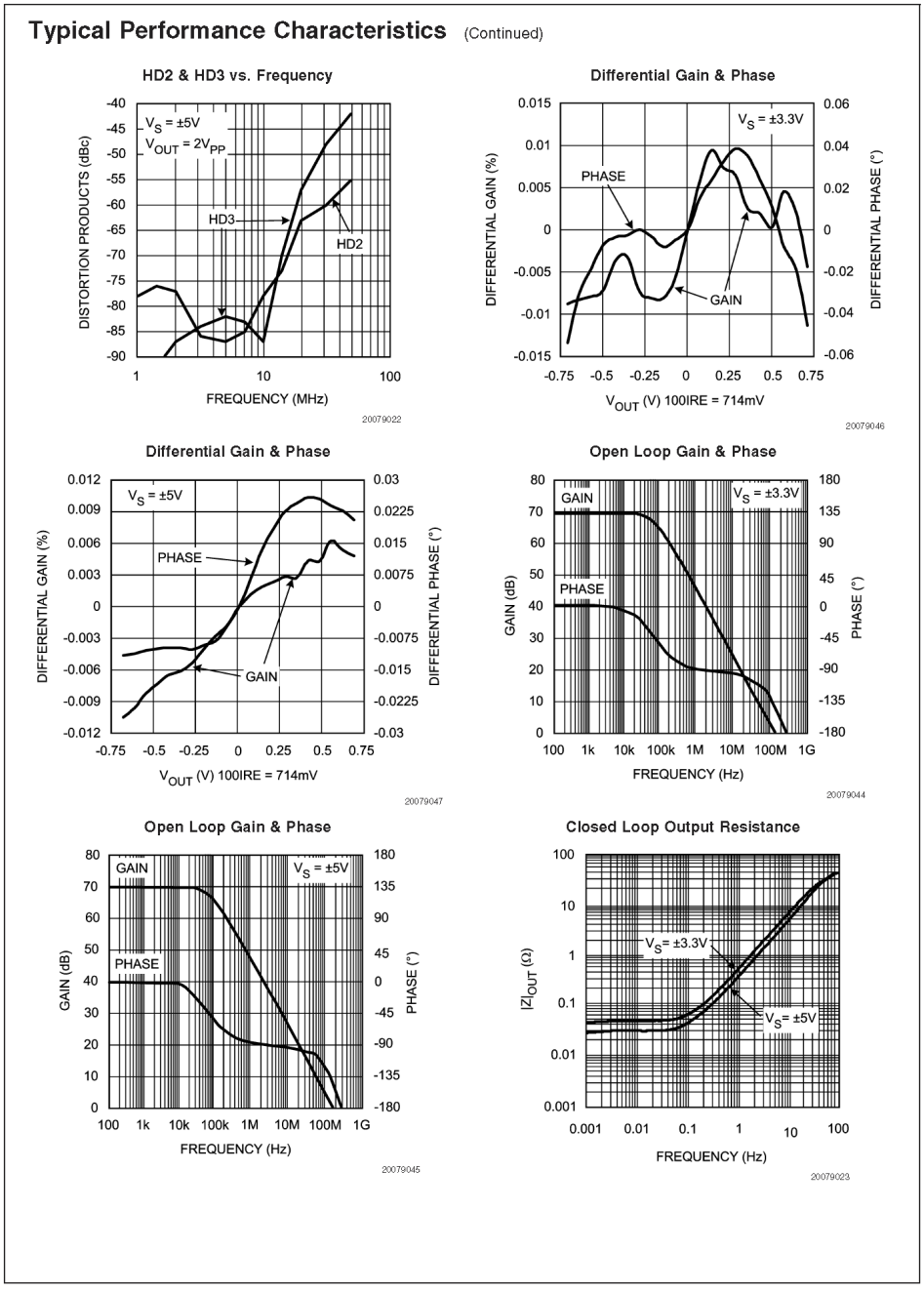

Figure B.28. LMH6609 wideband amplifier performance characteristics, continued

Wideband 4 GHz, 43 dB Isolation at 1 GHz, CMOS 1.65 V to 2.75 V, 2:1 Mux/SPDT Switches

ADG918/ADG919

FEATURES

Wideband switch: −3 dB @ 4 GHz
Absorptive/reflective switches
High off isolation (43 dB @ 1 GHz)
Low insertion loss (0.8 dB @1 GHz)
Single 1.65 V to 2.75 V power supply
CMOS/LVTTL control logic
8-lead MSOP and tiny 3 mm × 3 mm LFCSP packages
Low power consumption (<1 µA)

APPLICATIONS

Wireless communications
General-purpose RF switching
Dual-band applications
High speed filter selection
Digital transceiver front end switch
IF switching
Tuner modules
Antenna diversity switching

FUNCTIONAL BLOCK DIAGRAMS

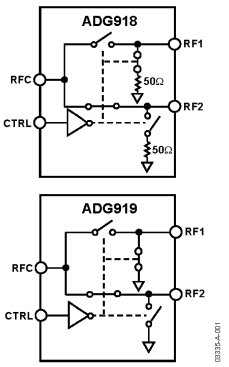

Figure 1.

GENERAL DESCRIPTION

The ADG918/ADG919 are wideband switches using a CMOS process to provide high isolation and low insertion loss to 1 GHz. The ADG918 is an absorptive (matched) switch having 50 Ω terminated shunt legs, while the ADG919 is a reflective switch. These devices are designed such that the isolation is high over the dc to 1 GHz frequency range. They have on-board CMOS control logic, thus eliminating the need for external controlling circuitry. The control inputs are both CMOS and LVTTL compatible. The low power consumption of these CMOS devices makes them ideally suited to wireless applications and general-purpose high frequency switching.

PRODUCT HIGHLIGHTS

1. −43 dB Off Isolation @ 1 GHz.
2. 0.8 dB Insertion Loss @ 1 GHz.
3. Tiny 8-Lead MSOP/LFCSP Packages.

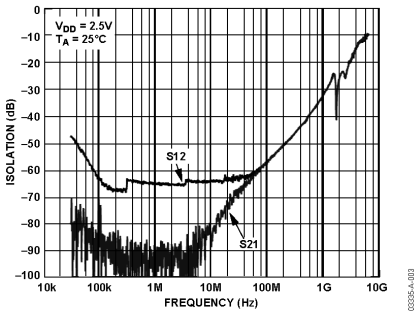

Figure 2. Off Isolation vs. Frequency

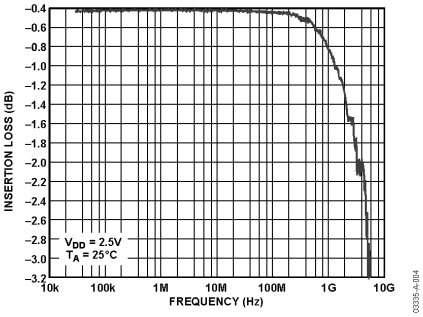

Figure 3. Insertion Loss vs. Frequency

One Technology Way, P.O. Box 9106, Norwood, MA 02062-9106, U.S.A.
Tel: 781.329.4700 **www.analog.com**
Fax: 781.326.8703

Figure B.29. ADG918 wideband switch features and general description

SPECIFICATIONS

Table 1. V_{DD} = 1.65 V to 2.75 V, GND = 0 V, input power = 0 dBm, all specifications T_{MIN} to T_{MAX}, unless otherwise noted.[1]

			B Version			
Parameter	**Symbol**	**Conditions**	**Min**	**Typ[2]**	**Max**	**Unit**
AC ELECTRICAL CHARACTERISTICS						
Operating Frequency[3]			DC		2	GHz
3 dB Frequency[4]					4	GHz
Input Power[4]		0 V dc Bias			7	dBm
		0.5 V dc Bias			16	dBm
Insertion Loss	S_{21}, S_{12}	DC to 100 MHz; V_{DD} = 2.5 V ± 10%		0.4	0.7	dB
		500 MHz; V_{DD} = 2.5 V ± 10%		0.5	0.8	dB
		1000 MHz; V_{DD} = 2.5 V ± 10%		0.8	1.25	dB
Isolation—RFC to RF1/RF2	S_{21}, S_{12}	100 MHz	57	60		dB
(CP Package)		500 MHz	46	49		dB
		1000 MHz	36	43		dB
Isolation—RFC to RF1/RF2	S_{21}, S_{12}	100 MHz	55	60		dB
(RM Package)		500 MHz	43	47		dB
		1000 MHz	34	37		dB
Isolation—RF1 to RF2 (Crosstalk)	S_{21}, S_{12}	100 MHz	55	58		
(CP Package)		500 MHz	41	44		
		1000 MHz	31	37		
Isolation—RF1 to RF2 (Crosstalk)	S_{21}, S_{12}	100 MHz	54	57		
(RM Package)		500 MHz	39	42		
		1000 MHz	31	33		
Return Loss (On Channel)[4]	S_{11}, S_{22}	DC to 100 MHz	21	27		dB
		500 MHz	22	27		dB
		1000 MHz	22	26		dB
Return Loss (Off Channel)[4]	S_{11}, S_{22}	DC to 100 MHz	18	23		dB
ADG918		500 MHz	17	21		dB
		1000 MHz	16	20		dB
On Switching Time[4]	t_{ON}	50% CTRL to 90% RF		6.6	10	ns
Off Switching Time[4]	t_{OFF}	50% CTRL to 10% RF		6.5	9.5	ns
Rise Time[4]	t_{RISE}	10% to 90% RF		6.1	9	ns
Fall Time[4]	t_{FALL}	90% to 10% RF		6.1	9	ns
1 dB Compression[4]	$P_{-1\ dB}$	1000 MHz		17		dBm
Third Order Intermodulation Intercept	IP_3	900 MHz/901 MHz, 4 dBm	30	36		dBm
Video Feedthrough[5]				2.5		mV p-p
DC ELECTRICAL CHARACTERISTICS						
Input High Voltage	V_{INH}	V_{DD} = 2.25 V to 2.75 V	1.7			V
	V_{INH}	V_{DD} = 1.65 V to 1.95 V	0.65 V_{CC}			V
Input Low Voltage	V_{INL}	V_{DD} = 2.25 V to 2.75 V			0.7	V
	V_{INL}	V_{DD} = 1.65 V to 1.95 V			0.35 V_{CC}	V
Input Leakage Current	I_I	$0 \le V_{IN} \le 2.75$ V		± 0.1	± 1	µA
CAPACITANCE[4]						
RF1/RF2, RF Port On Capacitance	C_{RF} ON	f = 1 MHz		1.6		pF
CTRL Input Capacitance	C_{CTRL}	f = 1 MHz		2		pF
POWER REQUIREMENTS						
V_{DD}			1.65		2.75	V
Quiescent Power Supply Current	I_{DD}	Digital inputs = 0 V or V_{DD}		0.1	1	µA

[1]Temperature range B Version: −40°C to +85°C.
[2]Typical values are at V_{DD} = 2.5 V and 25°C, unless otherwise stated.
[3]Point at which insertion loss degrades by 1 dB.
[4]Guaranteed by design, not subject to production test.
[5]The dc transience at the output of any port of the switch when the control voltage is switched from high to low or low to high in a 50 Ω test setup, measured with 1 ns rise time pulses and 500 MHz bandwidth.

Figure B.30. ADG918 wideband switch specifications

ABSOLUTE MAXIMUM RATINGS[1]

Table 2. (T_A = 25°C, unless otherwise noted.)

Parameter	Rating
V_{DD} to GND	–0.5 V to +4 V
Inputs to GND	–0.5 V to V_{DD} + 0.3 V[2]
Continuous Current	30 mA
Input Power	18 dBm
Operating Temperature Range	
Industrial (B Version)	–40°C to +85°C
Storage Temperature Range	–65°C to +150°C
Junction Temperature	150°C
MSOP Package	
θ_{JA} Thermal Impedance	206°C/W
LFCSP Package	
θ_{JA} Thermal Impedance (2-layer board)	84°C/W
θ_{JA} Thermal Impedance (4-layer board)	48°C/W
Lead Temperature, Soldering (10 sec)	300°C
IR Reflow, Peak Temperature (<20 sec)	235°C
ESD	1 kV

NOTES

[1] Stresses above those listed under Absolute Maximum Ratings may cause permanent damage to the device. This is a stress rating only; functional operation of the device at these or any other conditions above those listed in the operational sections of this specification is not implied. Exposure to absolute maximum rating conditions for extended periods may affect device reliability. Only one absolute maximum rating may be applied at any one time.

[2] RF1/RF2 Off Port Inputs to Ground ..... –0.5 V to V_{DD} – 0.5 V

ESD CAUTION

ESD (electrostatic discharge) sensitive device. Electrostatic charges as high as 4000 V readily accumulate on the human body and test equipment and can discharge without detection. Although this product features proprietary ESD protection circuitry, permanent damage may occur on devices subjected to high energy electrostatic discharges. Therefore, proper ESD precautions are recommended to avoid performance degradation or loss of functionality.

Figure B.31. ADG918 wideband switch absolute maximum ratings

PIN CONFIGURATION AND FUNCTION DESCRIPTIONS

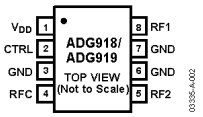

Figure 4. 8-Lead MSOP (RM-8)
8-Lead 3 mm x 3 mm LFCSP (CP-8)

Table 3. Truth Table

CTRL	Signal Path
0	RF2 to RFC
1	RF1 to RFC

Table 4. Pin Function Descriptions

Pin No.	Mnemonic	Function
1	V_{DD}	Power Supply Input. These parts can be operated from 1.65 V to 2.75 V, and V_{DD} should be decoupled to GND.
2	CTRL	CMOS or TTL Logic Level; 0->RF2 to RFC 1->RF1 to RFC
3, 6, 7	GND	Ground Reference Point for All Circuitry on the Part
4	RFC	COMMON RF Port for Switch
5	RF2	RF2 Port
8	RF1	RF1 Port

Figure B.32. ADG918 wideband switch pin configuration

TYPICAL PERFORMANCE CHARACTERISTICS

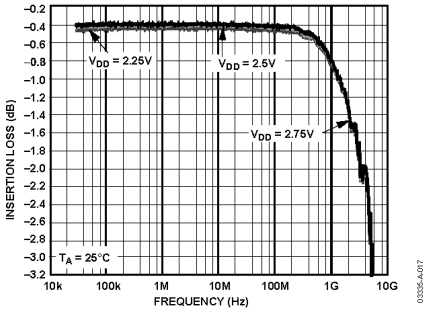

Figure 5. Insertion Loss vs. Frequency over Supplies (RF1/RF2, S12, and S21)

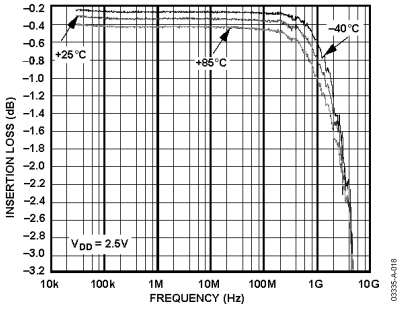

Figure 8. Insertion Loss vs. Frequency over Temperature (RF1/RF2, S12, and S21)

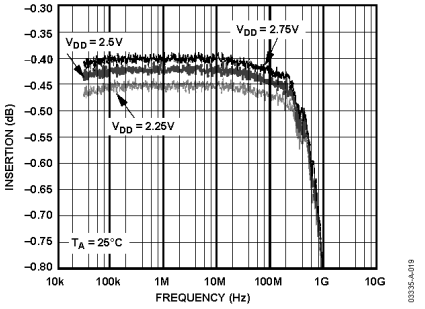

Figure 6. Insertion Loss vs. Frequency over Supplies (RF1/RF2, S12, and S21) (Zoomed Figure 5 Plot)

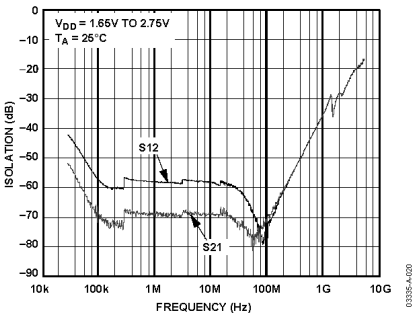

Figure 9. Isolation vs. Frequency over Supplies (RF1/RF2, ADG918)

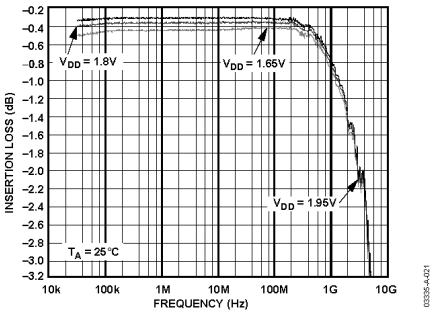

Figure 7. Insertion Loss vs. Frequency over Supplies (RF1/RF2, S12, and S21)

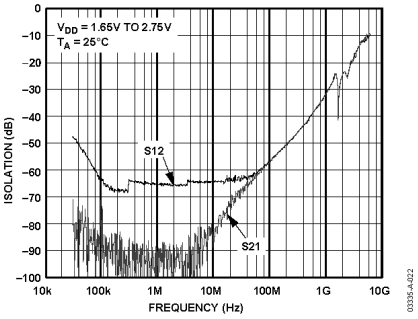

Figure 10. Isolation vs. Frequency over Supplies (RF1/RF2, ADG919)

Figure B.33. ADG918 wideband switch performance characteristics

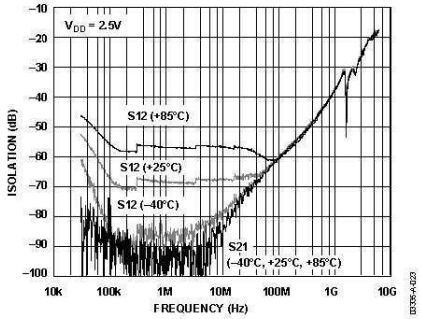

Figure 11. Isolation vs. Frequency over Temperature (RF1/RF2, ADG919)

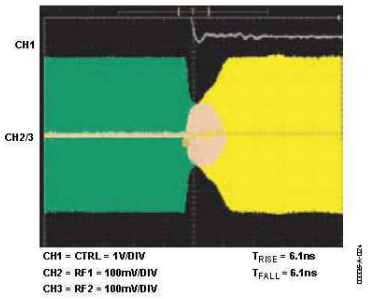

Figure 14. Switch Timing

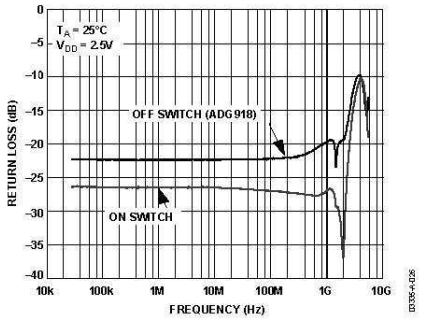

Figure 12. Return Loss vs. Frequency (RF1/RF2, S11)

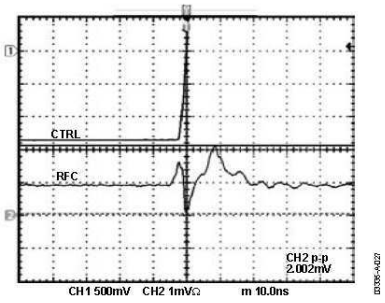

Figure 15. Video Feedthrough

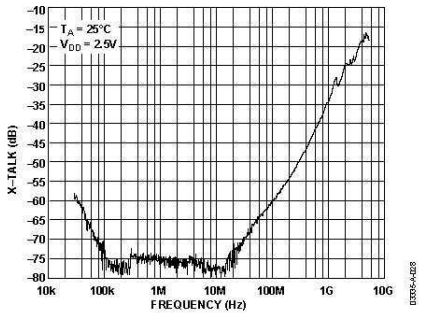

Figure 13. Crosstalk vs. Frequency (RF1/RF2, S12, S21)

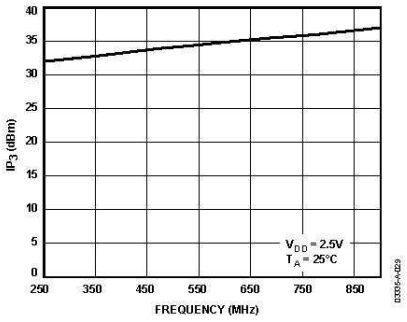

Figure 16. IP_3 vs. Frequency

Figure B.34. ADG918 wideband switch performance characteristics, continued

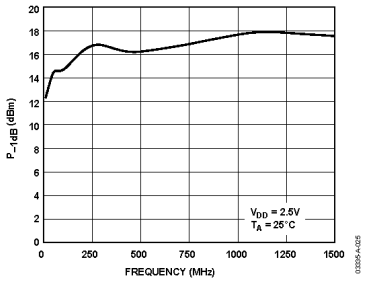

Figure 17. P_{1dB} vs. Frequency

Figure B.35. ADG918 wideband switch performance characteristics, continued

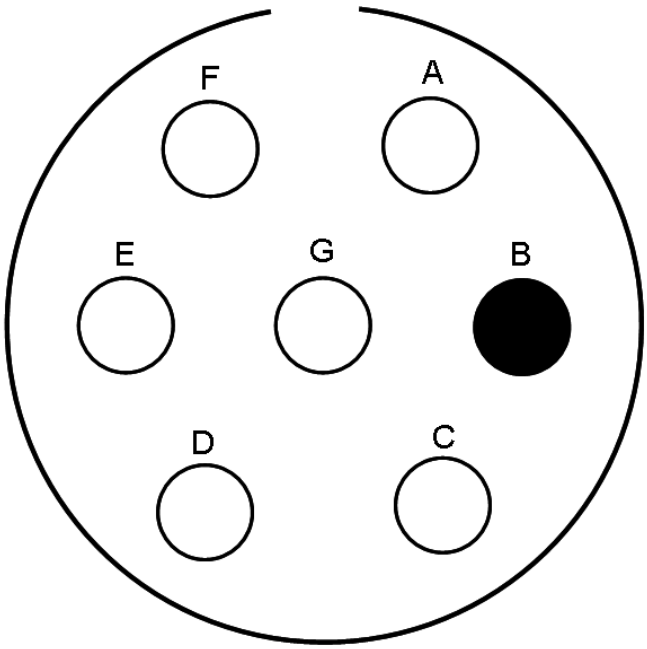

Figure B.36. Millitech power supply pinouts

Pin	Assignment
A	+15 VDC
B	Not Used
C	+12 VDC GND
D	+12 VDC GND
E	-12 VDC
F	+12 VDC
G	+15 VDC GND

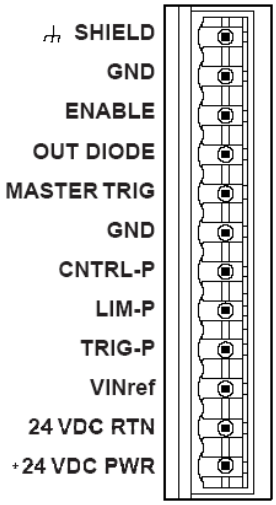

Figure B.37. 6K2 Auxiliary connections

Pin	Assignment
SHIELD	Connected to chassis earth ground
GND	Isolated logic ground
ENABLE	Connected to 6K2 GND
OUT DIODE	Internally connected to 24 VDC PWR
MASTER TRIG	Not connected
GND	Isolated logic ground
CNTRL-P	Not connected
LIM-P	Connected to 24 VDC PWR
TRIG-P	Connected to 6K2 GND
VINref	Internally connected to 24 VDC PWR
24 VDC RTN	Connected to - terminal of SOLA Supply
+24 VDC PWR	Connected to + terminal of SOLA Supply

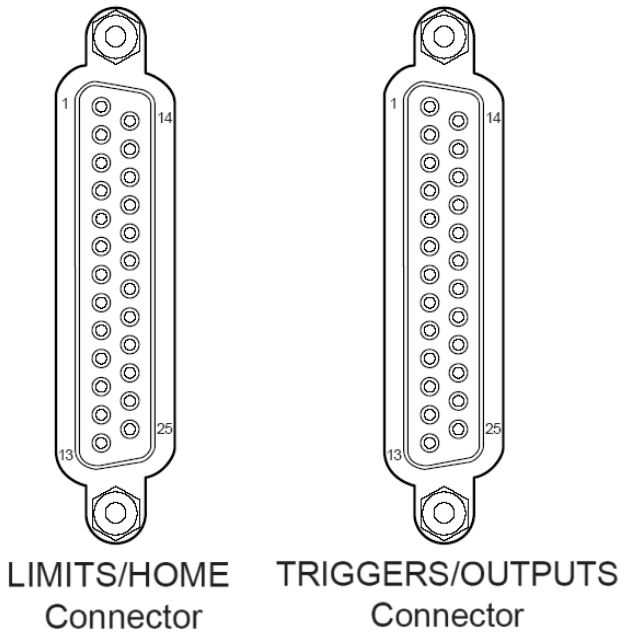

Figure B.38. Limits/Home and Triggers/Outputs pin outs

LIMITS/HOME Connector

Pin	Assignment
13	Home limit, axis 2
15	Negative end-of-travel limit, axis 2
17	Positive end-of-travel limit, axis 2

TRIGGERS/OUTPUTS Connector

Pin	Assignment
9	Home limit, axis 1
11	Negative end-of-travel limit, axis 1
13	Positive end-of-travel limit, axis 1

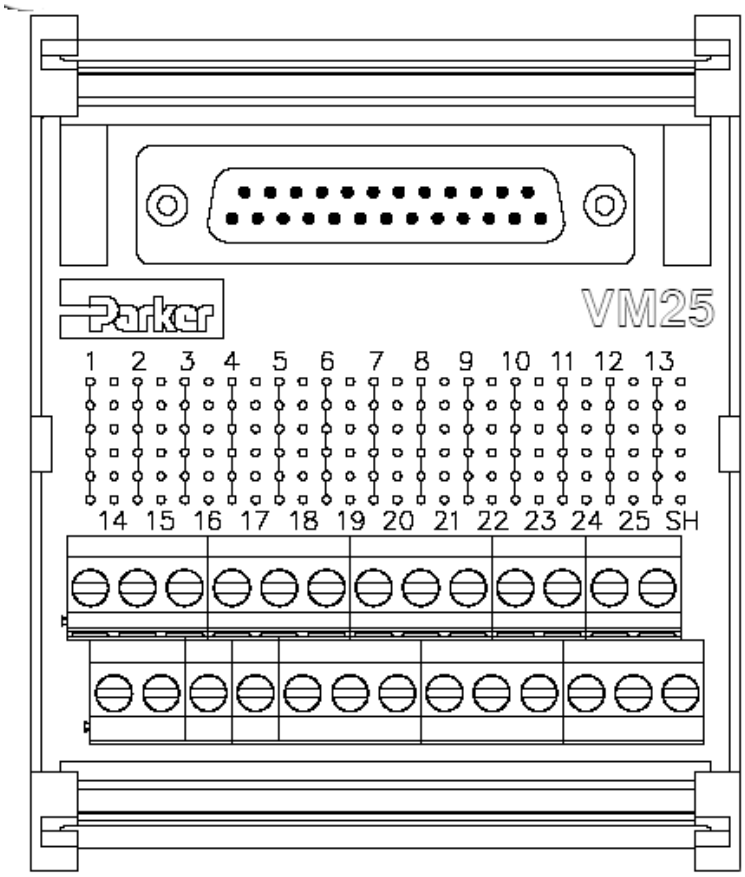

Figure B.39. VM25 pin outs

Pin	Assignment
13	Home limit, axis 2
15	Negative end-of-travel limit, axis 2
17	Positive end-of-travel limit, axis 2

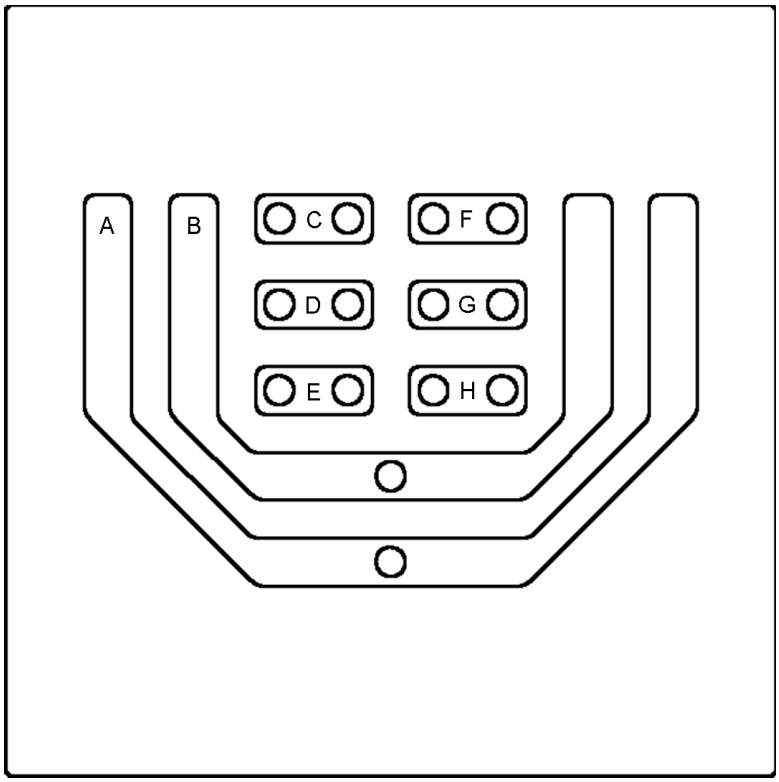

Figure B.40. Sensor switch printed circuit board schematic

Trace	Assignment
A	+24 VDC
B	DC Return
C	Negative end-of-travel limit, axis 2
D	Home limit, axis 2
E	Positive end-of-travel limit, axis 2
F	Negative end-of-travel limit, axis 1
G	Home limit, axis 1
H	Positive end-of-travel limit, axis 1

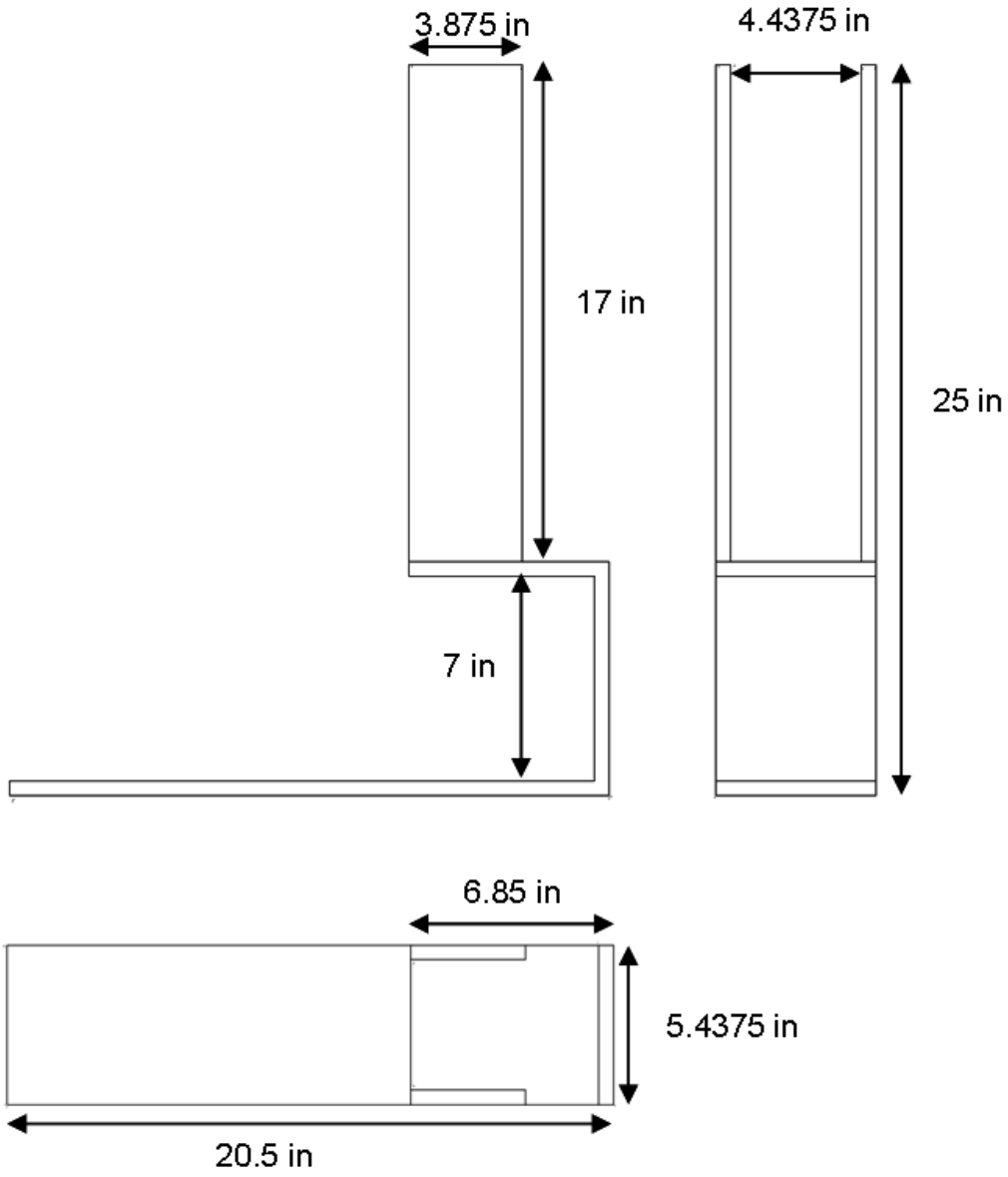

Figure B.41. Dimensions of stationary radiometer support structure

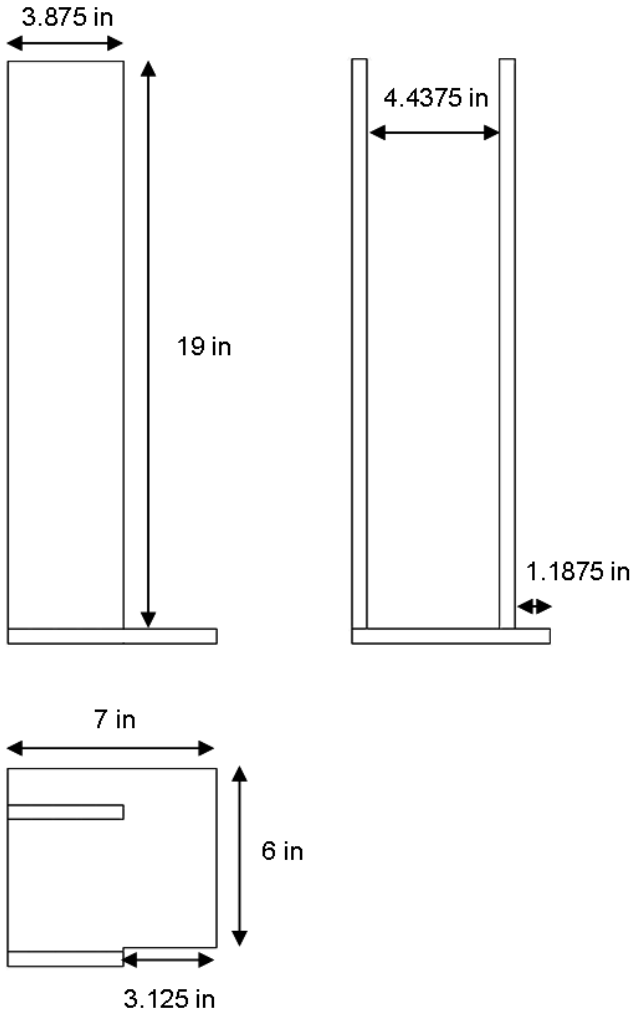

Figure B.42. Dimensions of mobile radiometer support structure

APPENDIX C

SYSTEM PICTURES

Figure C.1. Linear drive and antenna measurement hardware

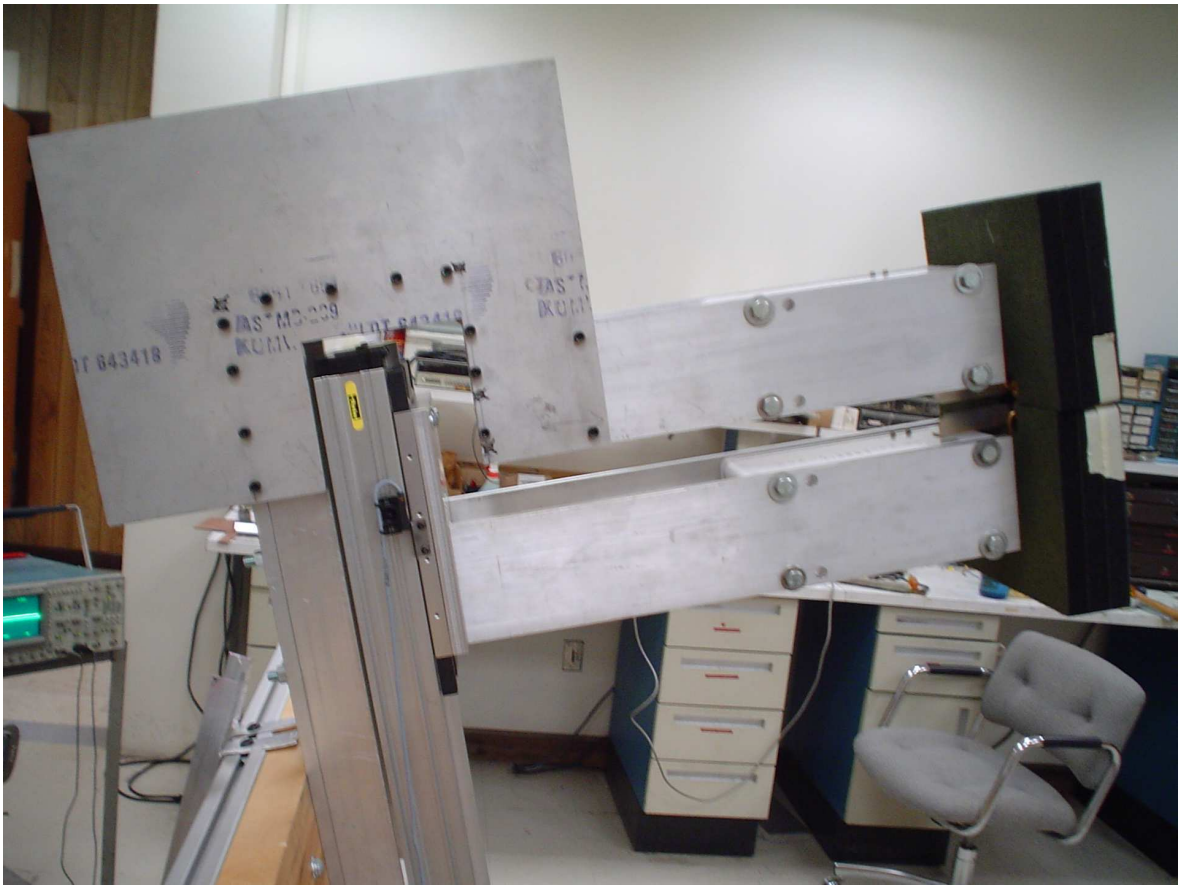

Figure C.2. Radiometer support structures

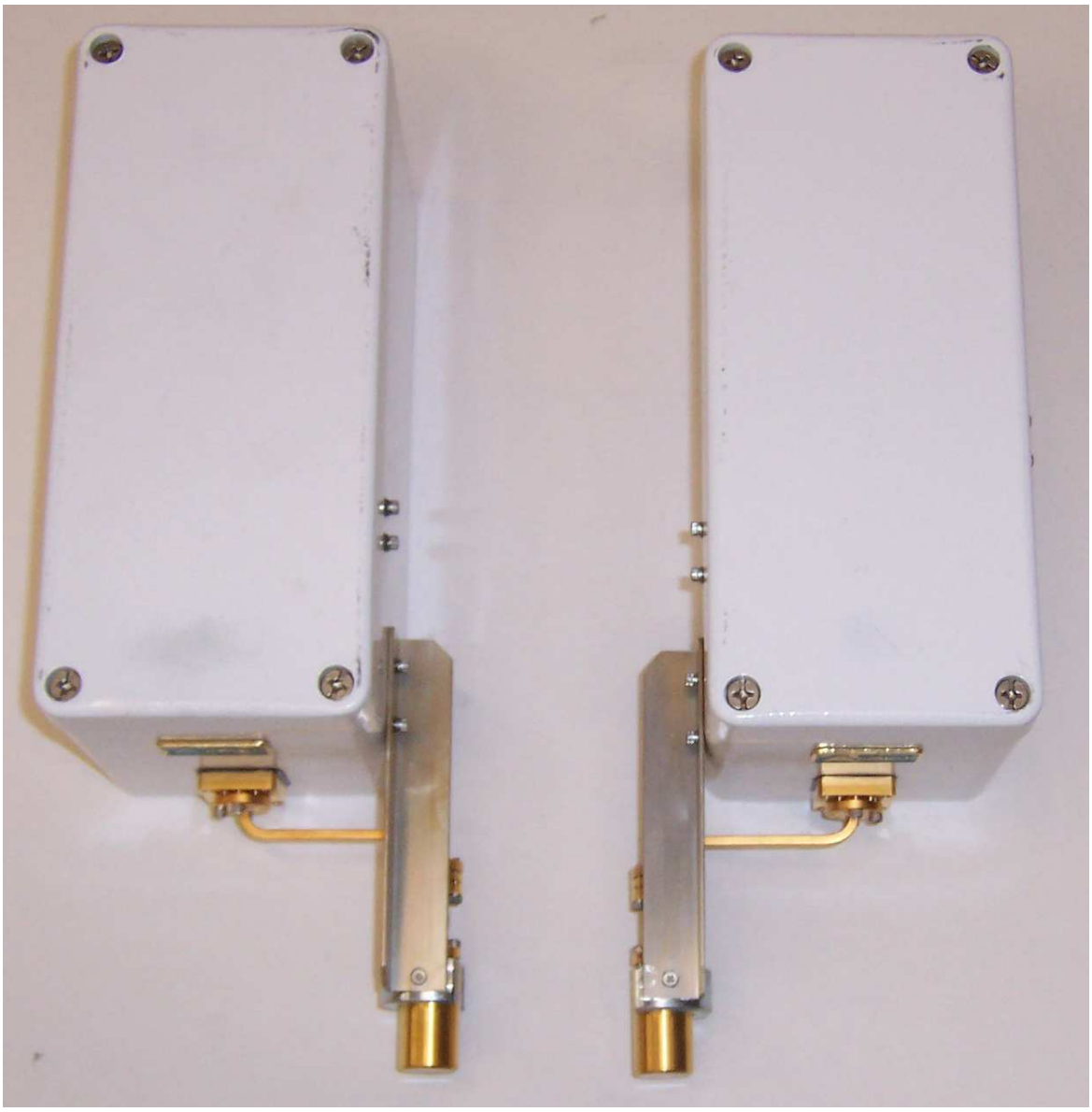

Figure C.3. 94.8 GHz Millitech radiometers

Figure C.4. 94.8 GHz Millitech radiometers on measurement structures with absorber

Figure C.5. 94.8 GHz Millitech noise source

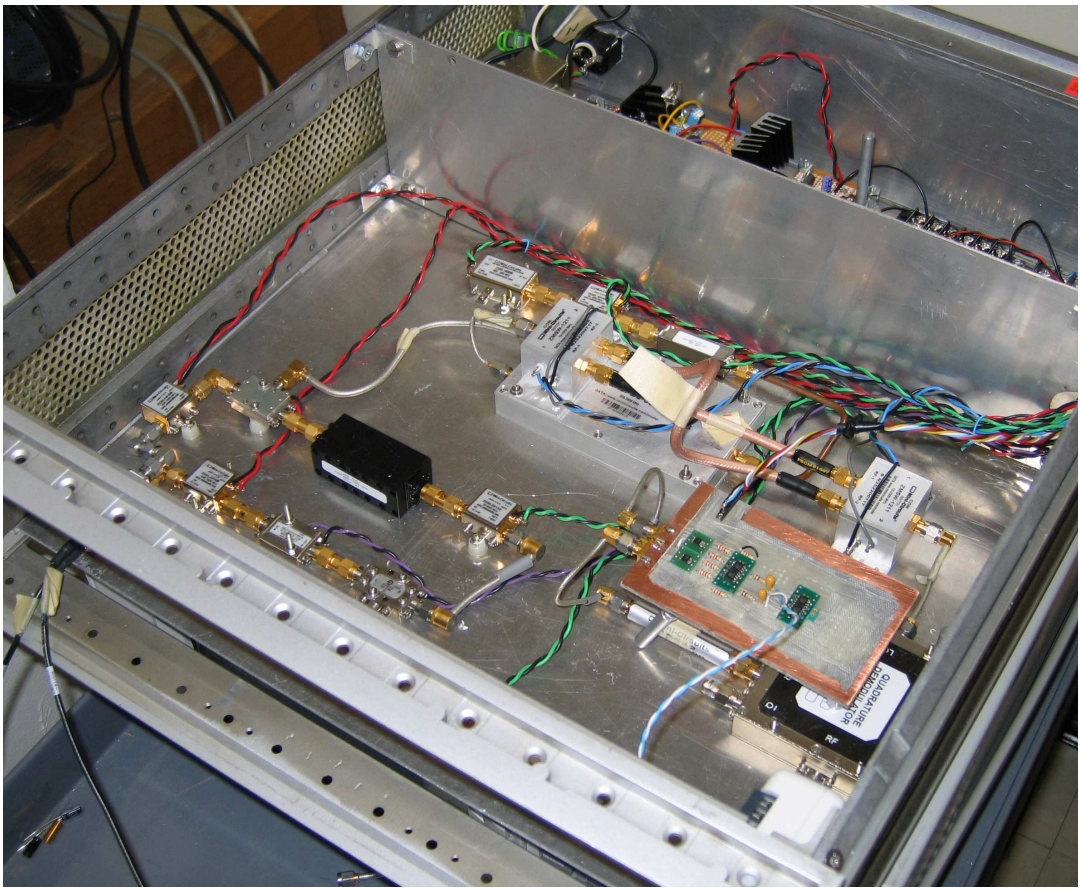

Figure C.6. Complex correlator and power supply packaging

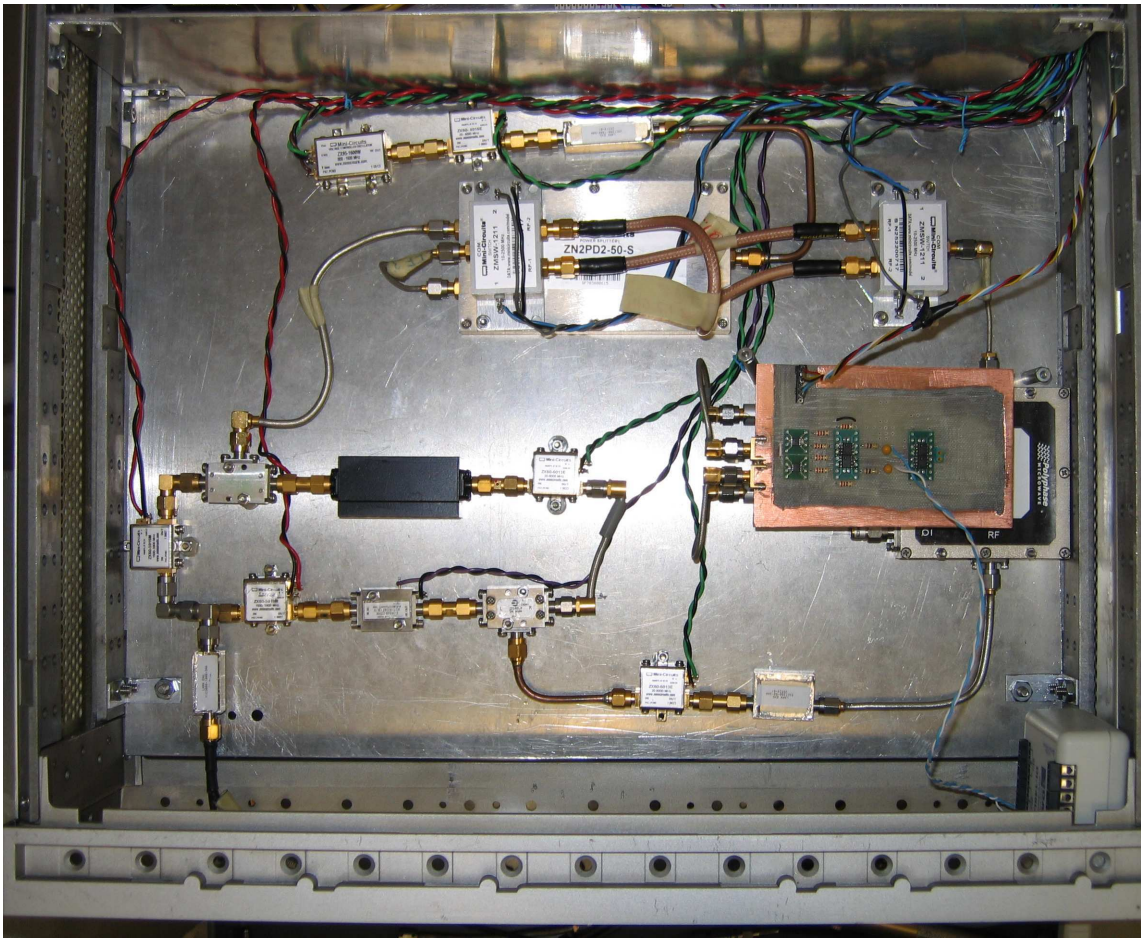

Figure C.7. Top view of complex correlator

APPENDIX D

GEMINI DIGITAL SERVO DRIVE AND 6K2 SETUP CODE

D.1 Gemini Digital Servo Drives

Both Gemini Digital Servo Drives require unique configuration before any drive movements can be taken place. The following code consists of the configuration code for the Servo Drives operating the 406XR1000 1 meter and 406XR2000 2 meter linear drives.

D.1.1 Configuration Code for 406XR1000

```
;Gemini GV Servo Drive Setup

;Motor Setup
DMTR 1803 ;Motor ID (BE232DJ)
DMTIC 1.83 ;Continuous Current (Amps-RMS)
DMTICD 16.90 ;Continuous Current Derating (% derating at rated speed)
DMTKE 48.3 ;Motor Ke (Volts (0-to-peak)/krpm)
DMTRES 7.72 ;Motor Winding Resistance (Ohm)
DMTJ 16.950 ;Motor Rotor Inertia (kg*m*m*10e-6)
DPOLE 4 ;Number of Motor Pole Pairs
DMTW 83.3 ;Motor Rated Speed (rev/sec)
DMTIP 5.49 ;Peak Current (Amps-RMS)
DMTLMN 38.1 ;Minimum Motor Inductance (mH)
DMTLMX 47.2 ;Maximum Motor Inductance (mH)
DMTD 0.000034 ;Motor Damping (Nm/rad/sec)
DMTRWC 0.56 ;Motor Thermal Resistance (degrees Celsius/Watt)
DMTTCM 15.0 ;Motor Thermal Time Constant (minutes)
DMTTCW 1.50 ;Motor Winding Time Constant (minutes)
DMTAMB 40.00 ;Motor Ambient Temperature (degrees Celsius)
DMTMAX 125.00 ;Maximum Motor Winding Temperature (degrees Celsius)
DHALL  1 ;Disable Hall Sensor Checking
MXPLUS  0 ;MAX PLUS MOTOR
DMTLQS  0 ;Set Q Axis Inductance Saturation
DMTLDS  0 ;Set D Axis Inductance Saturation
DTHERM  0 ;Disable motor thermal switch input
```

```
;Drive Setup
DMODE 2 ;Drive Control Mode
DRES 8000 ;Drive Resolution (counts/rev)
DPWM 8 ;Drive PWM Frequency (kHz)
SFB 1 ;Encoder Feedback
ERES 8000 ;Encoder Resolution (counts/rev)
ORES 8000 ;Encoder Output Resolution (counts/rev)
DMEPIT 0.00 ;Electrical Pitch (mm)
SHALL 0 ;Invert Hall Sensors
DMTLIM 3.1 ;Torque Limit (Nm)
DMTSCL 3.1 ;Torque Scaling (Nm)
DMVLIM 83.000000 ;Velocity Limit (rev/sec)
DMVSCL 83.000000 ;Velocity Scaling (rev/sec)

;Load Setup
LJRAT 27.9 ;Load-to-Rotor Inertia Ratio
LDAMP 0.0000 ;Load Damping (Nm/rad/sec)

;Fault Setup
FLTSTP 1 ;Fault on Startup Indexer Pulses Enable
FLTDSB 1 ;Fault on Drive Disable Enable
SMPER 8000 ;Maximum Allowable Position Error (counts)
SMVER 0.000000 ;Maximum Allowable Velocity Error (rev/sec)
DIFOLD 0 ;Current Foldback Enable

;Digital Input Setup
INLVL 11000000 ;Input Active Level
INDEB 50 ;Input Debounce Time (milliseconds)
INUFD 0 ;Input User Fault Delay Time (milliseconds)
LH 0 ;Hardware EOT Limits Enable

;Digital Output Setup
OUTBD 0 ;Output Brake Delay Time (milliseconds)
OUTLVL 0100000 ;Output Active Level

;Analog Monitor Setup
DMONAV 0 ;Analog Monitor A Variable
DMONAS 100 ;Analog Monitor A Scaling (% of full scale output)
DMONBV 0 ;Analog Monitor B Variable
DMONBS 100 ;Analog Monitor B Scaling (% of full scale ouput)

;Servo Tuning
DIBW 500 ;Current Loop Bandwidth (Hz)
DVBW 50 ;Velocity Loop Bandwidth (Hz)
DPBW 20.00 ;Position Loop Bandwidth (Hz)
SGPSIG 1.000 ;Velocity/Position Bandwidth Ratio
SGIRAT 1.000 ;Current Damping Ratio
SGVRAT 1.000 ;Velocity Damping Ratio
SGPRAT 1.000 ;Position Damping Ratio
DNOTAF 0 ;Notch Filter A Frequency (Hz)
DNOTAQ 1.0 ;Notch Filter A Quality Factor
DNOTAD 0.0000 ;Notch Filter A Depth
DNOTBF 0 ;Notch Filter B Frequency (Hz)
```

```
DNOTBQ 1.0 ;Notch Filter B Quality Factor
DNOTBD 0.0000 ;Notch Filter B Depth
DNOTLG 0 ;Notch Lag Filter Break Frequency (Hz)
DNOTLD 0 ;Notch Lead Filter Break Frequency (Hz)
SGINTE 1 ;Integrator Option
SGVF 0 ;Velocity Feedforward Gain (%)
SGAF 0 ;Acceleration Feedforward Gain (%)
```

D.1.2 Configuration Code for 406XR2000

```
;Gemini GV Servo Drive Setup

;Motor Setup
DMTR 1803 ;Motor ID (BE232DJ)
DMTIC 1.83 ;Continuous Current (Amps-RMS)
DMTICD 16.90 ;Continuous Current Derating (% derating at rated speed)
DMTKE 48.3 ;Motor Ke (Volts (0-to-peak)/krpm)
DMTRES 7.72 ;Motor Winding Resistance (Ohm)
DMTJ 16.950 ;Motor Rotor Inertia (kg*m*m*10e-6)
DPOLE 4 ;Number of Motor Pole Pairs
DMTW 83.3 ;Motor Rated Speed (rev/sec)
DMTIP 5.49 ;Peak Current (Amps-RMS)
DMTLMN 38.1 ;Minimum Motor Inductance (mH)
DMTLMX 47.2 ;Maximum Motor Inductance (mH)
DMTD 0.000034 ;Motor Damping (Nm/rad/sec)
DMTRWC 0.56 ;Motor Thermal Resistance (degrees Celsius/Watt)
DMTTCM 15.0 ;Motor Thermal Time Constant (minutes)
DMTTCW 1.50 ;Motor Winding Time Constant (minutes)
DMTAMB 40.00 ;Motor Ambient Temperature (degrees Celsius)
DMTMAX 125.00 ;Maximum Motor Winding Temperature (degrees Celsius)
DHALL  1 ;Disable Hall Sensor Checking
MXPLUS  0 ;MAX PLUS MOTOR
DMTLQS  0 ;Set Q Axis Inductance Saturation
DMTLDS  0 ;Set D Axis Inductance Saturation
DTHERM  0 ;Disable motor thermal switch input


;Drive Setup
DMODE 2 ;Drive Control Mode
DRES 8000 ;Drive Resolution (counts/rev)
DPWM 8 ;Drive PWM Frequency (kHz)
SFB 1 ;Encoder Feedback
ERES 8000 ;Encoder Resolution (counts/rev)
ORES 8000 ;Encoder Output Resolution (counts/rev)
DMEPIT 0.00 ;Electrical Pitch (mm)
SHALL 0 ;Invert Hall Sensors
DMTLIM 3.1 ;Torque Limit (Nm)
DMTSCL 3.1 ;Torque Scaling (Nm)
DMVLIM 83.000000 ;Velocity Limit (rev/sec)
DMVSCL 83.000000 ;Velocity Scaling (rev/sec)

;Load Setup
```

```
LJRAT 48.2 ;Load-to-Rotor Inertia Ratio
LDAMP 0.0000 ;Load Damping (Nm/rad/sec)

;Fault Setup
FLTSTP 1 ;Fault on Startup Indexer Pulses Enable
FLTDSB 1 ;Fault on Drive Disable Enable
SMPER 8000 ;Maximum Allowable Position Error (counts)
SMVER 0.000000 ;Maximum Allowable Velocity Error (rev/sec)
DIFOLD 0 ;Current Foldback Enable

;Digital Input Setup
INLVL 11000000 ;Input Active Level
INDEB 50 ;Input Debounce Time (milliseconds)
INUFD 0 ;Input User Fault Delay Time (milliseconds)
LH 0 ;Hardware EOT Limits Enable

;Digital Output Setup
OUTBD 0 ;Output Brake Delay Time (milliseconds)
OUTLVL 0100000 ;Output Active Level

;Analog Monitor Setup
DMONAV 0 ;Analog Monitor A Variable
DMONAS 100 ;Analog Monitor A Scaling (% of full scale output)
DMONBV 0 ;Analog Monitor B Variable
DMONBS 100 ;Analog Monitor B Scaling (% of full scale ouput)

;Servo Tuning
DIBW 500 ;Current Loop Bandwidth (Hz)
DVBW 50 ;Velocity Loop Bandwidth (Hz)
DPBW 20.00 ;Position Loop Bandwidth (Hz)
SGPSIG 1.000 ;Velocity/Position Bandwidth Ratio
SGIRAT 1.000 ;Current Damping Ratio
SGVRAT 1.000 ;Velocity Damping Ratio
SGPRAT 1.000 ;Position Damping Ratio
DNOTAF 0 ;Notch Filter A Frequency (Hz)
DNOTAQ 1.0 ;Notch Filter A Quality Factor
DNOTAD 0.0000 ;Notch Filter A Depth
DNOTBF 0 ;Notch Filter B Frequency (Hz)
DNOTBQ 1.0 ;Notch Filter B Quality Factor
DNOTBD 0.0000 ;Notch Filter B Depth
DNOTLG 0 ;Notch Lag Filter Break Frequency (Hz)
DNOTLD 0 ;Notch Lead Filter Break Frequency (Hz)
SGINTE 1 ;Integrator Option
SGVF 0 ;Velocity Feedforward Gain (%)
SGAF 0 ;Acceleration Feedforward Gain (%)
```

D.2 6K2 Controller

The following lines of code must be sent to the 6K2 controller before any movement can be taken. These lines of configuration code are included in the measurement

application and therefore do not need to be entered by the user beforehand. However, if troubleshooting is required outside of the measurement software, this code must be enabled.

D.2.1 Configuration Code for 6K2

```
AXSDEF11 ;Enable controller for Servo drives
ERES8000,8000 ;Encoder resolution (counts/rev)
SMPER0,0 ;Set maximum allowable position error
LH3,3 ;Enable Hardware end-of-limit checking
SCLD8000,8000 ;Set distance scaling value (counts/unit)
SCLV8000,8000 ;Set velocity scaling value (counts/unit)
SCLA8000,8000 ;Set acceleration scaling value (counts/unit)
SCALE1 ;Enable scaling
MA00 ;Enable Incremental mode
MC00 ;Enable Preset mode
A10,10 ;Acceleration rate (rev/sec/sec) THIS CAN BE CHANGED
AD10,10 ;Decceleration rate (rev/sec/sec) THIS CAN BE CHANGED
V1,1 ;Velocity rate (rev/sec) THIS CAN BE CHANGED
SGP3,12 ;Set proportional feedback gain
SGV3,5 ;Set velocity feedback gain
SGI2,3 ;Set integral feedback gain

;Limit/Home Sensor Initialization
INFNC6-1R ;Set INFNC6 to Axis 1 + end-of-travel limit
INFNC7-1S ;Set INFNC7 to Axis 1 - end-of-travel limit
INFNC8-1T ;Set INFNC8 to Axis 1 home limit
LIMFNC1-A ;Clear LIMFNC1 content
LIMFNC2-A ;Clear LIMFNC2 content
LIMFNC3-A ;Clear LIMFNC3 content
INLVL00000111 ;Set Input Active levels for Axis 1 triggers
LIMLVL111000 ;Set Limit Active levels for Axis 1 & 2 triggers
```

APPENDIX E

MOVEMENT AND DATA COLLECTION SOFTWARE

E.1 Code Overview

The software used for controlling the linear drives and Dataq A/D converter is a Visual Basic 6.0 application. The code is comprised of three separate file components, each of which is given. The code files are: global variables file, time delay program, and the main executable that contains all subroutines done in the application.

E.1.1 Measurement Code

modGlobal.bas

```
Global C6K As Object
Global ConnectReturnValue As Integer
Global vel As Double, accel As Double
Global N1lim As Double, N2lim As Double
Global P1lim As Double, P2lim As Double
Global A1hom As Double, A2hom As Double
Global A1or As Double, A2or As Double
Global Xap As Double, Yap As Double
Global M As Integer, N As Integer
Global DisArray() As Integer
Global X As Double, Y As Double
Global TPERx As Double, TPERy As Double
Global Vi As Double, Vq As Double
Global Vid As Double, Vqd As Double
```

modDelay.bas

```
Declare Function timeGetTime Lib "C:\WINNT\SYSTEM32\winmm.dll"...
            () As Long
'"C:\winnt\system32" for Windows NT.
'Units are in milli-seconds.
Sub Delay(ByVal dTime As Long)
    Dim sTime As Long
    sTime& = timeGetTime()
    Do
```

```
        dummy% = DoEvents
    Loop While ((timeGetTime() - sTime&) <= dTime)
End Sub
```

Communication.frm

```
Public Sub cmdCalibrate_Click()
'This section is going to calibrate the two axes
'It will go as so- home to the center, travel to the
'negative EoL, record point, travel to the positive EoL,
'record point, determine the true origin position and
'travel to it.
txtCalStat.Text = "Calibrating..."
Dim homv1 As Double, homv2  As Double
homv = 2
homa = 10
vel = Val(txtVel.Text) * 100
accel = Val(txtAccel.Text) * 100
C6K.Write ("PORT0:ECHO0:")
C6K.Write ("DRIVE00:AXSDEF11:ERES8000,8000:SMPER0,0:LH3,3:")
C6K.Write ("SCLD8000,8000:SCLV8000,8000:SCLA8000,8000:SCALE1:")
C6K.Write ("MA00:MC00:A" & accel & "," & accel & ":AD" &...
            accel & "," & accel & ":V" & vel & "," & vel & ":")
C6K.Write ("INFNC6-1R:INFNC7-1S:INFNC8-1T:")
C6K.Write ("LIMFNC1-A:LIMFNC2-A:LIMFNC3-A:")
C6K.Write ("INLVL00000111:LIMLVL111000:COMEXL11:PSET CLR:")
C6K.Write ("HOMA" & homa & "," & homa & ":HOMV" & homv &...
            "," & homv & ":")

Delay (300)
strReadStr = C6K.read()

C6K.Flush
C6K.Write ("DRIVE11:HOM11:DRIVE00:")
Delay (6000)
C6K.Flush
C6K.Write ("DRIVE11:D-110,-60:GO11:DRIVE00:")
Delay (110 / vel * 1000 + 1000)
C6K.Flush
C6K.Write ("TPE:")
Delay (50)
temp = C6K.read()
N1lim = Val(Mid$(temp, 5, 9))
N2lim = Val(Mid$(temp, 14, 9))
C6K.Flush
C6K.Write ("DRIVE11:D210,110:GO11:DRIVE00:")
Delay (210 / vel * 1000)
C6K.Flush
C6K.Write ("TPE:")
Delay (50)
temp = C6K.read()
P1lim = Val(Mid$(temp, 5, 9))
```

```
P2lim = Val(Mid$(temp, 14, 9))
A1hom = (P1lim - N1lim) / 2
A2hom = (P2lim - N2lim) / 2
A1or = A1hom
A2or = P2lim
C6K.Write ("DRIVE11:D-" & CStr(A1or) & ",0:GO11:DRIVE00:")
Open txtDirCalFile.Text For Output As #2
UltimaSerial.Start
Delay (1000)
UltimaSerial.GetDataEx V(0), 2 * srate
UltimaSerial.Stop
For z = 0 To UBound(V, 1) / 2 - 1
    Ch1(z) = V(2 * z) / 64 * 10 / 512
    Ch2(z) = V(2 * z + 1) / 64 * 10 / 512
    Write #2, Ch1(z), Ch2(z)
Next
txtCalStat.Text = "Calibration Complete"
End Sub

Private Sub cmdConnect_Click()
Dim CommPort As Integer
Dim V As Double, A As Double
'Connect to the 6K controller
Set C6K = CreateObject("COM6SRVR.RS232")
CommPort = 1
ConnectReturnValue = C6K.Connect(CommPort)
'Connect to the ADC
UltimaSerial.Device = 148
UltimaSerial.CommPort = Val(USB)
UltimaSerial.AcquisitionMode = NoCondition
UltimaSerial.ChannelCount = 2
UltimaSerial.EventLevel = 2 * Val(Combo1.Text)
UltimaSerial.SampleRate = Val(Combo1.Text)
UltimaSerial.PChannel(0) = Ch3
UltimaSerial.PChannel(1) = Ch4
End Sub

Private Sub cmdDisconnect_Click()
Set C6K = Nothing
End Sub

Private Sub cmdSend_Click()
txtStatus.Text = "Creating array..."
Xap = Val(txtXap.Text) * 100 'take entered value and convert to cm
Yap = Val(txtYap.Text) * 100 'take entered value and convert to cm
d = Val(txtElement.Text) * 100 'element separation in cm
vel = Val(txtVel.Text) * 100 'velocity in cm/s
accel = Val(txtAccel.Text) * 100 'acceleration in cm/s/s
srate = Val(Combo1.Text)
M = Xap / d + 1
N = Yap / d + 1
Xap = (M - 1) * d
Yap = (N - 1) * d
ReDim DisArray(0 To N - 1, 0 To M - 1)
```

```
For i = 0 To N - 1
    For j = 0 To M - 1
        DisArray(i, j) = 1
        If i <> 0 And j = 0 Then
            DisArray(i, j) = 2
        ElseIf i = 0 And j = 0 Then
            DisArray(i, j) = 3
        End If
    Next
Next
txtStatus.Text = "Array complete."
Select Case N Mod 2
Case 0
    Y1 = N / 2 * d
    Y2 = Yap - Y1
Case 1
    Y1 = Yap / 2
    Y2 = Y1
End Select
Dim V() As Integer
Dim Ch1() As Double, Ch2() As Double
Dim counter As Double
counter = 0
ReDim V(2 * srate) As Integer
ReDim Ch1(srate - 1) As Double
ReDim Ch2(srate - 1) As Double
Open txtDirFile.Text For Output As #1
For i = 0 To N - 1
    For j = 0 To M - 1
    Vit = 0
    Vqt = 0
    Vidt = 0
    Vqdt = 0
    Select Case DisArray(i, j)
    Case 1
        C6K.Write ("DRIVE00:D0,-" & CStr(d) &...
            ":DRIVE11:GO11:DRIVE00:")
        Delay ((2 * d / vel + (4 * vel / accel)) * 1000)
        C6K.Flush
        C6K.Write ("TPER:")
        Delay (100)
        temp = C6K.read()
        TPERy = CDbl(Mid$(temp, 6, 6))
        TPERx = CDbl(Mid$(temp, 13, 6))
        C6K.Flush
        UltimaSerial.Start
        Delay (1000)
        UltimaSerial.GetDataEx V(0), 2 * srate
        UltimaSerial.Stop
        For z = 0 To UBound(V, 1) / 2 - 1
            Ch1(z) = V(2 * z) / 64 * 10 / 512
            Ch2(z) = V(2 * z + 1) / 64 * 10 / 512
            Vit = Vit + Ch1(z)
            Vqt = Vqt + Ch2(z)
```

```
    Next
    Vi = Vit / (UBound(Ch1, 1) + 1)
    Vq = Vqt / (UBound(Ch2, 1) + 1)
    X = j * d
    Y = i * d - Y1
    txtStatus.Text = Format(counter * 100 / (M * N), "#0")...
        & "% Complete"
Case 2
    If Xap > Y2 Then
        del = Xap
    Else
        del = Y2
    End If
    C6K.Write ("DRIVE00:D" & CStr(d) & "," & CStr(Xap) &...
        ":DRIVE11:GO11:DRIVE00:")
    Delay ((2 * del / vel + (8 * vel / accel)) * 1000)
    C6K.Flush
    C6K.Write ("TPER:")
    Delay (100)
    temp = C6K.read()
    TPERy = CDbl(Mid$(temp, 6, 6))
    TPERx = CDbl(Mid$(temp, 13, 6))
    UltimaSerial.Start
    Delay (1000)
    UltimaSerial.GetDataEx V(0), 2 * srate
    UltimaSerial.Stop
    For z = 0 To UBound(V, 1) / 2 - 1
        Ch1(z) = V(2 * z) / 64 * 10 / 512
        Ch2(z) = V(2 * z + 1) / 64 * 10 / 512
        Vit = Vit + Ch1(z)
        Vqt = Vqt + Ch2(z)
    Next
    Vi = Vit / (UBound(Ch1, 1) + 1)
    Vq = Vqt / (UBound(Ch2, 1) + 1)
    X = j * d
    Y = i * d - Y1
    txtStatus.Text = Format(counter * 100 / (M * N), "#0")...
        & "% Complete"
Case 3
    C6K.Write ("DRIVE00:D-" & CStr(Y1) & ",0:DRIVE11:...
        GO11:DRIVE00:")
    Delay ((2 * Y1 / vel + (8 * vel / accel)) * 1000)
    C6K.Flush
    C6K.Write ("TPER:")
    Delay (100)
    temp = C6K.read()
    TPERy = CDbl(Mid$(temp, 6, 6))
    TPERx = CDbl(Mid$(temp, 13, 6))
    UltimaSerial.Start
    Delay (1000)
    UltimaSerial.GetDataEx V(0), 2 * srate
    UltimaSerial.Stop
    For z = 0 To UBound(V, 1) / 2 - 1
        Ch1(z) = V(2 * z) / 64 * 10 / 512
```

```
            Ch2(z) = V(2 * z + 1) / 64 * 10 / 512
            Vit = Vit + Ch1(z)
            Vqt = Vqt + Ch2(z)
        Next
        Vi = Vit / (UBound(Ch1, 1) + 1)
        Vq = Vqt / (UBound(Ch2, 1) + 1)
        X = j * d
        Y = i * d - Y1
        txtStatus.Text = Format(counter * 100 / (M * N), "#0")...
            & "% Complete"
    End Select
    For zz = 0 To UBound(V, 1) / 2 - 1
        Vidt = Vidt + (Ch1(z) - Vi)^2
        Vqdt = Vqdt + (Ch2(z) - Vq)^2
    Next
    Vid = (Vidt / (UBound(Ch1, 1) + 1))^0.5
    Vqd = (Vqdt / (UBound(Ch2, 1) + 1))^0.5
    Write #1, Y, X, TPERy, TPERx, Vi, Vq, Vid, Vqd
    counter = counter + 1
    Next
Next
Close #1
If Xap > Y2 Then
    del = Xap
Else
    del = Y2
End If
C6K.Write ("DRIVE00:D-" & CStr(Y2) & "," & CStr(Xap) &...
          ":DRIVE11:GO11:DRIVE00:")
Delay ((2 * del / vel + (8 * vel / accel)) * 1000)
C6K.Flush
C6K.Write ("TPER:")
Delay (100)
temp = C6K.read()
C6K.Flush
txtStatus.Text = "Measurement Complete"
txtReceive.Text = C6K.read
End Sub

Private Sub Form_Load()
Combo1.AddItem "2"
Combo1.AddItem "4"
Combo1.AddItem "8"
Combo1.AddItem "16"
Combo1.AddItem "32"
Combo1.AddItem "64"
Combo1.AddItem "128"
Combo1.AddItem "256"
Combo1.AddItem "512"
Combo1.AddItem "1024"
End Sub
```

APPENDIX F

IMAGE RECONSTRUCTION CODE

F.1 Reconstruction Code Overview

The Matlab code provided reproduces the measured scene from the visibility function samples. The user inputs the operating frequency, calibration file and measurement file. Additional changes to the code may be needed depending on the user's needs, such as signal gain correction or further DC bias removal.

F.1.1 Reconstruction Code

```
clear all;close all;
%input operating frequency
f0=3e9;lam=3e8/f0;

%enter the calibration file
a=dlmread('ENTER CALIBRATION FILE',',',0,0);
%enter the measured data file
c=dlmread('ENTER MEASUREMENT FILE',',',0,0);
c(:,1)=c(:,1)*1e-2;
c(:,2)=c(:,2)*1e-2;%+.023;

%Determine the average voltage offset caused by the ADC
%and remove from the measured data
am(1)=mean(a(:,5));am(2)=mean(a(:,6));
c(:,5)=c(:,5)-am(1);c(:,6)=c(:,6)-am(2);

%creates a matrix of the visibility data and plots it
x1 = min(c(:,1)):.05:max(c(:,1));
y1 = min(c(:,2)):.05:max(c(:,2));
lll = 1;
for e1 = 1:length(x1)
for e2 = 1:length(y1)
vi(e2,e1)=c(lll,5);
vq(e2,e1)=c(lll,6);
lll = lll +1;
end
end
if max(max(vi)) >= max(max(vq))
```

```
    vip = max(max(vi));
    vi = vi/vip;
    vq = vq/vip;
else
    vqp = max(max(vq));
    vi = vi/vqp;
    vq = vq/vqp;
end

figure;
subplot(2,1,1);imagesc(x1,y1,vi);axis equal;
xlim([min(c(:,1)) max(c(:,1))]);ylim([min(c(:,2)) max(c(:,2))]);
set(gca,'xtick',[min(c(:,1)) max(c(:,1))...
-(max(c(:,1))-min(c(:,1)))/2 max(c(:,1))]);
set(gca,'ytick',[min(c(:,2)) max(c(:,2))...
-(max(c(:,2))-min(c(:,2)))/2 max(c(:,2))]);
xlabel('D_y (m)');ylabel('D_x (m)');

subplot(2,1,2);imagesc(x1,y1,vq);axis equal;
xlim([min(c(:,1)) max(c(:,1))]);ylim([min(c(:,2)) max(c(:,2))]);
set(gca,'xtick',[min(c(:,1)) max(c(:,1))...
-(max(c(:,1))-min(c(:,1)))/2 max(c(:,1))]);
set(gca,'ytick',[min(c(:,2)) max(c(:,2))...
-(max(c(:,2))-min(c(:,2)))/2 max(c(:,2))]);
xlabel('D_y (m)');ylabel('D_x (m)');

%convert visibility function to complex number
cmod(:,1)=complex(c(:,5),c(:,6));

%enter the focusing distance ht
ht=1.54;
x=min(c(:,1)):.01:max(c(:,1));
y=min(c(:,2)):.01:max(c(:,2));
for i=1:length(x)
    for k=1:length(y)
    Wc(:,i,k)=cmod(:,1).*exp(-j*2*pi*c(:,1)./lam./ht.*...
(x(i)-c(:,1)./2)).*exp(-j*2*pi*c(:,2)./lam./ht.*...
(y(k)-c(:,2)./2));
    vc(i,k)=sum(Wc(:,i,k));
    Tc(i,k)=vc(i,k);
    end
end

%plot the reconstructed data
figure;
imagesc(x,y,(abs(Tc)./max(max(abs(Tc))))');
colorbar('location','eastoutside');
axis equal;xlim([min(c(:,1)) max(c(:,1))]);
ylim([min(c(:,2)) max(c(:,2))]);
set(gca,'xtick',[min(c(:,1)) max(c(:,1))...
-(max(c(:,1))-min(c(:,1)))/2 max(c(:,1))]);
set(gca,'ytick',[min(c(:,2)) max(c(:,2))...
-(max(c(:,2))-min(c(:,2)))/2 max(c(:,2))]);
xlabel('D_y (m)');ylabel('D_x (m)');
```

```
figure;
surface(x,y,(abs(Tc)./max(max(abs(Tc))))',’LineStyle’,’none’);
axis equal;xlim([min(c(:,1)) max(c(:,1))]);
ylim([min(c(:,2)) max(c(:,2))]);...
set(gca,’xtick’,[min(c(:,1)) max(c(:,1))...
-(max(c(:,1))-min(c(:,1)))/2 max(c(:,1))]);
set(gca,’ytick’,[min(c(:,2)) max(c(:,2))...
-(max(c(:,2))-min(c(:,2)))/2 max(c(:,2))]);
set(gca,’ztick’,[0 .5 1]);set(gca,’XDir’,’reverse’);
xlabel(’D_y (m)’);ylabel(’D_x (m)’);zlabel(’Normalized T_B’);
```

BIBLIOGRAPHY

[1] A. Tanner, *Aperture Synthesis for Passive Microwave Remote Sensing: The Electronically Scanned Thinned Array Radiometer*. Ph.D. thesis, Elec. Comput. Engg., Univ. of Massachusetts, Amherst MA, 1990.

[2] G.W. Swenson and N.C. Mathur, "The Interferometer in Radio Astronomy," *Proc. IEEE*, vol. AP-56, pp. 2114–2130, Dec. 1968.

[3] G. Gleason, *The Design and Development of an Analog Complex Correlator and Other Subsystems for a Thinned Array Microwave Radiometer*. M.S. thesis, Elec. Comput. Engg., Univ. of Massachusetts, Amherst MA, 1993.

[4] T. Hiett, *Construction of an Electronically Steered Thinned Array Radiometer*. M.S. thesis, Elec. Comput. Engg., Univ. of Massachusetts, Amherst MA, 1988.

[5] D.M. LeVine, A.J. Griffis, C.T. Swift and T.J. Jackson, "ESTAR: A Synthetic Aperture Microwave Radiometer for Remote Sensing Applications," *Proc. IEEE*, vol. 82, pp. 1787–1801, Dec. 1994.

[6] A.T. Moffet, "Minimum-Redundancy Linear Arrays," *IEEE Trans. Antennas and Propagation*, vol. 16, pp. 172–175, Mar. 1968.

[7] C.S. Ruf, C.T. Swift, A.B. Tanner and D.M. LeVine, "Interferometric Synthetic Aperture Microwave Radiometry for the Remote Sensing of the Earth," *IEEE Trans. Geosciences and Remote Sensing*, vol. 26, pp. 597–611, Sep. 1988.

[8] D.M. LeVine, "Synthetic Aperture Radiometer Systems," *IEEE Trans. Microwave Theory and Techniques*, vol. 47, pp. 2228–2236, Dec. 1999.